Journal of the Serbian Chemical Society

*e*version electronic

Available on line at

СХД 1897

www.shd.org.rs/JSCS/

CONTENTS*

* For colored figures in this issue please see electronic version at the Journal Home Page: http://www.shd.org.rs/JSCS/

Synthesis of novel menthol derivatives containing 1,2,3-triazole group and their *in vitro* antibacterial activities

MOHADESEH KARBASI[1], PEYMAN SALEHI[1]*, ATOUSA ALIAHMADI[2], MORTEZA BARARJANIAN[1] and FARZANEH ZANDI[2]

[1]*Department of Phytochemistry, Medicinal Plants and Drugs Research Institute, Shahid Beheshti University, G. C., Evin, 1983963113 Tehran, Iran and* [2]*Department of Biology, Medicinal Plants and Drugs Research Institute, Shahid Beheshti University, G. C., Evin, 1983963113 Tehran, Iran*

Abstract: New *N*-substituted α-aminonitrile derivatives from menthol were synthesized by consecutive succinic ester formation, propargylation, 1,3-dipolar Huisgen cycloaddition and Strecker reaction. The structures of the synthesized compounds were confirmed by diverse spectroscopic techniques including ^{1}H-NMR, ^{13}C-NMR, ESI-MS and IR. The novel synthesized compounds were evaluated for their *in vitro* antibacterial activities against *Staphylococcus aureus* as Gram-positive and *Escherichia coli* as Gram-negative bacteria. These compounds demonstrated a strong inhibitory effect against *S. aureus* with the minimum inhibitory concentration (*MIC*) values ranged from 32–128 μg mL^{-1}. Derivatives **6a$_2$**, **6b$_1$**, **6b$_4$** and **6b$_5$** with a *MIC* value of 32 μg mL^{-1} exhibited the best inhibitory effects.

Keywords: click reaction; strecker synthesis; α-aminonitrile; Huisgen reaction.

INTRODUCTION

Menthol is a naturally occurring terpenoid with three chiral carbon atoms. Among the optical isomers, (–)-menthol is the one that has been found most widely in nature.[1] Various studies have revealed that menthol has significant biological properties such as antimicrobial, anticancer, anti-inflammatory and antifungal.[2,3] What has drawn the researchers' attention more among these biological properties during the past several years is the antibacterial activity and its use in pharmaceutical products designed to care of the oral health, including toothpastes and mouthwashes to diminish bacterial growth and oral offensive odor.[4] Moreover, some menthol derivatives were reported with outstanding spectrum of antibacterial activities against several bacterial strains.[5–7]

577

1,2,3-Triazole is a famous scaffold, which can be prepared by 1,3-dipolar Huisgen cycloaddition reaction,[8] and broadly exists in the wide range of compounds with interesting biological properties such as antibacterial, antimalarial, anticancer, antitubercular, anti-inflammatory.[3,9–11] The structural attribute of 1,2,3-triazole allows it to mimic various functional groups such as esters and amides, leading to its widespread applications in the design of drugs and synthesis of chemical compounds to boost the efficacy of the lead molecule.[12] Most commonly, 1,4-disubstituted 1,2,3-triazoles are served as bioisosteres of the amide bond in different therapeutic contexts, such as anticancer, antitubercular and anti-microbial agents.[13–15]

α-Aminonitriles constitute an important class of naturally existing compounds and a salient intermediate to synthesize various *N*-containing heterocycles.[16,17] The *α*-aminonitrile motif is found in different medicines such as, vildagliptin and anagliptin, Fig. 1, as anti-diabetic drugs.[18] In addition, saframycin as a natural product and its synthetic derivative phthalascidin exhibited promising antitumor activities.[19,20] Several studies revealed that *α*-aminonitrile derivatives exhibit good biological properties, for instance: anticancer, antibacterial, antifungal, and antiviral as well as pesticidal agent.[21–23]
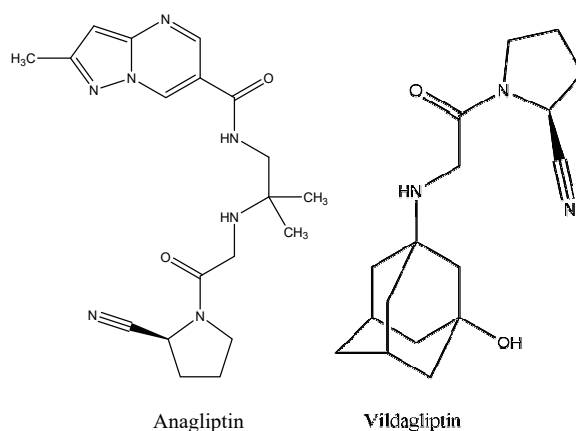
Fig. 1. Structures of biologically active derivatives of *α*-aminonitriles.

The Strecker reaction is a three-component condensation between an aldehyde, an amine and cyanide ion.[24] This valuable reaction leads to the synthesis of *α*-aminonitrile moiety which is of high importance as intermediate in organic synthesis as well as in the pharmaceutical industry.[23,25]

Based on the attributes mentioned above, and in continuation of our interest in evaluating the overall impact of the combination between 1,2,3-triazole ring and natural products,[26,27] here we report the synthesis of new menthol analog containing 1,2,3-triazole and investigation of their antimicrobial activity.

EXPERIMENTAL

General chemistry

Menthol and other starting materials and solvents were purchased from Sigma–Aldrich and Merck chemical companies and used without any further purification. Azides **4a–c** were synthesized according to the reported literature procedures.[28–30] ^{1}H- and ^{13}C-NMR spectra were recorded on a Bruker Avance III spectrometer at 300 and 75 MHz, respectively, in chloroform (CDCl$_3$) using tetramethylsilane (TMS) as the internal standard. Chemical shifts (δ) are given in ppm, and coupling constants (J) are given in Hz. FT-IR spectra were obtained on a Bruker Tensor 27 spectrometer. ESIMS spectra were prepared on a Thermo Fisher Scientific (Waltham, MA, USA) Finnigan TM LCQTM DECA in positive mode. Silica gel F$_{254}$ was employed in column chromatography and thin-layer chromatography (TLC). All analytical and spectral data of the synthesized compounds are given in the Supplementary material to this paper.

Preparation of menthyl succinate (2)

Menthyl succinate was synthesized as reported by a known method in the literature with some modifications.[31,32] To a solution of menthol (5.0 g, 32 mmol) in chloroform, 4-dimethylaminopyridine (0.78 g, 6.4 mmol) and succinic anhydride (3.86 g, 38 mmol) were added. This mixture was stirred overnight under reflux. After solvent evaporation, the crude product was purified using flash column chromatography on silica gel with hexane as eluent to give white crystals (8.0 g, 85 %).

Preparation of propargyl menthyl succinate (3)

Menthyl succinate (8.0 g, 30 mmol) was dissolved in acetonitrile (50 mL). Propargyl bromide (3.7 mL, 34.8 mmol) and NaHCO$_3$ (8.5 g, 60 mmol) were added. The suspension was stirred for 4 h under reflux condition. Then, acetonitrile was evaporated under vacuum and the reaction mixture was stirred with ethyl acetate. The light brown suspension was filtered and the solid was washed with ethyl acetate (2×30 mL) and dried under vacuum overnight.

General procedure for the preparation of menthyl di-substituted derivatives possessing 1,2,3--triazole ring (5a–c)

In a round-bottom flask, propargylic menthyl succinate **3** (441 mg, 1.5 mmol) and 1.5 mmol of azido-benzaldehyde derivatives **4a–c** were dissolved in methanol and dichloromethane mixture (1:1) in the presence of sodium ascorbate (118.8 mg, 0.4 mmol) and CuSO$_4$·5H$_2$O (149.5 mg, 0.2 mmol), the mixture was stirred at room temperature for 30 min to give exclusively disubstituted 1,2,3-triazoles **5a–c**. After completion of the reaction, confirmed by TLC, aqueous ammonia (25 mL, 6N) was added and the whole was extracted with dichloromethane (50 mL) and ethyl acetate (3×50 mL), consequently. In the following, H$_2$O (20 mL) was added and extracted with EtOAc (3×50 mL). The organic layers were combined and washed with H$_2$O (3×50 mL), dried over Na$_2$SO$_4$ and solvent was removed under reduced pressure. Final purification of analogs **5a–c** by flash chromatography on silica gel afforded pure products in 90, 80 and 75 % yields, respectively.

General procedure for the preparation of α-aminonitrile derivatives via *Strecker reaction (6a$_1$, a$_2$, 6b$_1$–b$_7$, 6c$_1$–c$_5$)*

A mixture of azido-benzaldehyde derivatives **4a–c** (0.5 mmol, 200 mg) and the corresponding aromatic amine (1.1 mmol) was stirred in acetic acid (10 mL) for 30 min. Then, 6 mmol of potassium cyanide was added to the mixture. Progress of the reaction mixture was monitored by TLC. The mixture was neutralized with (2×25 mL) potassium carbonate solut-

ion, 2 M, and extracted with ethyl acetate (3×50) mL. The organic layers were combined and washed with H_2O (3×50 mL) and dried over Na_2SO_4. Solvent was removed under reduced pressure. Final purification by crystallization afforded pure products in 60–80 % yields.

Biological tests

Antibacterial activity of the compounds (mixture of two diastereomers) was evaluated by determination of *MIC*, as the lowest concentration that could inhibit the visible growth of assessed bacterial strains. Broth micro-dilution technique was performed as recommended by Clinical Laboratory Standard Institute (J. Jorgensen). Concisely, a two-fold serial dilution of each compound was prepared using sterile Mueller Hinton broth (MHB) medium in 96 well plates in the concentration range from 0.128–0.256 μg mL^{-1}. Consequently, a freshly cultured *Staphylococcus aureus* ATCC 25923 and *Escherichia coli* ATCC 25922 were used to prepare a bacterial suspension with turbidity of 0.5 McFarland standard. Prior to adding bacterial suspensions to trays by sterile MHB, it was further diluted (1:100) to achieve 0.5–1×10^{6} colony forming unit mL^{-1}. *MIC* was documented after 20 h incubation at 37 °C. Each experiment was performed in triplicate and cefixime was assessed as a standard antibiotic.

RESULTS AND DISCUSSION

Chemistry

Our strategy for the synthesis of novel *α*-aminonitrile derivatives containing 1,2,3-triazole ring is illustrated in Scheme 1. Since succinate has been widely used as a linker in the synthesis of several chemical compounds and drugs with biological activities,[33] it was chosen in order to link to (–)-menthol (**1**), and as a result, the menthyl succinate (**2**) was obtained.[31]
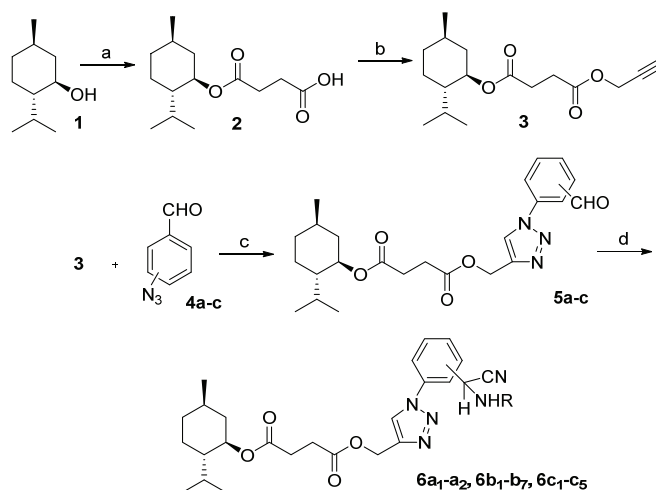
Scheme 1. Preparation of novel triazole derivatives from menthol.

Propargylation of the terminal oxygen in the presence of propargyl bromide and potassium carbonate resulted in the formation of the corresponding propergylated ester (**3**).[34] Then, derivatives **5a**–**c** were synthesized with three *ortho*,

meta and *para* substituted azido-benzaldehydes **4a**–**c** *via* 1,3-dipolar cycloaddition in high yields and purity, using $CuSO_4 \cdot 5H_2O$ and sodium ascorbate as catalysts at room temperature.[35] In the following, a series of α-aminonitriles were produced by adopting three-component Strecker reaction in the presence of various amines, potassium cyanide and compounds **5a**–**c** as the aldehyde source.[36]

Reagents and conditions: a) succinic anhydride, DMAP, $CHCl_3$, reflux overnight; b) propargyl bromide, K_2CO_3, ACN, 4 h, room temperature (r.t.); c) $CuSO_4 \cdot 5H_2O$, sodium ascorbate, $MeOH:H_2O$, r.t., 45 min; d) RNH_2, KCN, CH_3COOH, 2 h, r.t.

To synthesize a diverse range of products, three different azido benzaldehydes, *i.e.*, **4a**–**b** were employed. Also, several aromatic amines bearing halogens (F, Cl, Br) and other electron-withdrawing (NO_2, CN) and electron-releasing (CH_3, CH_2CH_3) functional groups were used to reach a library with a collection of pharmacophores (Table I).

TABLE I. Yields and structure of the synthesized α-aminonitriles
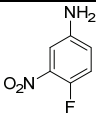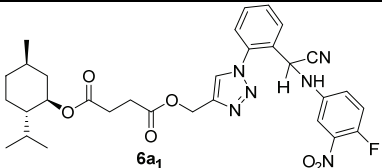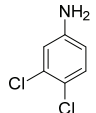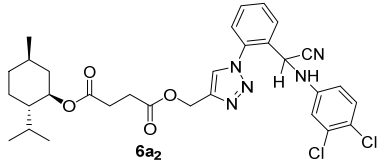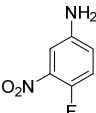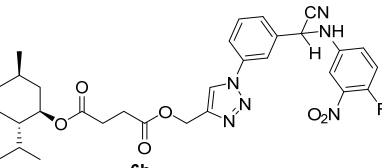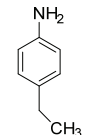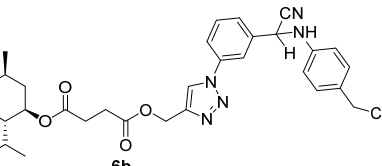
Aldehyde	Amine	Product	Yield, %
5a		**6a₁**	70
5a		**6a₂**	65
5b		**6b₁**	80
5b		**6b₃**	70

TABLE I. Continued
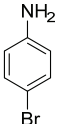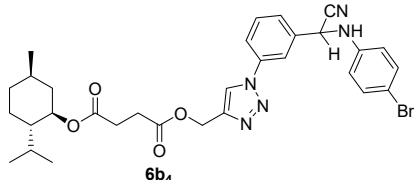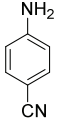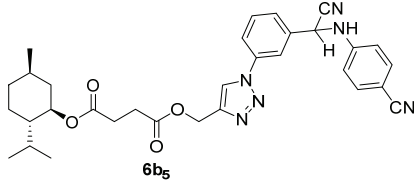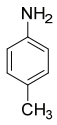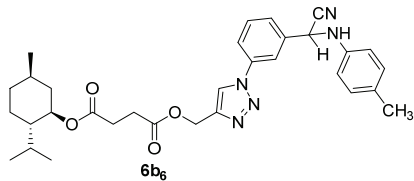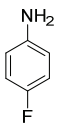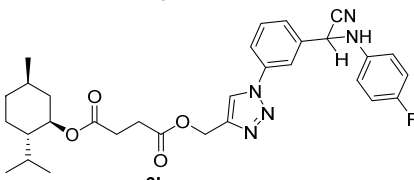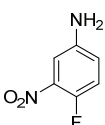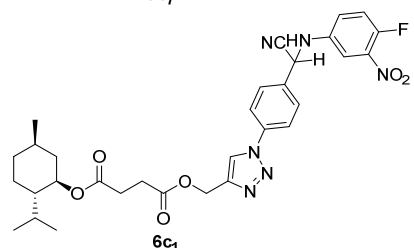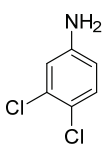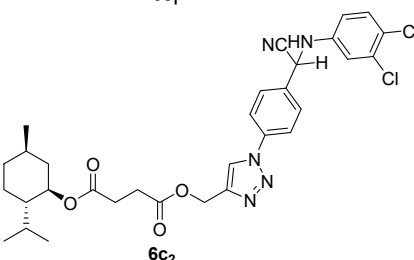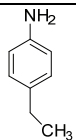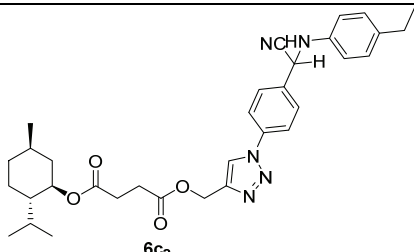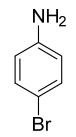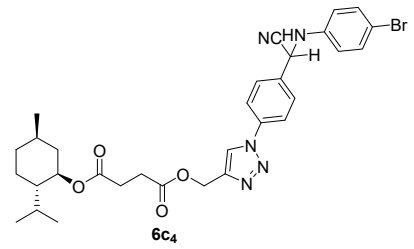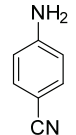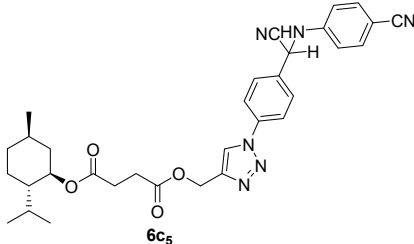
Aldehyde	Amine	Product	Yield, %
5b		6b₄	70
5b		6b₅	65
5b		6b₆	70
5b		6b₇	70
5c		6c₁	65
5c		6c₂	75

TABLE I. Continued

Aldehyde	Amine	Product	Yield, %
5c			70
5c			0
5c			70

Due to the similarity of structures and polarities of the produced diastereomers, we could not separate them by the conventional chromatographic techniques. Surprisingly, almost all of the twin diastereomers exhibited the same NMR spectra. The difference in NMR spectra was only observed for compound **6a1**. The large distance between the newly formed chiral center with other stereogenic centers could be an explanation for this observation.

Biological evaluation

Strong ability of menthol to inhibit different bacterial strains' growth, inspired us to choose it as a lead compound and link it to different scaffolds to discover and develop new antibacterial analogs. *In vitro* antibacterial activities of the newly synthesized compounds **6a**$_1$**, a**$_2$**, 6b**$_1$–**b**$_7$**, 6c**$_1$–**c**$_5$ against Gram-positive bacteria *Staphylococcus aureus* and Gram-negative bacteria *Escherichia coli* were evaluated by determining the minimum inhibitory concentrations (*MIC*), defined as the lowest concentration of the compound that inhibits the visible bacteria growth and compared them with menthol and cefixime (standard antibiotic). As shown in Table II, it is obvious that all novel synthesized compounds exhi-

bited better inhibition activity compared with menthol, however, neither of them was as potent as cefixime. It was revealed that compounds **6a₂**, **6b₁**, **6b₄** and **6b₅** showed promising antibacterial activity against *S. aureus* with *MIC* of 32 µg mL^{-1}. Apparently, the *meta*-substituted products bearing halogen and/or other electron--withdrawing moieties like NO_2 and CN groups exhibited the best antibacterial activities.

TABLE II. *In vitro* (*MIC* / µg mL^{-1}) antibacterial activity of the α-aminonitrile derivatives

Compound	Bacterium	
	S. aureus ATCC (25923)	*E. coli* ATCC (25922)
6a₁	64	>128
6a₂	32	>128
6b₁	32	>128
6b₃	64	>128
6b₄	32	>128
6b₅	32	>128
6b₆	>128	>128
6b₇	>128	>128
6c₁	64	>128
6c₂	64	>128
6c₃	> 128	>128
6c₄	64	>128
6c₅	64	>128
Cefixime	2	7.5
Menthol	> 128	>256

Also, all of them displayed weak activity but stronger than menthol, against *E. coli MIC* > 128 µg mL^{-1}. Due to the obtained results, the significant role of the 1,2,3-triazole ring in boosting the antibacterial activity of menthol derivatives was obvious. Several studies displayed a similar trend (synergistic effect) for improving the antibacterial activity of various lead compounds when linked with a triazole ring.[27,37]

CONCLUSION

One of the most underlying problems facing human beings is bacterial resistance. Menthol is the widely used natural compound in different areas of industries. Several reports have indicated the synergistic and boosting effects of triazoles in terms of biological activities. In this study we aimed to synthesize an α-aminonitrile library of novel 1,2,3-triazole tethered menthol derivatives by a combination of Huisgen 1,3-dipolar cycloaddition and Strecker reactions. Assessment of the antibacterial activity of the products against *Staphylococcus aureus* and *Escherichia coli* revealed that most of them had a stronger activity than menthol itself, while neither were as efficient as cefixime.

SUPPLEMENTARY MATERIAL

Additional data and information are available electronically at the pages of journal website: https://www.shd-pub.org.rs/index.php/JSCS/article/view/12030, or from the corresponding author on request.

И З В О Д
СИНТЕЗА НОВИХ ДЕРИВАТА МЕНТОЛА КОЈИ САДРЖЕ 1,2,3-ТРИАЗОЛСКУ ГРУПУ И ИСПИТИВАЊЕ ЊИХОВЕ *IN VITRO* АНТИБАКТЕРИЈСКЕ АКТИВНОСТИ

MOHADESEH KARBASI[1], PEYMAN SALEHI[1], ATOUSA ALIAHMADI[2], MORTEZA BARAJANIAN[1]
и FARZANEH ZANDI[2]

[1]*Department of Phytochemistry, Medicinal Plants and Drugs Research Institute, Shahid Beheshti University, G. C., Evin, 1983963113 Tehran, Iran и* [2]*Department of Biology, Medicinal Plants and Drugs Research Institute, Shahid Beheshti University, G. C., Evin, 1983963113 Tehran, Iran*

Синтетисани су нови *N*-супституисани α-аминонитрилни деривати ментола, узастопном секвенцом реакција коју чине добијање естра ћилибарне киселине, пропаргиловање, 1,3-диполарне Хизгенове (Huisgen) циклоадиције и Стрекерове (Strecker) синтезе. Структуре синтетисаних производа одређене су на основу анализе спектара, што укључује ^{1}H-NMR, ^{13}C-NMR, ESI-MS и IC. Испитана је *in vitro* антибактеријска активност нових једињења према Грам-позитивној бактерији *Staphylococcus aureus* и Грам-негативној бактерији *Escherichia coli*. Једињења су показала јаку инхибицију према *S. aureus* и минималне инхибиторне концентрације (*MIC*) у опсегу 32–128 µg mL^{-1}. Деривати **6a$_2$**, **6b$_1$**, **6b$_4$** и **6b$_5$** показују највећи инхибиторни ефекат и имају *MIC* вредност од 32 µg mL^{-1}.

REFERENCES

1. N. Kolassa, *Regul. Toxicol. Pharmacol.* **65** (2013) 115 (http://dx.doi.org/10.1016/J.YRTPH.2012.11.009)
2. G. Kamatou, I. Vermaak, A. Viljoen, B. Lawrence, *Phytochemistry* **96** (2013) 15 (http://dx.doi.org/10.1016/j.phytochem.2013.08.005)
3. W. A. Russin, J. D. Hoesly, C. E. Elson, M. A. Tanner, M. N. Gould, *Carcinogenesis* **10** (1989) 2161 (http://dx.doi.org/10.1093/carcin/10.11.2161)
4. I. Freires, C. Denny, B. Benso, S. Alencar, P. Rosalen, *Molecules* **20** (2015) 7329 (http://dx.doi.org/10.3390/molecules20047329)
5. S. Ismailova, E. Mammadbeyli, A. Gurbanov, S. Muradova, *Process. Petrochem. Oil Refin.* **20** (2019) 168
6. G. Zengin, *Chem. Nat. Compd.* **47** (2011) 550 (http://dx.doi.org/10.1007/S10600-011-9994-1)
7. R. Ejaz, S. Malik, M. Ahmad, H. Ali, S. Choudhry, *BCSRJ* (2020) 37 (http://dx.doi.org/10.54112/bcsrj.v2020i1.37)
8. N. S. Vatmurge, B. G. Hazra, V. S. Pore, F. Shirazi, M. V Deshpande, S. Kadreppa, S. Chattopadhyay, R. G. Gonnade, *Org. Biomol. Chem.* **6** (2008) 3823 (http://dx.doi.org/10.1039/b809221d)
9. X. Chu, C. Wang, W. Wang, L. Liang, W. Liu, K. Gong, K. Sun, *Eur. J. Med. Chem.* **166** (2019) 206 (http://dx.doi.org/10.1016/j.ejmech.2019.01.047)

10. Z. Xu, S. Zhao, Chemistry, Y. Liu, *Eur. J. Med. Chem.* **183** (2019) 111700 (http://dx.doi.org/10.1016/j.ejmech.2019.111700)
11. R. Raj, P. Singh, P. Singh, J. Gut, P. Rosenthal, V. Kumar, *Eur. J. Med. Chem.* **62** (2013) 590 (http://dx.doi.org/10.1016/j.ejmech.2013.01.032)
12. E. Bonandi, M. S. Christodoulou, G. Fumagalli, D. Perdicchia, G. Rastelli, D. Passarella, *Drug Discovery Today* **22** (2017) 1572 (http://dx.doi.org/10.1016/j.drudis.2017.05.014)
13. I. Głowacka, J. Balzarini, A. Wróblewski, *Eur. J. Med. Chem.* **70** (2013) 703 (http://dx.doi.org/10.1016/j.ejmech.2013.10.057)
14. J. E. Doiron, C. A. Le, B. K. Ody, J. B. Brace, S. J. Post, N. L. Thacker, H. M. Hill, G. W. Breton, M. J. Mulder, S. Chang, T. M. Bridges, L. Tang, W. Wang, S. M. Rowe, S. G. Aller, M. Turlington, *Chem. Eur. J.* **25** (2019) 3662 (http://dx.doi.org/10.1002/CHEM.201805919)
15. R. Reddyrajula, U. Dalimba, *Bioorg. Med. Chem. Lett.* **30** (2020) 126846 (http://dx.doi.org/10.1016/j.bmcl.2019.126846)
16. N. Otto, T. Opatz, *Chem. Eur. J.* **20** (2014) 13064 (http://dx.doi.org/10.1002/CHEM.201403956)
17. I. Echevarría, M. Vaquero, R. Quesada, G. Espino, *Inorg. Chem. Front.* **7** (2020) 3092 (http://dx.doi.org/10.1039/D0QI00580K)
18. K. Babanezhad, P. Salehi, S. Nejad, M. Bararjanian, M. Kaiser, H. Reza, A. Al-Harrasi, *Bioorg. Chem.* **91** (2019) 103116 (http://dx.doi.org/10.1016/j.bioorg.2019.103116)
19. J. D. Scott, R. M. Williams, *Chem. Rev.* **102** (2002) 1669 (http://dx.doi.org/10.1021/CR010212U)
20. D. Enders, J. Shilvock, *Chem. Soc. Rev.* **29** (2000) 359 (http://dx.doi.org/10.1039/a908290e)
21. B. Ganem, *Acc. Chem. Res.* **42** (2009) 463 (http://dx.doi.org/10.1021/AR800214S)
22. I. N. Shaikh, K. M. Hosamani, M. M. Kurjogi, *Arch. Pharm. (Weinheim)* **351** (2018) 1700205 (http://dx.doi.org/10.1002/ardp.201700205)
23. V. Kouznetsov, C. Galvis, *Tetrahedron* **74** (2018) 773 (http://dx.doi.org/10.1016/j.tet.2018.01.005)
24. E. Ezzatzadeh, Z. Hossaini, *Nat. Prod. Res.* **34** (2018) 923 (http://dx.doi.org/10.1080/14786419.2018.1542389)
25. R. Dalavai, K. Gomathi, K. Naresh, F. R. Nawaz Khan, *Polycycl. Arom. Compd.* **42** (2020) 1581 (http://dx.doi.org/10.1080/10406638.2020.1791917)
26. F. Nemati, P. Salehi, M. Bararjanian, N. Hadian, M. Mohebbi, G. Lauro, D. Ruggiero, S. Terracciano, G. Bifulco, I. Bruno, *Bioorg. Med. Chem. Lett.* **30** (2020) 127489 (http://dx.doi.org/10.1016/j.bmcl.2020.127489)
27. P. Khaligh, P. Salehi, M. Bararjanian, A. Aliahmadi, H. Khavasi, S. Nejad-Ebrahimi, *Chem. Pharmaceut. Bull.* **64** (2016) 1589 (http://dx.doi.org/10.1248/cpb.c16-00463)
28. J. R. Baker, J. Gilbert, S. Paula, X. Zhu, J. Sakoff, A. Mccluskey, *Chem. Eur.* **13** (2018) 1447 (http://dx.doi.org/10.1002/cmdc.201800256)
29. E. Pelkey, G. Gribble, *Tetrahedron Lett.* **38** (1997) 5603 (http://dx.doi.org/10.1016/S0040-4039(97)01272-0)
30. N. T. Pokhodylo, V. S. Matiychuk, M. D. Obushak, *Synthesis (Stuttgart)* (2009) 2321 (http://dx.doi.org/10.1055/S-0029-1216850)
31. P. A. Procopiou, S. P. D. Baugh, S. S. Flack, G. G. A. Inglis, *J. Org. Chem.* **63** (1998) 2342 (http://dx.doi.org/10.1021/JO980011Z)
32. A. Abu-Fayyad, S. Nazzal, *Int. J. Pharmaceut.* **528** (2017) 463 (http://dx.doi.org/10.1016/j.ijpharm.2017.06.031)

33. J. Czarnik-Kwaśniak, K. Kwaśniak, K. Tutaj, I. Filiks, Ł. Uram, M. Stompor, S. Wołowiec, *J. Drug Deliv. Sci. Technol.* **55** (2020) 101424 (http://dx.doi.org/10.1016/J.JDDST.2019.101424)
34. S. Keskin, M. Balci, *Org. Lett.* **17** (2015) 964 (http://dx.doi.org/10.1021/ACS.ORGLETT.5B00067)
35. S. E. Sadat-Ebrahimi, A. Rahmani, M. Mohammadi-Khanaposhtani, N. Jafari, S. Mojtabavi, M. Ali Faramarzi, M. Emadi, A. Yahya-Meymandi, B. Larijani, M. Biglar, M. Mahdavi, *Med. Chem. Res.* **29** (2020) 868 (http://dx.doi.org/10.1007/s00044-020-02522-7)
36. J. Wang, X. Liu, X. Feng, *Chem. Rev.* **111** (2011) 6947 (http://dx.doi.org/10.1021/CR200057T/ASSET/CR200057T.FP.PNG_V03)
37. H. Y. Guo, Z. A. Chen, Q. K. Shen, Z. S. Quan, *J. Enzyme Inhib. Med. Chem.* **36** (2021) 1115 (http://dx.doi.org/10.1080/14756366.2021.1890066).

Synthesis of novel menthol derivatives containing 1,2,3-triazole group and their *in vitro* antibacterial activities

MOHADESEH KARBASI[1], PEYMAN SALEHI[1]*, ATOUSA ALIAHMADI[2],
MORTEZA BARARJANIAN[1] and FARZANEH ZANDI[2]

[1]*Department of Phytochemistry, Medicinal Plants and Drugs Research Institute, Shahid Beheshti University, G. C., Evin, 1983963113 Tehran, Iran and* [2]*Department of Biology, Medicinal Plants and Drugs Research Institute, Shahid Beheshti University, G. C., Evin, 1983963113 Tehran, Iran*

(1-(2-(RS(4-Fluoro-3-nitrophenylamino)(cyano)methyl)phenyl)-1H-1,2,3-triazol-4-yl)methyl(1R,2S,5R)-2-isopropyl-5-methylcyclohexyl succinate (6a₁)

Yield: 70 % , white powder; M.p.: 106 – 109 ºC; IR(KBr, cm^{-1}): 3448.9, 2926.2, 2362.7, 1729.5, 1616.3, 1540.9; ^{1}H NMR (300 MHz, CDCl$_3$), (δ, ppm): mixture of two isomers 7.97 (s, 2H, H$_{Tr}$), 7.90 - 7.83 (m, 2H, H$_{Ar}$), 7.71 - 7.61 (m, 4H, H$_{Ar}$), 7.53 - 7.44 (m, 2H, H$_{Ar}$), 7.39 - 7.32 (m, 2H, H$_{Ar}$), 7.21 - 7.08 (m, 2H, H$_{Ar}$), 7.02 - 6.94 (m, 2H, H$_{Ar}$), 5.77 (d, J = 9.2 Hz, 1H, -CH-CN, one isomer), 5.76 (d, J = 9.2 Hz, 1H, -CH-CN, another isomer), 5.35 - 5.26 (m, 4H, -O-CH$_2$-C$_{Triazile}$), 5.17 (d, J = 9.2 Hz, 1H, NH, one isomer), 5.16 (d, J = 9.2 Hz, 1H, NH, another isomer), 4.71 – 4.61 (m, 2H, -CH-O-), 2.63 (s, 8H, -CO-CH$_2$-CH$_2$-CO-), 1.99 - 1.86 (m, 2H, CH), 1.87 - 1.80 (m, 2H, CH), 1.77 - 1.61 (m, 4H, CH$_2$), 1.45 - 1.35 (m, 2H, CH), 1.36 - 1.28 (m, 2H, CH), 1.24 - 0.90 (m, 6H, CH), 0.89 - 0.86 (m, 12H, 4CH$_3$), 0.71 (dd, J = 6.9Hz, 6H, 2CH$_3$). ^{13}C-NMR (75 MHz, CDCl$_3$), (δ, ppm): 172.32, 172.05, 149.80 (d, J = 257 Hz), 143.97, 140.85, 137.29, 135.36, 131, 27, 130.97, 130.48, 128.56, 126.54, 125.75, 121.72, 119.56, 116.31, 110.90, 74.79, 57.50, 47.60, 46.88, 40.78, 34.14, 31.37, 29.29, 29.04, 26.21, 23.37, 21.99, 20.37, 16.29. MS (ESI): [M+H]$^{+}$ C$_{31}$H$_{35}$FN$_6$O$_6$ calcd 607.66, found 607.70.

(1-(2-(RS(3,4-Dichlorophenylamino)(cyano)methyl)phenyl)-1H-1,2,3-triazol-4-yl)methyl(1R,2S,5R)-2-isopropyl -5-methylcyclohexyl succinate (6a₂)

Yield: 68 %, cream powder; M.p.: 106 - 108 ºC; IR (KBr, cm^{-1}): 3444.4, 2924.5, 2357.2, 1733.1, 1632.7; ^{1}H NMR (300 MHz, CDCl$_3$), (δ, ppm): mixture of two isomers 7.93 (m, 1H, H$_{Triazole}$),7.86 - 7.83 (m, 1H, H$_{Ar}$), 7.68 - 7.61 (m,

---

* Corresponding author. E-mail: p-salehi@sbu.ac.ir

2H, H$_{Ar}$), 7.52- 7.43 (m, 1H, H$_{Ar}$), 7.25 (s, 1H, H$_{Ar}$), 6.80 (d, J = 2.9 Hz, 1H, H$_{Ar}$), 6.56 (dd, J = 8.9, 2.9 Hz, 1H, H$_{Ar}$), 5.69 (d, J = 9.4 Hz, 1H, -CH-CN), 5.31 (s, 2H, H –O-CH$_2$-C$_{Triazol}$), 4.81 (d, J = 9.3, 1H, -NH-), 4.67 (td, J = 11.0, 4.6 Hz, 1H, -CH-O-), 2.62 (s, 4H, -CO-CH$_2$CH$_2$-CO-), 2.00 - 1.90 (m, 1H, CH-Me$_2$), 1.87-1.74 (m, 1H, CH-CHO), 1.67 (s, 2H, CH$_2$), 1.46 - 1.38 (m, 1H, CH), 1.37 - 1.27 (m, 1H, CH), 1.14-0.94 (m, 3H, CH),0.87 (d, J = 6.8 Hz, 6H, 2CH$_3$), 0.76 (d, J = 6.9 Hz, 3H, CH$_3$). ^{13}C-NMR (75 MHz, CDCl$_3$), (δ, ppm): 172.3, 171.9, 143.8, 143.7, 135.3, 133.1, 131.0, 130.1, 130.2, 128.9, 126.6, 125.7, 123.5, 116.6, 116.3, 114.3, 74.8, 57.5, 47.2, 46.9, 40.8, 34.1, 31.4, 29.3, 29.0, 26.2, 23.4, 22.0, 20.7, 16.3. MS (ESI): [M+H]$^{+}$ C$_{31}$H$_{35}$ Cl$_2$N$_5$O$_4$ calcd   613.55, found 613.58.

*(1-(3-(RS(4-fluoro-3-nitrophenylamino)(cyano)methyl)phenyl)-1H-1,2,3-triazol-4-yl)methyl(1R,2S,5R)-2-isopropyl-5-methylcyclohexyl succinate (**6b$_1$**)*

Yield**:** 85 %, white powder; 59-62 °C; IR (KBr, cm^{-1}): 3446.99, 2926.28, 2359.09, 1734.28, 1622.52, 1542.80. ^{1}H NMR (300 MHz, CDCl$_3$), (δ, ppm): mixture of two isomers 8.14 (s, 1H, H$_{Tr}$), 8.06 (s, 1H, H$_{Ar}$), 7.77 (d, J = 8.0 Hz, 1H, H$_{Ar}$), 7.71 (d, J = 8.1 Hz, 1H, H$_{Ar}$), 7.63 (dd, 7.9 Hz 1H, H$_{Ar}$), 7.52 – 7.44 (m, 1H, H$_{Ar}$), 7.23 - 7.12 (m, 1H, H$_{Ar}$), 7.10 - 6.97 (m, 1H, H$_{Ar}$), 5.66 (d, J = 8.6, Hz, 1H, -HC-CN), 5.40 - 5.18 (m, 3H, -O-CH$_2$-C$_{Triazile}$, -NH-), 4.66 (td, J = 10.9, 4.4 Hz, 1H, -CH-O-), 2.78 – 2.50 (m, 4H, -CO-CH$_2$-CH$_2$-CO-), 1.97 - 1.88 (m, 1H, CH), 1.86 - 1.78 (m, 1H, CH), 1.69 - 1.61 (m, 2H, CH$_2$), 1.45 - 1.39 (m, 1H, CH), 1.37-1.31 (m, 1H, CH), 1.12-0.89 (m, 3H, CH), 0.87 (d, J = 7.0 Hz, 3H, CH$_3$), 0.86 (d, J = 6.4 Hz, 3H, CH$_3$), 0.71 (d, J = 6.9 Hz, 3H, CH$_3$).^{13}C-NMR (75 MHz, CDCl$_3$), (δ, ppm): 172.3, 171.9, 149.5 (d, J = 256.5 Hz), 143.9, 141.2, 137.5, 137.4, 135.3, 131.0, 127.6, 122.2, 121.4, 121.2, 119.5, 119.3, 110.4, 74.8, 57.6, 49.6, 46.9, 40.8, 34.1, 31.3, 29.3, 29.1, 26.2, 23.3, 21.9, 20.7, 16.3. MS (ESI): [M+H]$^{+}$ C$_{31}$H$_{36}$FN$_6$O$_6$ calcd 607.66, found 607.68.

*(1-(3-(RS(4-Ethylphenylamino)(cyano)methyl)phenyl)-1H-1,2,3-triazol-4-yl)methyl(1R,2S,5R)-2-isopropyl-5-methylcyclohexyl succinate (**6b$_3$**)*

Yield: 70 %, white powder; M.p.: 53 – 55 ºC; IR(KBr, cm^{-1}): 3424.5, 2923.8, 2358.7, 1731.5, 1614.7; ^{1}H NMR (300 MHz, CDCl$_3$), (δ, ppm): mixture of two isomers 8.12 (s, 1H, H$_{Triazole}$), 8.03 (s, 1H, H$_{Ar}$), 7.82 (d, J = 8.1 Hz, 1H, H$_{Ar}$), 7.74 (d, J = 8.0 Hz, 1H, H$_{Ar}$), 7.63 (dd, J = 8.0 Hz, 1H, H$_{Ar}$), 7.13 (d, J = 8.6 Hz, 2H, H$_{Ar}$), 6.75 (d, J = 8.6 Hz, 2H, H$_{Ar}$), 5.54 (br s, 1H, -CH-CN), 5.41 - 5.27 (m, 2H, -O-CH$_2$-C$_{Triazole}$,), 4.69 (td, J = 10.8, 4.4 Hz, 1H, -CH-O-), 4.18 (br s, 1H, -NH), 2.74 - 2.62 (m, 4H, -CO-CH$_2$-CH$_2$-CO-), 2.60 (q, J = 7.6 Hz, 2H, CH$_2$), 1.99 - 1.91 (m, 1H, CH), 1.90 - 1.80 (m, 1H, CH), 1.71 - 1.60 (m, 2H, CH$_2$), 1.49 - 1.40 (m, 1H, CH), 1.39 - 1.32 (m, 1H, CH), 1.22(t, J = 7.6 Hz, 3H, CH$_3$), 1.11-0.91 (m, 3H, CH), 0.89 (d, J = 7.0 Hz, 3H, CH$_3$), 0.88 (d, J = 6.4 Hz, 3H, CH$_3$), 0.74 (d, J = 6.9 Hz, 3H, CH$_3$). ^{13}C-NMR (75 MHz, CDCl$_3$), (δ, ppm): 172.3, 171.8, 143.8, 142.1, 137.5, 136.5, 136.4, 130.7, 128.9, 127.4, 122.0, 121.2,

119.2, 117.8, 114.7, 74.7, 57.7, 50.1, 46.9, 40.8, 34.1, 31.3, 29.3, 29.1, 27.9, 26.2, 23.3, 22.0, 20.7, 16.3, 15.8. MS (ESI): [M+H] $^+$ $C_{33}H_{41}N_5O_4$ calcd 572.72, found 572.75.

(1-(3-(RS(4-Bromophenylamino)(cyano)methyl)phenyl)-1H-1,2,3-triazol-4-yl)methyl(1R,2S,5R)-2-isopropyl-5-methylcyclohexyl succinate (6b₄)

Yield: 70 % , white powder; M.p.: 53 – 55 °C; IR(KBr, cm^{-1}): 3423.7, 2925.3, 1730.8, 1602.5; ^{1}H NMR (300 MHz, CDCl$_3$), (δ, ppm): mixture of two isomers 8.13 (s, 1H, H$_{Triazolr}$), 8.03 (s, 1H, H$_{Ar}$), 7.79 (d, J = 8.1 Hz, 1H, H$_{Ar}$), 7.68 (d, J = 8.0 Hz, 1H, H$_{Ar}$), 7.63 (dd, J = 7.8 Hz 1H, H$_{Ar}$), 7.38 (d, J = 8.8 Hz, 2H, H$_{Ar}$), 6.68 (d, J = 8.8 Hz, 2H, H$_{Ar}$), 5.54 (s, 1H, -CH-CN), 5.40 - 5.26 (m, 2H, -O-CH$_2$-C$_{Triazol}$), 4.68 (td, J = 10.9, 4.4 Hz, 1H, -CH-O-), 4.52 (br s, 1H, -NH-), 2.73 - 2.58 (m, 4H, -CO-CH$_2$CH$_2$CO), 2.00 - 1.91 (m, 1H, CH), 1.88 - 1.79 (m, 1H ,CH), 1.73 - 1.59 (m, 2H, CH$_2$), 1.44 - 1.38 (m, 1H, CH), 1.37 - 1.24 (m, 1H, CH), 1.12 - 0.91 (m, 3H, CH), 0.88 (d, J = 7.0 Hz, 3H, CH$_3$), 0.87 (d, J = 6.4 Hz, 3H, CH$_3$), 0.73 (d, J = 6.9 Hz, 3H, CH$_3$). ^{13}C-NMR (75 MHz, CDCl$_3$), (δ, ppm): 172.3, 171.9, 143.9, 143.3, 137.5, 135.8, 132.4, 130.9, 127.4, 122.1, 121.4, 119.3, 117.3, 116.0, 112.6, 74.8, 57.7, 49.6, 46.9, 40.8, 34.1, 31.3, 29.3, 29.1, 26.2, 23.3, 22.0, 20.7, 16.3 ppm. MS (ESI): [M+Na] $^+$ $C_{31}H_{36}BrN_5O_4$ calcd 645.54 found 645.59.

(1-(3-(RS(4-Cianobenzylamino)(cyano)methyl)phenyl)-1H-1,2,3-triazol-4-yl)methyl(1R,2S,5R)-2-isopropyl-5-methylcyclohexyl succinate (6b₅)

Yield: 65 % , cream powder; M.p.: 59 – 62 °C; IR(KBr, cm^{-1}): 3432.7, 2926.1, 2368.1, 1734.4, 1610.6; ^{1}H NMR (300 MHz, CDCl$_3$), (δ, ppm):): mixture of two isomers 8.13 (s, 1H, H$_{Triazole}$), 8.04 (s, 1H, H$_{Ar}$), 7.79 (d, J = 7.9 Hz, 1H, H$_{Ar}$), 7.71 (d, J = 8.0 Hz, 1H, H$_{Ar}$), 7.64 (dd, J = 7.8 Hz, 1H, H$_{Ar}$), 7.53 (d, J = 8.7 Hz, 2H, H$_{Ar}$), 6.81 (d, J = 8.7 Hz, 2H, H$_{Ar}$), 5.66 (d, J = 8.0 Hz, 1H, -CH-CN), 5.45 - 5.21 (m, 3H, -O-CH$_2$-C$_{Triazole}$, -NH-), 4.67 (td, J = 10.8, 4.4 Hz, 1H, -CH-O-), 2.73 - 2.56 (m, 4H, -CO-CH$_2$-CH$_2$-CO-), 1.97 – 1.89 (m, 1H, CH), 1.87 - 1.80 (m , 1H, CH), 1.71 - 1.61 (m, 2H, CH$_2$), 1.49 - 1.41 (m, 1H, CH), 1.38 - 1.32 (m, 1H, CH), 1.05 - 0.92 (m, 3H, CH), 0.87 (d, J = 7.0 Hz , 3 Hz, 3H, CH$_3$), 0.86 (d, J = 6.4 Hz, 3H, CH$_3$), 0.72 (d, J = 6.9 Hz, 3H , CH$_3$). ^{13}C-NMR (75 MHz, CDCl$_3$), (δ, ppm): 172.3, 171.9, 147.9, 143.9, 137.5, 135.2, 133.8, 130.9, 127.5, 122.1, 121.4, 119.5, 119.3, 116.9, 113,9, 102.1, 74.8, 57.6, 48.6, 46.8, 40.7, 34.1, 31.3, 29.2, 29.0, 26.2, 23.3, 22.0, 20.7, 16.3. MS (ESI): [M+H] $^+$ $C_{32}H_{36}N_6O_4$ calcd 569.68, found 569.75.

(1-(3-(SR(4-Tolylamino)(cyano)methyl)phenyl)-1H-1,2,3-triazol-4-yl)methyl(1R,2S,5R)-2-isopropyl-5-methylcyclohexyl succinate (6b₆)

Yield: 70 %, white powder; M.p.: 53 – 54 °C; IR(KBr, cm^{-1}): 3440.8, 2923.2, 1730.0, 1619.1; ^{1}H NMR (300 MHz, CDCl$_3$), (δ, ppm):): mixture of two isomers 8.13 (s, 1H, H$_{Triazole}$), 8.03 (s, 1H, H$_{Ar}$), 7.82 (d, J = 7.9 Hz, 1H, H$_{Ar}$), 7.73 (d, J = 8.1 Hz, 1H, H$_{Ar}$), 7.63 (dd, J = 8.0 Hz, 1H, H$_{Ar}$), 7.10 (d, J = 8.3 Hz, 2H, H$_{Ar}$),

6.72 (d, J = 8.3 Hz, 2H, H$_{Ar}$), 5.53(br s, 1H, -CH-CN), 5.38-5.31 (m, 2H, -O-CH$_2$-C$_{Triazole}$), 4.68 (td, J = 10.8, 4.3 Hz, 1H, -CH-O-), 4.17 (br s, 1H, -NH-), 2.71 - 2.62 (m, 4H, -CO-CH$_2$CH$_2$-CO-), 2.29 (s, 3H, CH$_3$), 2.25 – 2.16 (m, 1H, CH), 1.98 - 1.80 (m, 1H, CH), 1.71 - 1.65(m, 2H, CH$_2$), 1.49 - 1.40 (m, 1H,CH), 1.39 - 1.32 (m, 1H, CH), 1.14 - 0.92 (m, 3H, CH), 0.90 – 0.86 (m, 6H, 2CH$_3$), 0.74 (d, J = 6.9 Hz, 3H, CH$_3$). ^{13}C-NMR (75 MHz, CDCl$_3$), (δ, ppm): 172.3, 171.8, 143.9, 141.9, 137.6, 136.4, 130.8, 130.2, 130.1, 127.5, 122.1, 121.3, 119.3, 117.8, 114.8, 74.7, 57.8, 50.2, 46.9, 40.8, 34.2, 31.4, 29.3, 29.1, 26.2, 23.4, 22.0, 20.8, 20.5, 16.3 ppm. MS (ESI): [M+H]$^+$ C$_{32}$H$_{39}$N$_5$O$_4$ calcd 558.70, found 558.72.

(1-(3-(RS(4-Fluorophenylamino)(cyano)methyl)phenyl)-1H-1,2,3-triazol-4-yl)methyl(1R,2S,5R)-2-isopropyl-5-methylcyclohexyl succinate (6b$_7$)

Yield: 70 %, yellow oil; IR(KBr, cm^{-1}): 3348.4, 2952.4,1729.9, 1510.9,1223.5, 1159.2; ^{1}H NMR (300 MHz, CDCl$_3$), (δ, ppm): mixture of two isomers 8.13 (s, 1H, H$_{Triazole}$), 8.04 (s, 1H, H$_{Ar}$), 7.81 (d, J = 8.2 Hz, 1H, H$_{Ar}$), 7.73 (d, J = 8.1 Hz, 1H, H$_{Ar}$), 7.63 (dd, J = 7.9 Hz, 1H, H$_{Ar}$), 7.05 - 6.92 (m, 2H, H$_{Ar}$), 6.81 - 6.69 (m, 2H, H $_{Ar}$), 5.50 (s, 1H, -CH-CN), 5.40 – 5.25 (m, 2H, -O-CH$_2$-C$_{Triazole}$), 4.68 (td, J = 10.8, 4.3 Hz, 1H, -CH-O-), 2.78 - 2.48 (m, 4H, -CO-CH$_2$-CH$_2$-CO-), 2.00 - 1.91 (m, 1H, CH), 1.89 - 1.79 (m, 1H, CH), 1.72 - 1.63 (m, 2H, CH$_2$), 1.48 - 1.39 (m, 1H,CH), 1.37 - 1.28 (m, 1H, CH), 1.08 - 0.91 (m, 3H, CH), 0.88 (d, J = 7.0 Hz, 3H), 0.87 (d, J = 6.4 Hz, 3H, CH$_3$), 0.73 (d, J = 6.9 Hz, 3H, CH$_3$). ^{13}C-NMR (75 MHz, CDCl$_3$), (δ, ppm): 172.4, 171.9, 157.4 (d, J = 237 Hz), 143.8, 140.6, 137.4, 136.1, 130.7, 127.5, 122.1, 121.2, 119.2, 117.7, 116.2, 116.0, 74.7, 57.7, 50.4, 46.8, 40.7, 34.1, 31.3, 29.3, 29.0, 26.20, 23.3, 21.9, 20.7, 16.2 ppm. MS (ESI): [M+Na] $^+$ C$_{31}$H$_{36}$FN$_5$O$_4$ calcd 584.64, found 584.68.

(1-(4-(RS(4-Fluoro-3-nitrophenylamino)(cyano)methyl)phenyl)-1H-1,2,3-triazol-4-yl)methyl(1R,2S,5R)-2-isopropyl-5-methylcyclohexyl succinate (6c$_1$)

Yield: 63 % , white powder; M.p.: 114 – 116 ºC; IR (KBr, cm^{-1}): 3445.7, 2924.6, 2358.6, 1733.9, 1627.7; ^{1}H NMR (300 MHz, CDCl$_3$), (δ, ppm): mixture of two isomers 8.14 (s, 1H, H$_{Triazole}$), 7.82 (d, J = 8.7 Hz, 2H, H$_{Ar}$), 7.75 (d, J = 8.7 Hz, 2H, H$_{Ar}$), 7.55 – 7.42 (m, 1H, H$_{Ar}$), 7.25 – 7.16 (m, 1H, H$_{Ar}$), 7.09 – 7.01 (m, 1H, H$_{Ar}$), 5.61 (d, J = 8.6 Hz, 1H, -CH-CN), 5.38 - 5.24 (m, 2H, -O-CH$_2$-C$_{Triazole}$), 5.00 (d, J = 8.6 Hz, 1H, NH), 4.68 (td, J = 10.9, 4.3 Hz, 1H, -CH-O-), 2.76 - 2.55 (m, 4H, -CO-CH$_2$CH$_2$-CO-), 2.00 - 1.90 (m, 1H, CH), 1.88 - 1.78 (m, 1H, CH), 1.70 - 1.61 (m, 2H, CH$_2$), 1.46 - 1.38 (m, 1H, CH), 1.37 - 1.29 (m, 1H, CH), 1.14 - 0.90 (m, 3H, CH), 0.89 (d, J = 7.0 Hz, 3H, CH$_3$), 0.87 (d, J = 6.4 Hz, 3H, CH$_3$), 0.74 (d, J = 6.9 Hz, 3H, CH$_3$). ^{13}C-NMR (75 MHz, CDCl$_3$), (δ, ppm): 172.4, 171.9, 149.6 (d, J = 256.5 Hz), 144.0, 141.2, 137.6, 137.3, 133.5, 128.8, 122.1, 121.1, 119.6, 119.3, 117.0, 110.4, 74.8, 57.7, 49.5, 46.9, 40.8, 34.1, 31.4, 29.1, 29.0, 26.2, 23.3, 21.9, 20.7, 16.3. MS (ESI): [M+H] $^+$ C$_{31}$H$_{35}$FN$_6$O$_6$ calcd 607.66, found 607.69.

(1-(4-(RS(3,4-Dichlorophenylamino)(cyano)methyl)phenyl)-1H-1,2,3-triazol-4-yl)methyl(1R,2S,5R)-2-isopropyl-5-methylcyclohexyl succinate (6c₂):

Yield: 72 % , cream powder; M.p.: 100 – 102 °C; IR (KBr, cm^{-1}): 3434.11, 2927.53, 2366.45, 1730.02, 1602.00; ^{1}H NMR (300 MHz, CDCl$_3$), (δ, ppm): mixture of two isomers 8.13 (s, 1H,H$_{Triazole}$), 7.85 (d, J = 8.7 Hz, 2H , H$_{Ar}$), 7.76 (d, J = 8.7 Hz, 2H , H$_{Ar}$), 7.32 (d, J = 8.7 Hz, 1H , H$_{Ar}$), 6.91 (d, J = 2.7 Hz, 1H, H$_{Ar}$), 6.65 (dd, J = 8.7, 2.7 Hz, 1H, H$_{Ar}$), 5.53 (d, J = 8.7 Hz, 1H, -CH-CN), 5.38 - 5.28 (m ,2H, -O-CH$_2$-C$_{Triazole}$), 4.68 (td, J = 10.8, 4.4 Hz, 1H, -CH-O-), 4.5 (d, J = 8.7 Hz, 1H, NH), 2.71 - 2.61 (m, 4H, -CO-CH$_2$CH$_2$-CO-), 1.98 - 1.91 (m, 1H, CH), 1.89 - 1.80 (m, 1H, CH), 1.72 - 1.63 (m, 2H, CH$_2$), 1.46 - 1.38 (m, 1H, CH), 1.38 - 1.30 (m, 1H, CH), 1.16 - 0.90 (m, 3H, CH), 0.89 (d, J = 7.0 Hz, 3H, CH$_3$), 0.88 (d, J = 6.4 Hz, 3H, CH$_3$), 0.74 (d, J = 6.9 Hz, 3H, CH$_3$). ^{13}C-NMR (75 MHz, CDCl$_3$), (δ, ppm): 172.3, 171.9, 144.1, 143.9, 137.5, 133.9, 133.1, 130.9, 128.7, 123.1, 121.9, 121.0, 117.3, 115.9, 113.8, 74.8, 57.7, 49.2, 46.9, 40.8, 34.1, 31.8, 29.3, 29.10, 26.2, 23.4, 22.0, 20.7, 16.3. MS (ESI): [M+H]$^+$ C$_{31}$H$_{35}$Cl$_2$N$_5$O$_4$ calcd 612.55, found 612.58.

(1-(4-(RS(4-Ethylphenylamino)(cyano)methyl)phenyl)-1H-1,2,3-triazol-4-yl)methyl(1R,2S,5R)-2-isopropyl-5-methylcyclohexyl succinate (**6c₃**)

Yield: 70 % , white powder; M.p.: 101 – 102 ºC; IR(KBr, cm^{-1}): 3437.1, 2924.9, 2359.1, 1733.5, 1618.3; ^{1}H NMR (300 MHz, CDCl$_3$), (δ, ppm): mixture of two isomers 8.13 (s, 1H, H$_{Triazole}$), 7.85 (d, J = 8.9Hz, 2H, H$_{Ar}$), 7.78 (d, J = 8.9 Hz, 2H, H$_{Ar}$), 7.12 (d, J = 8.9 Hz, 2H, H$_{Ar}$), 6.74 (d, J = 8.9 Hz, H$_{Ar}$), 5.53 (d, J = 8.9 Hz, 1H, -CH-CN), 5.40 - 5.26 (m, 2H, -O-CH$_2$-C$_{Triazole}$), 4.68 (td, J = 10.9, 4.3 Hz, 1H, -CH-O-), 4.22 (d, J = 8.8 Hz, 1H, NH), 2.72 - 2.64 (m, 4H, -CO-CH$_2$-CH$_2$-CO-), 2.59 (q, J = 7.7 Hz, 2H, CH$_2$), 1.97 - 1.90 (m, 1H, CH), 1.88 - 1.80 (m, 1H, CH), 1.71 - 1.63 (m, 2H, CH$_2$), 1.48 - 1.34 (m, 1H, CH), 1.35 - 1.20 (m, 1H, CH), 1.20 (t, J = 7.6 Hz, 3H, CH$_3$), 1.12 - 0.90 (m, 3H, CH), 0.9 (d, J = 6.9 Hz, 3H, CH$_3$), 0.87 (d, J = 6.4 Hz, 3H, CH$_3$), 0.74 (d, J = 6.8 Hz, 3H, CH$_3$). ^{13}C-NMR (75 MHz, CDCl$_3$), (δ, ppm): 172.3, 171.9, 143.9, 142.2, 137.4, 136.5, 134.9, 128.9, 128.7, 121.9, 120.9, 117.9, 114.7, 74.8, 57.8, 49.9, 46.9, 40.8, 34.1, 29.3, 29.1, 28.0, 26.2, 23.4, 22.02, 20.7, 16.3, 15.8. MS (ESI): [M+Na]$^+$ C$_{33}$H$_{41}$N$_5$O$_4$ calcd 594.70, found 594.71.

(1-(4-(RS(4-Bromophenylamino)(cyano)methyl)phenyl)-1H-1,2,3-triazol-4-yl)methyl(1R,2S,5R)-2-isopropyl-5-methylcyclohexyl succinate (6c₄)

Yield: 68 %, white powder; M.p.: 109 – 111 ºC; IR (KBr, cm^{-1}): 3437.10, 2924.58, 2358.34, 1734.01, 1636.93; ^{1}H NMR (300 MHz, CDCl$_3$), (δ, ppm): mixture of two isomers 8.13 (s, 1H, H$_{Triazole)}$, 7.85 (d, J = 8.8 Hz, 2H, H$_{Ar}$), 7.76 (d, J = 8.8 Hz, 2H, H$_{Ar}$), 7.37 (d, J = 8.8 Hz, 2H, H$_{Ar}$), 6.69 (d, J = 8.8 Hz, H$_{Ar}$), 5.53 (d, J = 8.7 Hz, 1H, -CH-CN), 5.40 - 5.28 (m, 2H, -O-CH$_2$-C$_{Triazole}$), 4.68 (td, J = 10.9, 4.4 Hz, 1H, -CH-O-), 4.44 (d, J = 8.7 Hz, 1H, NH), 2.73 - 2.59 (m, 4H, -CO-CH$_2$CH$_2$-CO-), 2.00 - 1.90 (m, 1H, CH), 1.89 -1.79 (m, 1H, CH), 1.72 - 1.62

(m, 2H, CH$_2$), 1.47 - 1.36 (m, 1H, CH), 1.35 - 1.21 (m, 1H, CH), 1.12 - 0.90 (m, 3H, CH), 0.9 (d, *J* = 6.9 Hz, 3H, CH$_3$), 0.87 (d, *J* = 6.4 Hz, 3H, CH$_3$), 0.74 (d, *J* = 6.9 Hz, 3H, CH$_3$). ^{13}C-NMR (75 MHz, CDCl$_3$), (δ, ppm): 172.3, 171.9, 143.9, 143.33, 137.5, 134.1, 132.4, 128.7, 121.9, 121.1, 117.4, 116.1, 112.6, 74.8, 57.8, 49.5, 46.9, 40.8, 34.1, 31.4, 29.3, 29.1, 26.2, 23.4, 22.0, 20.7, 16.3. MS (ESI): [M+H]$^+$ C$_{31}$H$_{36}$BrN$_5$O$_4$ calcd 623.56, found 623.57.

(1-(4-(RS(4-Cianobenzylamino)(cyano)methyl)phenyl)-1H-1,2,3-triazol-4-yl)methyl(1R,2S,5R)-2-isopropyl-5-methylcyclohexyl succinate (6c$_5$)

Yield: 70 % , cream powder; M.p.: 110 – 112 °C; IR(KBr, cm^{-1}): 3436.34, 2924.18, 2362.89, 1733.88, 1611.49; ^{1}H NMR (300 MHz, CDCl$_3$), (δ, ppm): mixture of two isomers 8.13 (s, 1H, H$_{Triazole}$), 7.86 (d, *J* = 8.7 Hz, 2H, H$_{Ar}$), 7.76 (d, *J* = 8.7Hz, 2H, H$_{Ar}$), 7.54 (d, *J* = 8.7 Hz, 2H, H$_{Ar}$), 6.82 (d, *J* = 8.7 Hz, 2H, H$_{Ar}$), 5.63 (d, *J* = 8.0 Hz, 1H, -CH-CN), 5.42 - 5.23 (m, 3H, -O-CH$_2$-C$_{Triazole}$, -NH-), 4.68 (td, *J* = 10.9, 4.4 Hz, 1H, -CH-O-), 2.74 - 2.75 (m, 4H, -CO-CH$_2$CH$_2$-CO-), 2.01 - 1.89 (m, 1H, CH), 1.89 - 1.78 (m, 1H, CH), 1.72 - 1.59 (m, 2H, CH$_2$), 1.47 - 1.39 (m ,1H, CH), 1.39 - 1.29 (m,1H, CH), 1.11 - 0.90 (m, 3H, CH), 0.87 (d, *J* = 6.9 Hz, 3H, CH$_3$), 0.86 (d, *J* = 6.4 Hz, 3H, CH$_3$), 7.3 (d, *J* = 6.9 Hz, 3H, CH$_3$). ^{13}C-NMR (75 MHz, CDCl$_3$), (δ, ppm): 172.4, 171.9, 147.9, 144.0, 137.7, 133.9, 133.5, 128.8, 121.9, 121.1, 119.5, 116.9, 113.9, 102.3, 74.8, 57.7, 48.5, 46.9, 40.8, 34.1, 31.4, 29.3, 29.1, 26.2, 23.4, 22.0, 20.7, 16.3. MS (ESI): [M+H]$^+$ C$_{32}$H$_{36}$N$_6$O$_4$ calcd 569.68, found 569.71.

(1-(2-Formylphenyl)-1H-1,2,3-triazol-4-yl)methyl(1R,2S,5R)-2-isopropyl-methylcyclohexyl succinate (5a)

Yield: 90 %, white powder, M.P: 76 - 78 °C. IR (KBr, cm^{-1}): 2927.30, 1730.91, 1601.86, 1158.25, ^{1}H NMR (300 MHz, CDCl$_3$), (δ, ppm): 9.94 (s, 1H, -CHO-), 8.14 (dd, *J* = 7.8 Hz, 1.3 Hz,1H, H$_{Ar}$), 8.06 (s, 1H, H$_{Triazole}$), 7.79 - 7.65 (td, *J* = 7.6, 1.3 Hz, 1H, H$_{Ar}$), 7.70 (t, *J* = 7.4 Hz, 1H, H$_{Ar}$), 7.55 (d, *J* = 7.8 Hz, 1H, H$_{Ar}$), 5.41-5.32 (m, 2H, -O-CH$_2$-C$_{Triazole}$), 4.72 – 4.60 (m, 1H, -CH-O-), 2.71 - 2.60 (m, 4H, -CO-CH$_2$-CH$_2$-CO-), 1.97 - 1.90 (m, 1H, CH), 1.89 –1.82 (m, 1H, CH), 1.71 - 1.62 (m, 2H, CH$_2$), 1.47 - 1.36 (m, 1H, CH), 1.39 - 1.29 (m, 1H, CH), 1.05 - 0.93 (m, 3H, CH), 0.87 (d, *J* = 7.0 Hz, 3H, CH$_3$), 0.86 (d, *J* = 6.6 Hz, 3H, CH$_3$), 0.73 (d, *J* = 6.9 Hz, 3H, CH$_3$) ppm. ^{13}C-NMR (75 MHz, CDCl$_3$), (δ, ppm): 188.28, 172.19, 171.66, 143.71, 138.08, 134.57, 130.38, 130.10, 129.52, 125.75, 125.35, 74.67, 57.69, 46.94, 40.81, 34.17, 31.34, 29.33, 29.12, 26.26, 23.45, 21.94, 20.66, 16.31. MS (ESI): [M+H]$^+$ C$_{24}$H$_{31}$N$_3$O$_5$ calcd 442.53, found 442.63.

(1-(3-Formylphenyl)-1H-1,2,3-triazol-4-yl)methyl(1R,2S,5R)-2-isopropyl-5-methylcyclohexyl succinate (5b)

Yield: 80 %, yellow oil, IR (KBr, cm^{-1}): 2951.69, 1732.41, 1228.82, 1157.42, ^{1}H NMR (300 MHz, CDCl$_3$), (δ, ppm): 10.10 (s, 1H, -CHO-), 8.27 – 8.23 (m, 1H, H$_{Ar}$), 8.21 (s, 1H, H$_{Triazole}$), 8.13 – 8.05 (m, 1H, H$_{Ar}$), 8.01 – 7.92 (m, 1H, H$_{Ar}$), 7.74 (t, *J* = 7.8 Hz, 1H, H$_{Ar}$), 5.40 - 5.31 (m, 2H, -O-CH$_2$-C$_{Triazole}$), 4.68

(td, J = 10.9, 4.4 Hz, 1H, -CH-O-), 2.72 - 2.61(m, 4H, -CO-CH$_2$-CH$_2$-CO), 1.96 - 1.92 (m, 1H, CH), 1.86 - 1.82 (m,1H, CH), 1.69 - 1.62 (m, 2H, CH$_2$), 1.47 - 1.39 (m, 1H, CH), 1.38 - 1.30 (m, 1H, CH), 1.08 - 0.93(m, 3H, CH), 0.87 (d, J = 7.0 Hz, 3H, CH$_3$), 0.86 (d, J = 6.6 Hz, 3H, CH$_3$), 0.73 (d, J = 6.9 Hz, 3H, CH$_3$) ppm. ^{13}C-NMR (75 MHz, CDCl$_3$), (δ, ppm): 190.79, 172.25, 171.79, 144.07, 137.72, 137.52, 130.71, 129.97, 125.77, 121.96, 120.33, 74.64, 57.74, 46.85, 40.75, 34.10, 31.29, 29.29, 29.07, 26.17, 23.32, 21.94, 20.68, 16.25. MS (ESI): [M+H] $^+$ C$_{24}$H$_{31}$N$_3$O$_5$ calcd 442.53, found 422.58.

*(1-(4-Formylphenyl)-1H-1,2,3-triazol-4-yl)methyl(1R,2S,5R)-2-isopropyl-5-methylcyclohexyl succinate (**5c**)*

Yield: 75 %, white powder, M.P: 80 - 81 °C. IR (KBr, cm-1): 2924.08, 1735.64, 1628.80, 1159.27, 1H NMR (300 MHz, CDCl3), (δ, ppm): 10.03 (s, 1H, -CHO-), 8.21 (s, 1H, HTriazole), 8.02 (d, J = 8.6 Hz, 2H, HAr), 7.95 (d, J = 8.6 Hz, 2H, HAr), 5.36 – 5.25 (m, 2H, -O-CH2-CTriazole), 4.62 (td, J = 10.8, 4.3 Hz, 1H, -CH-O-), 2.67 – 2.57 (m, 4H, -CO-CH2-CH2-CO), 1.93 - 1.84 (m, 1H, CH), 1.83 - 1.74 (m, 1H, CH), 1.65 - 1.56 (m, 2H, CH2), 1.44 - 1.34 (m, 1H, CH), 1.35 - 1.24 (m, 1H, CH), 1.03 - 0.86 (m, 3H, CH), 0.83 (d, J = 7.0 Hz, 3H, CH3), 0.81 (d, J = 6.4 Hz, 3H, CH3), 0.68 (d, J = 6.9 Hz, 3H, CH3) ppm. 13C-NMR (75 MHz, CDCl3), (δ, ppm): 190.70, 172.28, 171.82, 144.25, 140.80, 136.01, 131.34, 121.90, 120.45, 74.70, 57.74, 46.87, 40.78, 34.11, 31.35, 29.30, 29.09, 26.20, 23.36, 21.97, 20.70, 16.27. MS (ESI): [M+H] + C24H31N3O5 calcd 442.53, found 442.60.

*(1R,2S,5R)-2-Isopropyl-5-methylcyclohexyl prop-2-yl succinate (**3**)*

Yield: 80 %, brown liquid, IR (KBr, cm^{-1}): 3289, 2952, 1738, 1375, 1157, 995, 672. 1H NMR (300 MHz, CDCl3), (δ, ppm): 4.78 - 4.62 (m, 3H, -CH-O- and C Acetylene –CH2), 2.75 - 2.59 (m, 4H, -CO-CH2-CH2-CO-), 2.49 (t, J = 2.5 Hz, 1H, H Acetylene), 2.02 - 1.93 (m, 1H, CH), 1.93 - 1.78 (m, 1H, CH), 1.75 - 1.58 (m, 2H, CH2), 1.54 - 1.41 (m, 1H, CH), 1.40 - 1.25 (m, 1H, CH), 1.19 - 0.92 (m, 3H, CH2), 0.90 (d, J = 6.9 Hz, 3H, CH3), 0.89 (d, J = 7.1 Hz, 3H, CH3), 0.75 (d, J = 6.9 Hz, 3H, CH3) ppm. 13C-NMR (75 MHz, CDCl3), (δ, ppm): 171.52, 171.49, 75.00, 74.63, 52.14, 46.93, 40.79, 34.19, 31.35, 29.26, 28.98, 26.19, 23.37, 22.00, 20.75, 16.27. MS (ESI): [M+Na] + C17H26O4 calcd 317.37, found 317.37.

In vitro study of redox properties of azolyl-lactones in human serum

MILENA R. SIMIĆ[1*#], JELENA M. KOTUR-STEVULJEVIĆ[2**], PREDRAG M. JOVANOVIĆ[1#], MILOŠ R. PETKOVIĆ[1#], MILOŠ D. JOVANOVIĆ[1#], GORDANA D. TASIĆ[1#] and VLADIMIR M. SAVIC[1#]

[1]*University of Belgrade-Faculty of Pharmacy, Department of Organic Chemistry, Vojvode Stepe 450, 11221 Belgrade, Serbia and* [2]*University of Belgrade-Faculty of Pharmacy, Department of Medical Biochemistry, Vojvode Stepe 450, 11221 Belgrade, Serbia*

Abstract: Disruption of the redox balance in the body causes oxidative stress that can initiate many diseases. While antioxidants reduce the level of oxidizing compounds in the medium, prooxidants promote the opposite process and have been used in therapies in particular those of cancer diseases. In this study, a series of azolyl lactones, were tested in human serum as a biological matrix and the obtained values of their oxy scores (*OS*) were compared. The antioxidative properties of these compounds were also tested under conditions of induced oxidative stress using an external prooxidant, *t*-butylhydroperoxide. The results showed that the sulphur analogue 4-azolyl coumarin **5** has the best antioxidant properties (*OS* –2.2), while the halogenated derivatives of pyrazolyl-coumarin **7** and **8** act as prooxidants, but successfully resist oxidative stress (*OS* 2.7 and 2.0, respectively). Related phthalides and isocoumarins showed prooxidative properties, but azolyl isocoumarins **10** and **11** show the strongest resistance to oxidative stress, reflected in their negative oxy score value (*OS* –2.1 and –1.1, respectively). The results demonstrated that combining two pharmacophores with known redox properties can produce potent compounds in both directions, with the antioxidative and the prooxidative characteristics.

Keywords: oxidative stress; antioxidant; prooxidant; biological matrix; coumarins; azoles.

INTRODUCTION

Oxidative processes are common reactions that are the part of various metabolic transformations in the body. Small quantities of reactive oxidative species, such as free radicals, have their role in the body and participate in the regulation

589

of certain biochemical processes, contributing in homeostasis maintenance.[1] Constitutive production of reactive oxygen species (ROS) is an inevitable phenomenon called physiological eustress.[2] However, if oxidative species are present in organism (tissues, cells) in a large amount and an imbalance occurs, oxidative stress can arise and cause organs' damage and thus many diseases such as cancer, diabetes, atherosclerosis and neurodegenerative processes.[3] Tumour cells proliferation takes place in high ROS environment, which is followed by antioxidants accumulation promoted by antioxidant transcription factors activation. Otherwise, critical ROS level will cause cancer cells' senescence and subsequently their death.[4] This tumour driven interplay between ROS and antioxidants, should be interrupted by cytostatic therapy, intended to increase cancer cells' ROS concentration. Ideal cytostatic should have high prooxidant activity with concomitant high selectivity for tumour cells in order to protect adjacent health tissue. This is a reason why the simultaneous use of antioxidants with cytostatic therapy should not be advised to patients, in order to preserve therapy potency. New cytostatic therapy design should rely on its prooxidant potency improvement and accompanied by new, sophisticated carriers to enable its cancer cells directed activity. Contrary to prooxidants, antioxidants promote the opposite process and can be used as prophylactic agents or as therapeutics that can reduce the side effects of anticancer drugs. Our previous study analysed several tyrosine kinase inhibitors with anticancer properties in order to reveal its redox activity, finding their clear prooxidant properties.[5]

Typical representatives of class of compounds with antioxidative properties are ascorbic acid and polyphenols. Compounds with the phenolic or stable enolic functionalities are capable of scavenging free radicals. A large number of various natural products are known as antioxidants, such as coumarins,[6–8] flavonoids,[9,10] phthalides,[11] stilbenes[12] and others. Antioxidative properties of vitamin E are also well known and have been extensively studied showing whole range of beneficial effects. Due to the importance of compounds with antioxidant properties, many synthetic compounds of these types have been produced and widely biologically profiled.[13,14] In this sense, coumarins are particularly interesting compounds as they can reduce the risk of diseases with high mortality rate such as cancer and cardiovascular diseases. This effect was attributed, at least in part, to their radical scavenging ability as the result of their antioxidative properties. Their appealing biological profile attracted much attention and this class of compounds was intensively studied in recent decades.[7,15–18]

Our involvement in this area encompassed the investigation of various azolyl derived coumarins and some structurally related lactones.[19] In our previous study, the coumarins possessing azole substituent at C-4 position showed anticancer properties against several tumour cell lines.[20] In continuation of that work we explored their antioxidative/prooxidative potential and the same properties of

related, structurally similar azolyl phthalides and azolyl isocoumarins in biological medium (serum pool of healthy subjects), and that work is outlined herein.

EXPERIMENTAL

Chemistry

Procedures for obtaining compounds **1**–**8**, **10**, **11**, **13** and **14** as well as their spectral characteristics, are described in our previous works.[19,20] Compounds **12** and **15** were synthesized according to literature procedures.[14,21] Commercially available 4-hydroxycoumarin (**9**) was purchased from Merck Schuchardt (Hohenbrunn, Germany).

Sample collection

Serum pool was formed by collecting samples from apparently healthy individuals, remaining after the every-day laboratory work. This study was created without using any patients' data.

The only samples included were of subjects whose basic biochemical parameters were within metabolite reference ranges, as a confirmation of subjects' good health. Serum pool's aliquots were frozen at −80 °C and used several months after the initial collection. Tested substances dissolved in dimethyl sulfoxide (DMSO, initial concentration 10 mmol/L), were mixed with serum pool aliquots (in 1:9 ratio in order to limit sample dilution at 10 %, because of bio-matrix preservation, thus final concentration for all tested substances were 1 mmol/L) and subjected to 2 h incubation at 37 °C. All analyses were performed in duplicate, alone or in combination with exogenously added prooxidant *tert*-butyl-hydroperoxide (TBH, conc. 0.25 mmol/L) in equi-volume ratio.

Evaluation of biochemical parameters

We performed four redox status parameters analyses, two of them were for prooxidants: total oxidative status (*TOS*) and prooxidant–antioxidant balance (*PAB*) and two of them were for antioxidants: total antioxidative status (*TAS*) and total sulfhydryl groups (SHG), by already published spectrophotometric methods.

Serum TOS presents a sum of lipid hydroperoxides and H_2O_2 concentrations and was determined using Erel's method and modified in our laboratory.[22,23] Oxidants from the sample oxidize the ferrous ion in *o*-dianisidine complex to ferric ion. The standard used for the assay calibration was water solution of hydrogen peroxide (2–200 μmol/L). Results are expressed as μmol H_2O_2 equivalent/L.

Serum PAB is a H_2O_2 concentration in an antioxidative environment and is measured according to a previously published method.[24] 3,3',5,5'-Tetramethylbenzidine (TMB) reacts with hydrogen peroxide and antioxidants like uric acid, simultaneously. Hydrogen peroxide and chromogen reaction is enzymatically catalysed with peroxidase, whereas the reaction of serum antioxidants and chromogen is non-enzymatic, *i.e.*, chemical reaction. Standard solutions were prepared by mixing varying proportions (0–100 %) of 1 mmol/L H_2O_2 with 6 mmol/L uric acid. The absorbance was measured at 450 nm. *PAB* values are expressed in arbitrary units, which correspond to the percentage of H_2O_2 in the standard solution. All measurement were performed using the micro-plate reader SPECTROstar Nano microplate reader (BMG Labtech, Ortenberg, Germany).

TAS is a parameter which represents the total concentration of all reductive substances in blood and was measured using 10 mmol/L 2,2'-azino-bis(3-ethylbenzothiazoline-6-sulphonic acid) (ABTS) as a chromogen. ABTS molecule is oxidized to $ABTS^{\bullet+}$ radical cation using hydrogen peroxide in acidic medium (an acetate buffer 30 mmol/L, pH 3.6). Under defined

conditions, emerald green ABTS[•+] molecules are stable for 6 months.[22-25] The antioxidants present in the sample cause the reagent discoloration to a degree proportional to their antioxidative potential. The reaction is calibrated with Trolox, a water-soluble vitamin E analog in the measurement range of 200–2000 μmol/L, the absorbance is measured at 660 nm, and the assay results are expressed in micromoles Trolox equivalent/L.

The levels of SHG were measured by Ellman's method modified by Kotur-Stevuljevic *et al.*, using 10 mM 5,5'-dithiobis(2-nitrodithiobenzoic acid) (DTNB) as a reagent.[23,26] DTNB reacts with aliphatic thiol compounds in a basic environment (pH 9.0) and this reaction generates equimolar quantities of mixed disulphide and 5-thio-2-nitrobenzoic acid (TNB) anion, which has absorbance maximum at 412 nm.[27,28] The method calibration was performed with the reduced glutathione as a standard, in the concentration range from 0.01–4.0 mM.

Prooxidative score, antioxidative score and oxy score

Oxy score (*OS*) is calculated as the difference between prooxidative score (average value of *Z* scores of all measured oxidants) and antioxidative score (average value of *Z* scores of all measured antioxidants). A larger oxy score means worse redox status (weaker antioxidative protection, higher prooxidants content). *Z* score is the difference between the original value and the control value divided by *SD* of control values (or population means and *SD*s).

Statistical analysis

Data are presented as median values (25th–75th percentile values). For the inter-groups comparison Kruskal–Wallis ANOVA and post-hoc Mann–Whitney U test were used. The *P* value below 0.05 was considered as statistically significant.

RESULTS AND DISCUSSION

A series of azolyl-coumarin derivatives including related isocoumarins and phthalides were previously synthesised an biologically profiled in various assays. As an extension of our interest in biological properties of these compounds, we further explored the antioxidative/prooxidative potential of these molecules as well. In fact, these compounds combine two pharmacophores, coumarin and diazole moieties, which are known to have redox properties individually, but their synergistic activity in this direction was not assessed.

As an addition, the redox properties of hydroxy analogues of coumarin, isocoumarin and phthalide were also tested due to their structure similarity to azolyl-coumarins.

The redox features of all these compounds in human serum as biological matrix were probed under conditions that mimic realistic physiological conditions. All structures are outlined in Fig. 1.

In order to determine the antioxidative and prooxidative properties of our compounds several parameters were measured as showed in Table I. The experiments were performed without (entries **a**–**o**, Table I) or with (entries **a′**–**o′**, Table I) the externally added *t*-butyl hydroperoxide in order to mimic conditions existing during pathological processes development.

The determined values for thePAB, TAS and SHG parameters were then used to calculate the prooxidative and antioxidative scores, as well as the oxy

scores, as the simple difference of the previous two factors (Table II). The calculation was performed for all compounds and experiments carried out without (entries **a**–**o**) and with the addition of TBH as exogenous prooxidant (entries **a′**––**o′**). Generally, a low value of the oxy score is associated with the pronounced antioxidant properties of tested compounds. The oxy scores with the addition of TBH indicate the ability of the system to resist the influence of exogenous prooxidant.
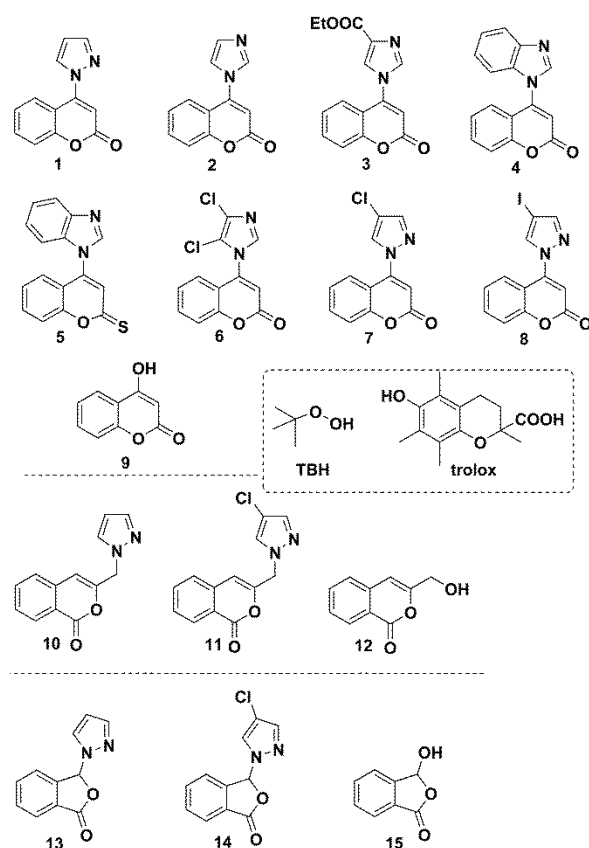
Fig 1. Structures of tested heterocycles, trolox and TBH.

TABLE I. Redox status parameters concentration in serum samples with tested compounds; data presented as medians and 25th–75th percentile values in brackets; entries **a**–**o**: samples without TBH; entries **a′**–**o′**: samples with TBH

Entry	Compound	PAB / U L^{-1}	TOS / µmol L^{-1}	TAS / µmol L^{-1}	SHG / µmol L^{-1}
–	Blank (0)	78.6	<2	920	0.209
		(77.9–79.2)		(878–963)	(0.207–0.210)
a	1	73.9	<2	930	0.212
		(73.7–74.1)		(903–958)	(0.206–0.219)

TABLE I. Continued

Entry	Compound	*PAB* / U L⁻¹	*TOS* / µmol L⁻¹	*TAS* / µmol L⁻¹	*SHG* / µmol L⁻¹
b	2	73.0 (72.3–73.7)	<2	1058 (990–1125)	0.176 (0.157–0.196)
c	3	74.8 (73.4–76.3)	<2	858 (690–1025)	0.180 (0.175–0.184)
d	4	73.5 (72.9–74.0)	<2	903 (858–948)	0.157 (0.146–0.167)
e	5	67.3 (66.7–68.0)	<2	980 (950–1010)	0.244 (0.242–0.246)
f	6	73.9 (72.3–75.4)	2.2 (2.1–2.3)	878 (850–905)	0.222 (0.216–0.228)
g	7	166.4 (165.9–166.9)	29.1 (28.1–30.1)	1160 (1088–1233)	0.315 (0.310–0.320)
h	8	159.3 (158.0–160.7)	8.5 (6.8–10.2)	1069 (1048–1090)	0.271 (0.267–0.275)
i	9	72.9 (71.9–73.8)	3.6 (3.3–4.0)	789 (683–895)	0.151 (0.125–0.177)
j	10	146.9 (146.3–147.5)	8.7 (8.5–8.8)	1247 (1233–1260)	0.313 (0.299–0.328)
k	11	150.7 (150.5–150.8)	10.9 (9.9–11.9)	1248 (1120–1375)	0.295 (0.290–0.300)
l	12	161.3 (157.4–165.1)	7.0 (5.6–8.4)	1174 (1138–1210)	0.274 (0.244–0.304)
m	13	159.8 (158.3–161.4)	12.7 (11.2–14.3)	1147 (940–1353)	0.304 (0.296–0.312)
n	14	151.8 (151.7–152.0)	16.0 (15.7–16.3)	1145 (1120–1170)	0.307 (0.290–0.325)
o	15	160.3 (160.2–160.4)	12.4 (12.0–12.9)	1109 (1078–1140)	0.279 (0.270–0.289)
a′	101	79.5 (78.8–80.3)	65.8 (65.7–65.9)	987 (815–1158)	0.121 (0.116–0.126)
b′	102	80.0 (79.7–80.2)	69.5 (68.8–70.1)	1062 (963–1160)	0.117 (0.110–0.125)
c′	103	78.8 (77.5–80.1)	57.1 (56.4–57.9)	1087 (846–1328)	0.116 (0.099–0.133)
d′	104	77.9 (77.5–78.2)	62.9 (61.2–64.6)	868 (838–898)	0.116 (0.115–0.117)
e′	105	74.2 (74.0–74.5)	65.4 (57.0–73.8)	978 (833–1123)	0.125 (0.116–0.133)
f′	106	79.8 (78.9–80.7)	69.6 (66.0–73.3)	1179 (1165–1193)	0.146 (0.106–0.187)
g′	107	109.2 (108.9–109.4)	43.3 (42.4–44.1)	998 (985–1010)	0.188 (0.181–0.196)
h′	108	108.7 (104.2–113.3)	38.5 (36.2–40.9)	1015 (993–1038)	0.182 (0.162–0.202)
i′	109	78.9 (77.9–79.9)	74.5 (70.5–78.4)	1064 (960–1168)	0.054 (0.020–0.087)

TABLE I. Continued

Entry	Compound	PAB / U L^{-1}	TOS / μmol L^{-1}	TAS / μmol L^{-1}	SHG / μmol L^{-1}
j′	110	104.6	28.4	1123	0.181
		(103.4–105.7)	(27.1–29.6)	(1030–1215)	(0.172–0.188)
k′	111	105.2	35.7	1108	0.175
		(105.1–105.4)	(33.7–37.7)	(1088–1128)	(0.167–0.183)
l′	112	107.5	35.6	1007	0.168
		(105.7–109.3)	(34.3–36.8)	(963–1050)	(0.158–0.178)
m′	113	175.4	39.7	1102	0.170
		(172.5–178.3)	(39.0–40.4)	(1050–1153)	(0.162–0.177)
n′	114	171.9	32.2	1053	0.177
		(170.8–173.1)	(31.7–32.7)	(1038–1068)	(0.168–0.186)
o′	115	173.7	35.6	1019	0.183
		(172.3–175.0)	(32.3–38.8)	(990–1048)	(0.175–0.190)
–	1000	81.4	126.4	873	0.046
	(TBH)	(80.1–82.6)	(123.6–129.2)	(843–903)	(0.014–0.078)
–	Trolox	119.0	6.5	784	0.247
		(118.0–120.0)	(5.9–7.1)	(750–818)	(0.203–0.291)

TABLE II. Calculated values of prooxy, antioxy and oxy score of azolyl lactones; data presented as medians and 25th–75th percentile values in brackets; entries **a–o**: samples without TBH; entries **a′–o′**: samples with TBH

Entry	Compound	Prooxy score	Antioxy score	Oxy score
–	Blank (0)	0.8	–0.7	1.5
		(0.40–1.3)	(–1.0–(–)0.3)	(1.4–1.6)
a	1	–0.4	–0.4	0.0
		(–0.5–(–) 0.3)	(–0.9–0.1)	(–0.4–0.4)
b	2	0.0	–1.4	1.4
		(–0.2–0.2)	(–2.8–0.0)	(0.2–2.7)
c	3	0.1	–2.5	2.6
		(–0.3–0.6)	(–3.8–(–)1.2)	(0.9–4.4)
d	4	0.1	–3.4	3.5
		(0.0–0.3)	(–4.1–(–)2.6)	(2.9–4.1)
e	5	–0.8	1.5	–2.2
		(–0.9–(–)0.6)	(1.4–1.6)	(–2.3–(–)2.2)
f	6	0.5	–0.3	0.7
		(0.4–0.5)	(–0.8–0.2)	(0.3–1.1)
g	7	31.4	2.1	29.3
		(31.1–31.8)	(1.2–2.9)	(28.1–30.6)
h	8	26.4	0.5	25.9
		(25.6–27.2)	(0.2–0.8)	(25.3–26.4)
i	9	0.8	–4.4	5.2
		(0.6–1.0)	(–6.4–(–)2.4)	(3.0–7.3)
j	10	19.7	3.1	16.6
		(19.4–20.0)	(2.8–3.4)	(16.0–17.2)
k	11	21.9	3.0	18.9
		(21.8–21.9)	(1.3–4.6)	(17.3–20.5)

TABLE II. Continued

Entry	Compound	Prooxy score	Antioxy score	Oxy score
l	12	27.3 (25.3–29.3)	1.9 (1.7–2.0)	25.5 (23.3–27.6)
m	13	26.9 (26.0–27.8)	1.8 (–0.8–4.4)	25.1 (23.4–26.8)
n	14	22.8 (22.7–22.9)	1.8 (1.7–2.0)	21.0 (20.8–21.2)
o	15	27.1 (27.1–27.2)	1.1 (0.6–1.6)	26.0 (25.5–26.6)
a′	101	12.8 (12.7–12.9)	–4.6 (–6.0–(–)3.3)	17.4 (15.9–18.8)
b′	102	13.5 (13.3–13.6)	–4.3 (–4.6–(–)4.1)	17.8 (17.4–18.2)
c′	103	11.1 (11.1–11.1)	–4.3(–6.6–(–)1.8)	15.4 (12.9–17.8)
d′	104	12.1 (17.8–12.4)	–5.6 (–5.8–(–)5.5)	17.7 (17.3–18.1)
e′	105	12.1 (10.6–13.6)	–4.5 (–5.0–(–)4.0)	16.6 (15.6–17.6)
f′	106	13.5 (12.7–14.2)	–2.1 (–4.1–(–)0.2	15.6 (14.4–16.8)
g′	107	1.6 (1.4–1.8)	–1.1 (–1.3–(–)0.9)	2.7 (2.6–2.8)
h′	108	1.1 (–1.2–3.4)	–0.9 (–1.4–(–)0.5)	2.0 (–0.7–4.8)
i′	109	14.3 (13.6–14.9)	–7.5 (–9.8–(–)5.2)	21.8 (18.8–24.7)
j′	110	–1.7 (–2.3–(–)1.2)	0.4 (–0.8–1.5)	–2.1 (–2.8–(–)1.5)
k′	111	–0.9 (–1.0–(–)0.9)	0.1 (0.0–0.3)	–1.1 (–1.3–(–)0.9)
l′	112	0.3 (–0.8–1.3)	–1.2 (–1.6–(–)0.7)	1.4 (–0.1–2.9)
m′	113	36.9 (35.3–38.5)	0.0 (–0.7–0.7)	36.9 (36.0–37.8)
n′	114	34.6 (34.0–35.2)	–0.5 (–0.8–(–)0.3)	35.1 (34.8–35.4)
o′	115	35.7 (35.2–36.2)	–0.9 (–1.2–(–)0.6)	36.6 (35.8–37.4)
–	1000 (TBH)	23.9 (23.6–24.3)	–9.1 (–10.5–(–)7.7)	33.0 (31.2–34.8)
–	Trolox	–11.7 (–12.0–(–) 11.5)	1.7 (0.8–2.6)	–12.7 (–13.2–(–)12.2)

The lowest value of oxy score (*OS*) in experiments performed without TBH was shown by derivative **5** (*OS* –2.2, entry **e**, Table II), which is the only one

with a thionoester group in the lacton ring. This is not surprising, bearing in mind the fact that thiocarbonyl compounds are known as good radical scavengers.[29–31] Additional unambiguous proof for the essential role of the thiono group is the antioxidative potential for compound **4**, the derivative with oxygen in place of sulphur, showing weaker antioxidative properties (*OS* 3.5, entry **d**, Table II). Further structure–activity relationship (SAR) analysis demonstrated some additional facts. The compound **2** possessing simple imidazole substituent showed better antioxidative properties (*OS* 1.4, entry **b**, Table II) than the benzimidazol derivative **4**. This might suggest that imidazole moiety directly contributes to the antioxidative properties and that this effect is hampered by the benzene ring in case of **4**. Going further along this line, the derivatives with chlorine **6** and carbethoxy group **3** compared with the parent **2** demonstrated different results. While the chloro derivative **6** showed slightly better antioxidative properties the ester derived compound **3** demonstrated worse profile, but in both cases the effect is relatively small (*OS* 2.6 and 0.7, entries **c** and **f**, respectively, Table II). It is known that amino acid histidine, which contains imidazole ring has antioxidative properties with the position C-2 prone to the oxidative transformation.[32] 2-Oxo histidine occurs in peptides as a product of its oxidation. Since this position in all our imidazole derived compounds is unsubstituted, it may contribute to the overall antioxidative feature of these derivatives. It was also interesting to compare the effect of pyrazole ring in place of imidazole. The compound **1** has simple pyrazole substituent and its oxy score is close to 0 (entry **a**, Table II), placing it in front of the complementary imidazole derivatives. It is also the most potent compound after the tiono derivative **5**. The preferred oxidative metabolic transformation of pyrazole leads to the formation of 4-hydroxy derivatives.[33] This could provide an explanation for the antioxidative properties of **1**, in particular when compared with the corresponding compounds **7** and **8** which demonstrated significantly lower antioxidative potential (entries **g** and **h**, Table II). Actually, these two compounds have prooxidative properties. It is noticeable that the influence of halogenated azole ring on antioxidative properties is more pronounced in the case of pyrazoles than in imidazoles. A possible explanation is that the halogen-occupied position C-4 in the compounds **7** and **8** cannot be oxidized as in the unsubstituted derivative **1** while in the case of compound **6**, as mentioned above, the unsubstituted position C-2 might be a key structural feature for the antioxidative character. In our previous study the compound **7** showed antiproliferative activity against tumor cell line K562 ($IC_{50} \approx 3.06$ μmol).[20]

In order to determinate the significance of the azole attached to the coumarin, the antioxidative properties of 4-hydroxycoumarin (**9**) in human serum were also examined.[34,35] Under our experimental conditions, it shows weaker antioxidant properties than most azolyl coumarins, but still doesn't have a high oxy score (*OS* 5.2, entry **i**, Table II).

The oxy score was also determined in the presence of *t*-butyl hydroperoxide indicating potential of the compounds to resist to oxidative stress. It is interesting that the two coumarin derivatives with initial prooxidative properties (**7** and **8**) in the presence of TBH become antioxidants and their *OS* value becomes about ten times lower (2.7 and 2.0, entries **g'** and **h'**, Table II). This result could be attributed to the potential formation of an oxidized form of pyrazoles due to the action of strong exogenous prooxidants.[32] Namely, that would lead to the formation of hydroxypyrazoles, or some of their tautomeric forms, which are known to be strong radical scavengers.[36,37] Other coumarin derivatives in the presence of TBH lose their antioxidative properties and values of their oxy score increases.

The next small class of tested compounds have isocoumarin core linked to azole via a methylene group at C(3), as well as isocoumaryl alcohol itself. The isocoumarin derivatives with pyrazole (**10**) and chloropyrazole ring (**11**) don't show antioxidant properties, however they act as prooxidants (*OS* 19.7 and 21.9, entries **j** and **k**, Table II). The key difference compared to the above compounds is the presence of the benzylic C–H moiety which might be involved in the formation of radical intermediates. An interesting phenomenon which was observed with the coumarins **7** and **8**, also occurs here: in the presence of TBH, oxy score of azolyl-isocoumarins decreases even to a negative value (*OS* –2.1 and –1.1, entries **j'** and **k'**, Table II). This means that their role changes in the presence of exogenous prooxidants. Similar to them, isocoumaril alcohol shows better antioxidative properties with TBH, but its value of *OS* is positive. Based on these results, it can be concluded that azole ring has some influence on the antioxidative properties of that class of compounds.

As a part of overall SAR studies the phthalide derivatives, **13** and **14**, with an azolyl group as well as the hydroxyphthalide **15** were also investigated. All three phthalide derivatives are prooxidants, without and in the presence of TBH.

Oxy scores for all compounds are also outlined in Fig. S-7 of the Supplementary material to this paper which summaries the results from both experiments (without and with TBH) after 2 h incubation at 37 °C in comparison with trolox used as standard.

CONCLUSION

Our study of the substituted coumarines and the related isocoumarins and phthalides demonstrated the beneficial effect of azolyl substituents on antioxidative/prooxidative balance of these compounds. While in the case of azol-substituted coumarins majority of compounds, but not all, showed reasonable antioxidative properties, the effect of heterocyclic substituent was opposite in the case of isocoumarins and phthalides displaying prooxidative characteristics. Although some general trends can be recognised by analysing the current results,

further study would be necessary to understand the substituent effect on the anti-oxidative/prooxidative balance in detail, which is now underway.

SUPPLEMENTARY MATERIAL

Additional data and information are available electronically at the pages of journal website: https://www.shd-pub.org.rs/index.php/JSCS/article/view/12184, or from the corresponding author on request.

И З В О Д

IN VITRO СТУДИЈА РЕДОКС ОСОБИНА АЗОЛИЛ-ЛАКТОНА У ХУМАНОМ СЕРУМУ

МИЛЕНА Р. СИМИЋ[1], ЈЕЛЕНА М. КОТУР-СТЕВУЉЕВИЋ[2], ПРЕДРАГ М. ЈОВАНОВИЋ[1], МИЛОШ Р. ПЕТКОВИЋ[1], МИЛОШ Д. ЈОВАНОВИЋ[1], ГОРДАНА Д. ТАСИЋ[1] и ВЛАДИМИР М. САВИЋ[1]

[1]*Универзитет у Београду-Фармацеутски факултет, Катедра за органску хемију, Војводе Степе 450, 11221 Београд и* [2]*Универзитет у Београду-Фармацеутски факултет, Катедра за медицинску биохемију, Војводе Степе 450, 11221 Београд*

Поремећај редокс баланса у организму може узроковати оксидативни стрес, који је окидач за настанак многих болести. Антиоксиданси снижавају ниво оксидујућих једи-њења у медијуму у коме се налазе, док прооксиданси делују супротно и као такви могу наћи примену у терапији канцера. У овом истраживању, испитиване су антиоксидативне и прооксидативне особине серије азолил-лактона у хуманом серуму као биолошком матриксу. Антиоксидативне особине су представљене помоћу окси скорова (*OS*), а испи-тивано је и понашање ових једињења у условима индукованог оксидативног стреса нас-талог додатком *терц*-бутил-хидропероксида као спољног прооксиданса. Резултати су показали да сумпорни дериват, 4-бензимидазолил кумарин **5** има најизраженије анти-оксидативне особине (*OS* −2,2), док халогеновани деривати пиразолил-кумарина **7** и **8** реагују као прооксиданси (*OS* 2,7 и 2,0). Утицају додатог прооксиданса се најбоље опиру једињења **7** и **8**. Испитивани деривати изокумарина и фталида такође показују проокси-дативне особине, док се оксидативном стресу најбоље опиру азолил-изокумарини (*OS* < 0).

(Примљено 21. децембра 2022, ревидирано 12. фебруара, прихваћено 23. марта 2023)

REFERENCES

1. C. H. Foyer, G. Noctor, *The Plant Cell* **17** (2005) 1866 (https://doi.org/10.1105/tpc.105.033589)
2. H. Sies, *Antioxidants* **9** (2020) 852 (https://doi.org/10.3390/antiox9090852)
3. I. Liguori, G. Russo, F. Curcio, G. Bulli, L. Aran, D. Della-Morte, G. Gargiulo, G. Testa, F. Cacciatore, D. Bonaduce, P. Abete, *Clin. Interv. Aging* **13** (2018) 757 (https://doi.org/10.2147/CIA.S158513)
4. J. D. Hayes, A. T. Dinkova-Kostova, K. D. Tew, *Cancer Cell* **38** (2020) 167 (https://doi.org/10.1016/j.ccell.2020.06.001)
5. M. Mihajlovic, B. Ivkovic, B. Jancic-Stojanovic, A. Zeljkovic, V. Spasojevic--Kalimanovska, J. Kotur-Stevuljevic, D. Vujanovic, *Anticancer Drugs* **31** (2020) 942 (https://doi.org/10.1097/cad.0000000000000924)

6. I. Kostova, S. Bhatia, P. Grigorov, S. Balkansky, V. S. Parmar, A. K. Prasad, L. Saso, *Curr. Med. Chem.* **18** (2011) 3929 (https://doi.org/10.2174/092986711803414395)

7. Z. Rehakova, V. Koleckar, L. Jahodar, L. Opletal, K. Macakova, L. Cahlikova, D. Jun, K. Kuca, *J. Enzyme Inhib. Med. Chem.* **29** (2014) 49 (https://doi.org/10.3109/14756366.2012.753589)

8. G. B. Bubols, D. da R. Vianna, A. Medina-Remon, G. von Poser, R. M. Lamuela-Raventos, V. L. Eifler-Lima, S. C. Garcia, *Mini Rev. Med. Chem.* **13** (2013) 318 (https://doi.org/10.2174/138955713804999775)

9. D. Procházková, I. Boušová, N. Wilhelmová, *Fitoterapia* **82** (2011) 513 (https://doi.org/10.1016/j.fitote.2011.01.018)

10. M. Sökmen, M. Akram Khan, *Inflammopharmacol* **24** (2016) 81 (https://doi.org/10.1007/s10787-016-0264-5)

11. K. Tianpanich, S. Prachya, S. Wiyakrutta, C. Mahidol, S. Ruchirawat, P. Kittakoop, *J. Nat Prod* **74** (2011) 79 (https://doi.org/10.1021/np1003752)

12. M. Frombaum, S. Le Clanche, D. Bonnefont-Rousselot, D. Borderie, *Biochimie* **94** (2012) 269 (https://doi.org/10.1021/np1003752)

13. T. Janković, N. Turković, J. Kotur-Stevuljević, Z. Vujić, B. Ivković, *Chem. Biol. Interact.* **324** (2020) 109084 (https://doi.org/10.1016/j.cbi.2020.109084)

14. X. Qiang, Y. Li, X. Yang, L. Luo, R. Xu, Y. Zheng, Z. Cao, Z. Tan, Y. Deng, *Bioorganic & Med Chem Lett* **27** (2017) 718 (https://doi.org/10.1016/j.bmcl.2017.01.050)

15. W. S. Hamama, M. A. Berghot, E. A. Baz, M. A. Gouda, *Arch. Pharm.* **344** (2011) 710 (https://doi.org/10.1002/ardp.201000263)

16. A. A. Al-Amiery, Y. K. Al-Majedy, A. A. H. Kadhum, A. B. Mohamad, *PLOS ONE* **10** (2015) e0132175 (https://doi.org/10.1371/journal.pone.0132175)

17. E. Y. Ahmed, O. M. Abdelhafez, D. Zaafar, A. M. Serry, Y. H. Ahmed, R. F. A. El-Telbany, Z. Y. Abd Elmageed, H. I. Ali, *Arch. Pharm.* **355** (2022) 2100327 (https://doi.org/10.1002/ardp.202100327)

18. I. A. M. Radini, D. A. Ibrahim, R. E. Khidre, *Acta Pol. Pharm.* **79** (2019) 453 (https://doi.org/10.32383/appdr/102651)

19. M. R. Simić, S. Erić, I. Borić, A. Lubelska, G. Latacz, K. Kiec-Kononowicz, S. Vojnović, J. Nikodinović-Runić, V. M. Savić, *J. Serb. Chem. Soc.* **86** (2021) 639 (https://doi.org/10.2298/JSC201201025S)

20. M. Simic, M. Petkovic, P. Jovanovic, M. Jovanovic, G. Tasic, I. Besu, Z. Zizak, I. Aleksic, J. Nikodinovic-Runic, V. Savic, *Arch. Pharm.* **354** (2021) 2100238 (https://doi.org/10.1002/ardp.202100238)

21. K. G. Guimarães, R. P. de Freitas, A. L. T. G. Ruiz, G. F. Fiorito, J. E. de Carvalho, E. F. F. da Cunha, T. C. Ramalho, R. B. Alves, *Eur. J. Med. Chem.* **111** (2016) 103 (https://www.sciencedirect.com/science/article/pii/S0223523416300599)

22. O. Erel, *Clin. Biochem.* **38** (2005) 1103 (https://doi.org/10.1016/j.clinbiochem.2005.08.008)

23. J. Kotur-Stevuljevic, N. Bogavac-Stanojevic, Z. Jelic-Ivanovic, A. Stefanovic, T. Gojkovic, J. Joksic, M. Sopic, B. Gulan, J. Janac, S. Milosevic, *Atherosclerosis* **241** (2015) 192 (https://doi.org/10.1016/j.atherosclerosis.2015.05.016)

24. O. Erel, *Clin. Biochem.* **37** (2004) 277 (https://doi.org/10.1016/j.clinbiochem.2003.11.015)

25. D. H. Alamdari, K. Paletas, T. Pegiou, M. Sarigianni, C. Befani, G. Koliakos, *Clin. Biochem.* **40** (2007) 248 (https://doi.org/10.1016/j.clinbiochem.2006.10.017)

26. G. L. Ellman, *Arch. Biochem. Biophys.* **82** (1959) 70 (https://doi.org/10.1016/0003-9861(59)90090-6)
27. E. Taylan, H. Resmi, *Turkish J. Biochem.* **35** (2010) 275 (https://web.citius.technology/upload/turkjbiochem/2010/275-278.pdf)
28. C. K.Riener, G. Kada, H.J. Gruber, *Anal. Bioanal. Chem,* **373** (2002) 266 (https://doi.org/10.1007/s00216-002-1347-2)
29. D. Crich, L. Quintero, *Chem. Rev.* **89** (1989) 1413 (https://doi.org/10.1021/cr00097a001)
30. N. Ivanović, L. Jovanović, Z. Marković, V. Marković, M. D. Joksović, D. Milenković, P. T. Djurdjević, A. Ćirić, L. Joksović, *ChemistrySelect* **1** (2016) 3870 (https://doi.org/10.1002/slct.201600738)
31. F. Denés, M. Pichowicz, G. Povie, P. Renaud, *Chem. Rev.* **114** (2014) 2587 (https://doi.org/10.1021/cr400441m)
32. Q. Cai, G. Takemura, M. Ashraf, *J. Cardiovasc. Pharmacol.* **25** (1995) 147 (https://doi.org/10.1097/00005344-199501000-00023)
33. S. Puntarulo, A. I. Cederbaum, *Arch. Biochem. Biophys.* **255** (1987) 217 (https://doi.org/10.1016/0003-9861(87)90388-2)
34. L. F. da Cruz, C. G. Santos, T. P. R. Gonçalves, G. D. Marena, I. L. A. Souza, L. A. R. dos S. Lima, F. M. D. Chequer, F. C. H. Pinto, F. A. R. Nogueira, M. G. de F. Araujo, *Res. Soc. Dev.* **10** (2021) e7910816948 (https://doi.org/10.33448/rsd-v10i8.16948)
35. E. H. Avdović, I. P. Petrović, M. J. Stevanović, L. Saso, J. M. Dimitrić Marković, N. D. Filipović, M. Ž. Živić, T. N. Cvetić Antić, M. V. Žižić, N. V. Todorović, M. Vukić, S. R. Trifunović, Z. S. Marković, *Oxid. Med. Cell. Longev.* **2021** (2021) e8849568 (https://doi.org/10.1155/2023/9979397)
36. M. Tanaka, S. Motomiya, A. Fujisawa, Y. Yamamoto, *J. Clin. Biochem. Nutr.* **61** (2017) 164 (https://doi.org/10.3164/jcbn.17-75)
37. L. A. Clejan, A. I. Cederbaum, *Biochim. Biophys. Acta Gen. Subj.* **1034** (1990) 233 (https://doi.org/10.1016/0304-4165(90)90082-8).

In vitro study of redox properties of azolyl-lactones in human serum

MILENA R. SIMIĆ[1]*, JELENA M. KOTUR-STEVULJEVIĆ[2]**, PREDRAG M. JOVANOVIĆ[1], MILOŠ R. PETKOVIĆ[1], MILOŠ D. JOVANOVIĆ[1], GORDANA D. TASIĆ[1] and VLADIMIR M. SAVIC[1]

[1]*University of Belgrade-Faculty of Pharmacy, Department of Organic Chemistry, Vojvode Stepe 450, 11221 Belgrade, Serbia and* [2]*University of Belgrade-Faculty of Pharmacy, Department of Medical Biochemistry, Vojvode Stepe 450, 11221 Belgrade, Serbia*

PROOXIDATIVE-ANTIOXIDATIVE BALANCE (PAB)
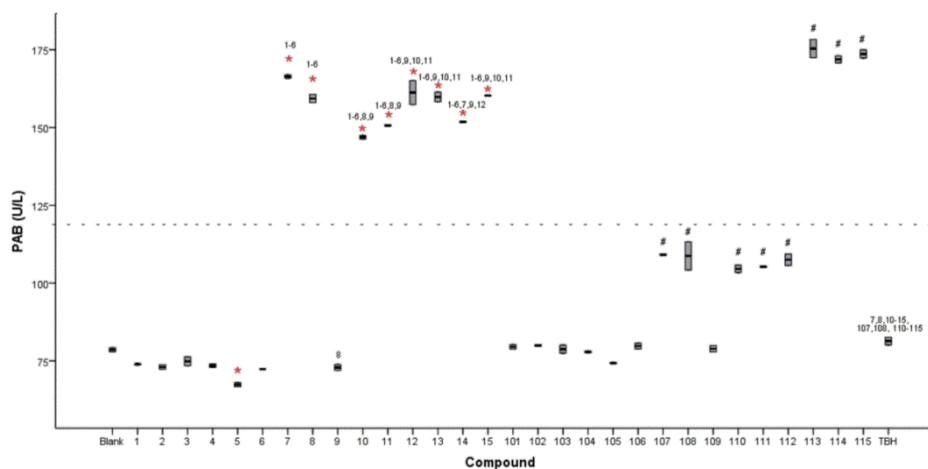
Figure S-1. PAB concentration (U/L) in compounds (1-15) and its combination with TBH (101-115) after 2h incubation in human serum pool (37° C). * $p < 0.05$ vs. blank sample (serum pool); # $p < 0.05$ compound + TBH in human serum pool vs. the same compound in human serum pool without TBH. TBH is a sample of TBH in human serum pool. Numbers above the boxes mean $p < 0.05$ vs. compound signed with the distinct number - - - median PAB value for human serum pool sample with Trolox.

* Corresponding authors. E-mail: milena@pharmacy.bg.ac.rs; jelena.kotur@pharmacy.bg.ac.rs

TOTAL OXIDATIVE STATUS (TOS)
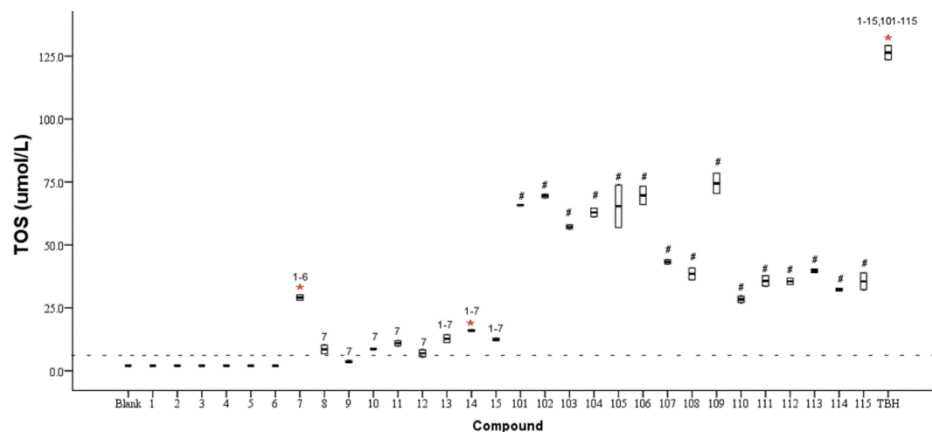
Figure S-2. TOS concentration (µmol/L) in compounds (1-15) and its combination with TBH (101-115) after 2h incubation in human serum pool (37° C). *p<0.05 vs. blank sample (serum pool); # p<0.05 compound + TBH in human serum pool vs. the same compound in human serum pool without TBH. TBH is a sample of TBH in human serum pool. Numbers above the boxes mean p<0.05 vs. compound signed with the distinct number - - - median TOS value for human serum pool sample with Trolox.

TOTAL ANTIOXIDATIVE STATUS (TAS)
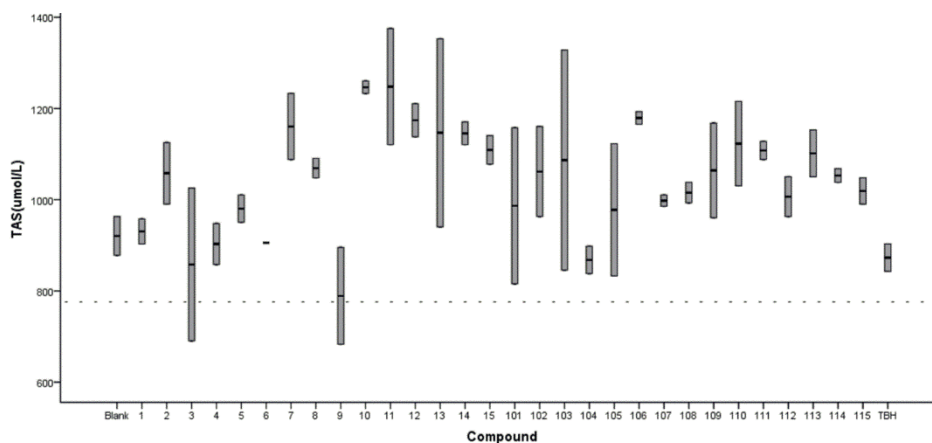
Figure S-3. TAS concentration (µmol/L) in compounds (1-15) and its combination with TBH (101-115) after 2h incubation in human serum pool (37° C). All differences in TAS concentration between different compounds were statistically non-significant. TBH is a sample of TBH in human serum pool. Numbers above the boxes mean p<0.05 vs. compound signed with the distinct number - - - median TAS value for human serum pool sample with Trolox.

TOTAL SULFHYDRYL GROUP (SHG)
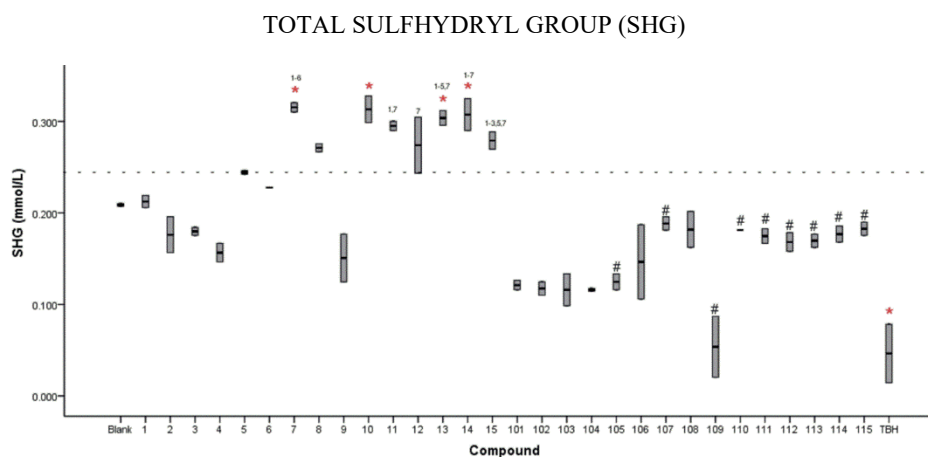
Figure S-4. Total SH groups concentration (mmol/L) in compounds (1-15) and its combination with TBH (101-115) after 2h incubation in human serum pool (37° C). *p<0.05 vs. blank sample (serum pool); # p<0.05 compound + TBH in human serum pool vs. the same compound in human serum pool without TBH. TBH is a sample of TBH in human serum pool. Numbers above the boxes mean p<0.05 vs. compound signed with the distinct number - - - - - median SHG value for human serum pool sample with Trolox.

PROOXIDATIVE SCORE
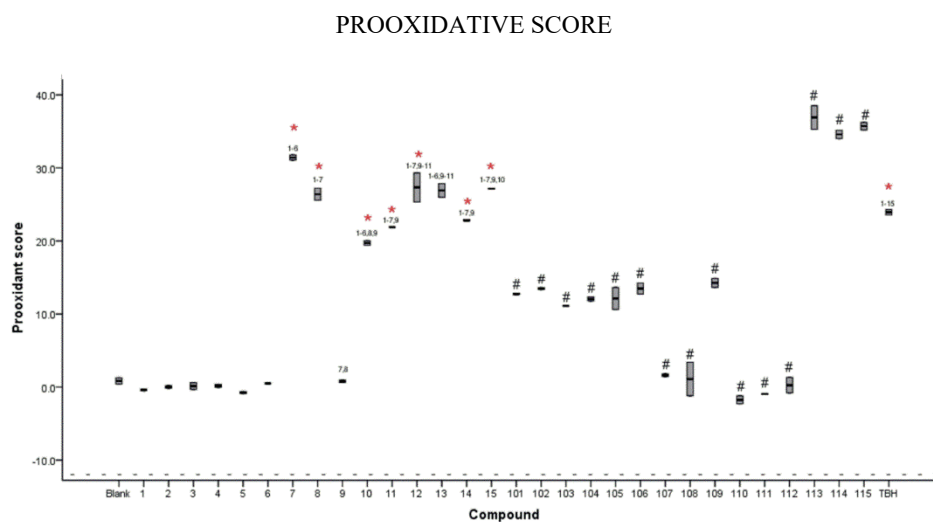
Figure S-5. Prooxidant score value in compounds (1-15) and its combination with TBH (101-115) after 2h incubation in human serum pool (37° C). *p<0.05 vs. blank sample (serum pool); # p<0.05 compound + TBH in human serum pool vs. the same compound in human serum pool without TBH. TBH is a sample of TBH in human serum pool. Numbers above the boxes mean p<0.05 vs. compound signed with the distinct number - - - median Prooxidant score value in serum sample with Trolox.

ANTIOXIDANT SCORE
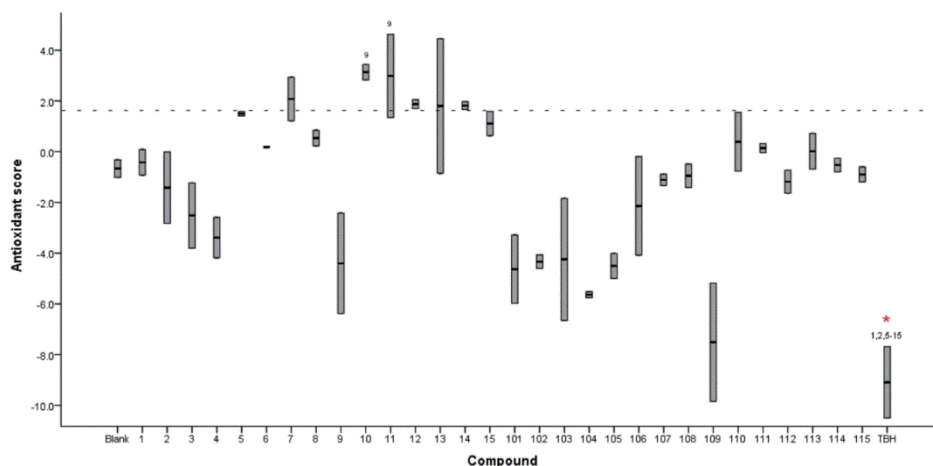
Figure S-6. Antioxidant score value in compounds (1-15) and its combination with TBH (101-115) after 2h incubation in human serum pool (37° C). *p<0.05 vs. blank sample (serum pool); # p<0.05 compound + TBH in human serum pool vs. the same compound in human serum pool without TBH. TBH is a sample of TBH in human serum pool. Numbers above the boxes mean p<0.05 vs. compound signed with the distinct number - - - median Antioxidant score value in serum sample with Trolox.
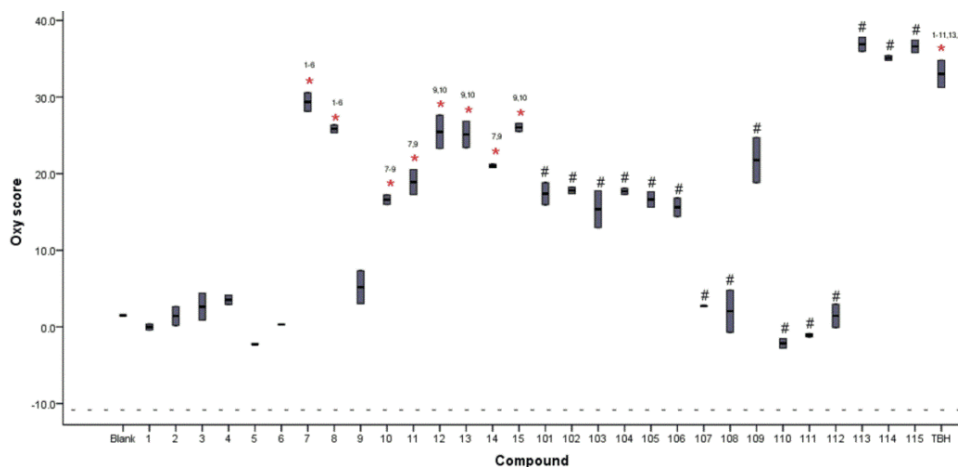
Figure S-7. Oxy score value in compounds **1**–**15** and its combination with TBH (**101**–**115**). *$p < 0.05$ *vs.* blank sample (serum pool); # $p < 0.05$ compound + TBH in human serum pool *vs.* the same compound in human serum pool without TBH. TBH is a sample of TBH in human serum pool. Numbers above the boxes mean $p < 0.05$ *vs.* compound signed with the distinct number; ---- median Oxy score value for human serum pool sample with Trolox.

Chemical characterization and antimicrobial activity of *Juglans nigra* L. nut and green husk

KATARINA M. RAJKOVIĆ[1]*, MILICA DROBAC[2], PETAR MILIĆ[3], VESNA VUČIĆ[4], ALEKSANDRA ARSIĆ[4], MIRIJANA PERIĆ[5], MILENA RADUNOVIĆ[6], SANJA JEREMIĆ[7] and JELENA ARSENIJEVIĆ[2]

[1]*Technical and technological department, The Academy of Applied Preschool Teaching and Health Studies, Kruševac, Serbia,* [2]*Department of Pharmacognosy, University of Belgrade-Faculty of Pharmacy, Serbia,* [3]*Department of Ćuprija Academy of Educational and Medical Vocational Studies, Serbia,* [4]*Group for Nutritional Biochemistry and Dietology, Institute for Medical Research, University of Belgrade, Serbia,* [5]*Department of Prosthodontics, Faculty of Dental Medicine, University of Belgrade, Serbia,* [6]*Department of Microbiology, Faculty of Dental Medicine, University of Belgrade, Serbia, and* [7]*Institute of Molecular Genetics and Genetic Engineering, University of Belgrade, Serbia*

Abstract: *Juglans nigra* (Black walnut) is a source of health-supporting biologically active compounds used in traditional medicine. The investigation of bioactive compounds in black walnut could lead to its broader application, as well as to the application of its by-products. Therefore, this study aimed to characterize *J. nigra* nut and green husk based on chemical analysis of their petroleum ether and ethanol extracts obtained by ultrasonic and reflux extraction methods, respectively. Different extract fractions were tested for their antimicrobial activities using Gram-negative bacteria (*Escherichia coli*, *Pseudomonas aeruginosa*), Gram-positive bacteria (*Enterococcus faecalis*, *Staphylococcus aureus*) and yeast (reference strain and clinical isolates of *Candida albicans*). The ethanol extracts analysis, performed by high performance liquid chromatography, singled out the ellagic acid as the most dominant compound in nut (($55.0\pm1.3)\times10^{-3}$ kg m^{-3}) and green husk (($114.1\pm0.5)\times10^{-3}$ kg m^{-3}) extracts. Non-polar compounds were evaluated using gas chromatography analysis of petroleum ether extracts. *Juglans nigra* nut and green husk contained two saturated fatty acids, palmitic acid (C16:0) and stearic acid (C18:0), then, monounsaturated fatty acids, palmitoleic (C16:1n-7), oleic (C18:1n-9) and vaccenic acid (C18:1n-7), as well as polyunsaturated fatty acids, linoleic (C18:2n-6), *γ*-linolenic (C18:3n-6) and *α*-linolenic (C18:3n-3) acids. Ethanol extracts of both *J. nigra* nut and green husk showed antimicrobial activity against *C. albicans*, which is the most common cause of yeast infections.

603

INTRODUCTION

Juglans nigra L. (Black walnut) is a deciduous tree whose different parts contain a variety of useful chemical compounds with numerous health benefits.[1–3] The walnut fruit consists of a husk, a hard shell, and kernel. The kernel is eaten raw or roasted, or pressed for oil and contains unsaturated fatty acids and toco-pherols that may have beneficial effect on cardiovascular disease risks.[4] The shells are used in a variety of applications ranging from abrasives, fillers, thick-eners, and dyes,[5] while the husk is commonly discarded although it contains phenolic compounds that exhibit antioxidant and antimicrobial properties.[4]

The majority of chemical research was focused on the *J. nigra* nuts, which represent a rich source of natural compounds proven to have various medicinal properties.[1,6–8] *J. nigra* nuts are of great biological importance, since they are an excellent source of phytochemical antioxidants, such as a complex mixture of phenolic compounds (phenolic acids, flavonoids and catechins).[3,7,9,10] Nuts of *J. nigra* are not only rich in phenolics, but also contain high levels of phytosterols, unsaturated fatty acids and tocopherols in fatty oil.[10] It is known that the fatty oil from all nuts species is an important parameter in assessing the quality of nuts and responsible for beneficial health effect as well.[6] The fatty acid profile of *J. nigra* kernel consist of unsaturated forms, whereas saturated forms are present in small quantities.[10] Among the unsaturated fatty acids, oleic, linoleic, and *α*-lino-lenic acids were found in *J. nigra* nuts.[6,10] In addition, *J. nigra* nuts are not only rich in mineral content.[6,11]

Regarding walnut husk, there have been a few studies involving the detailed characterization of phenolic compounds originating from the green husk of com-mon walnut (*J. regia*).[12–14] Generally, the green husk of common walnut is usu-ally discarded in processing, though it contains phenolic compounds that exhibit antioxidant and antimicrobial properties.[13–15] Cosmulescu *et al.*,[12] suggested that the green husk of common walnut as a by-product, is a good raw material for the extraction of phenolics. However, despite a diverse phytochemical composition of *J. regia* green husk,[12–14] there is no detailed chemical analysis of *J. nigra* green husk, except for the study of total phenolics content.[4]

The investigation of bioactive compounds in black walnut could lead to its broader application, as well as its by-products. To date, there is no study that sys-tematically characterizes and compares the chemical profiles between *J. nigra* nut and green husk. Accordingly, the aim of this research was to determine chemical composition and antimicrobial activity of *J. nigra* nut and green husk. The chemical analysis included high performance liquid chromatography (HPLC) and gas chromatography (GC).

EXPERIMENTAL

Plant material

Juglans nigra fruits (nuts with green husks) were collected during September 2021 from one location at Aleksinac in southeast region of Serbia (located at 43º 32′ 11″N/, 21º 42′ 11″E). There was not a significant variation among the provenances in number of fruits and fruit weight of different trees from plot. The voucher specimen was deposited at the Herbarium of the Department of Botany, University of Belgrade-Faculty of Pharmacy (HFF), under the number 3906HFF. The fruits were air dried for two weeks at the average temperature of 20 °C in a room with cross ventilation and out of direct sunlight. The green husks were manually removed from the nuts. It was not possible to separate the kernel from the shell, so the whole nut was ground. The nuts and green husks were ground thus obtaining the material particles of average size of 0.75 mm which were stored in a container at −18 °C until use. The extracts of nuts and green husks were made three weeks after collecting the fruits and stored in a container at −18 °C until the use for different analysis (10–20 days).

Extraction process

The 8×10^{-2} kg of powdered nut and green husk of *J. nigra* were extracted with 8×10^{-2} kg of petroleum ether (solvent-to-solid mass ratio 1:1) by indirect ultrasonication using ultrasonic thermostatic bath (Sonic, Niš, Serbia, power 120 W, frequency 40 kHz). Ultrasonic assisted extraction was performed during 80 min at 40 °C, and the obtained suspensions were vacuum filtered. The resulting liquid residues were labeled as the petroleum ether extracts. Each extractives modality was repeated twice.

The 5×10^{-2} kg defatted material of nut and green husk, remaining after the extraction with petroleum ether, was re-extracted with 0.20 dm^3 of 70 % ethanol for 4 h under reflux, at solvent-to-solid mass ratio of 4:1 and at boiling point of the solvent. After the filtration, the resulting liquid residues were labelled as the ethanol extracts. Each extractives modality was repeated twice.

HPLC analysis

The ethanol extracts of nut and green husk were dried under vacuum, dissolved in 70 % ethanol (5 mg cm^{-3}), filtered through 0.45×10^{-6} m filters and analyzed by HPLC using an Agilent LC 1260 system (Agilent Technologies, Waldbronn, Germany) with photodiode-array detector (PDA). Instrumental conditions were as follows: reversed-phase analytical column (Zorbax SB-aq column, 150 m$\times2.1\times10^{-3}$ m with 3.5×10^{-6} m particle size), 0.35×10^{-6} m^3 min^{-1} flow rate, 25 °C temperature, 2×10^{-9} m^3 injection volume. Solvent A, 0.1% formic acid in water , and solvent B, acetonitrile, were used for gradient elution: initial 10 % of B, rising to 30 % in 35 min, 35–45 min rising to 70 % of B and returning to initial conditions till 55 min. The wavelengths on which chromatograms were recorded were 210, 250, 320 and 350 nm. Qualitative analysis was performed by comparing the UV spectrum and the retention time of the detected component with those obtained for ellagic acid (Sigma–Aldrich). For the quantification of ellagic acid external standard method was used, with standard of ellagic acid at 250 nm ($y = 54x–209$, $R^2 = 0.9993$, working concentration range 17×10^{-3}–150×10^{-3} kg m^{-3}; *LoD* 6.3×10^{-3} kg m^{-3}, *LoQ* 19×10^{-3} kg m^{-3}, calculated according to ICH using residual standard deviation of calibration curve). HPLC analyses was performed in duplicate for each extractives modality.

GC analysis

The fatty acids composition of petroleum ether extracts of nut and green husk was determined using the method by Glaser *et al.*, with few modifications.[16] Briefly, in 100×10^{-9} m^3 of petroleum ether extracts 1.5×10^{-6} cm^3 of 3 M HCl in methanol was added and heated for 60 min at 85 °C. After cooling to room temperature, 1.5×10^{-6} m^3 of hexane was added and centrifuged for 15 min at 3000 rpm. The hexane layer was evaporated to dryness and stored in the freezer until analysis. Fatty acid methyl esters were analyzed by gas chromatography using a Shimadzu gas chromatograph with a flame ionization detector (model 2014) equipped with an Rtx 2330 column (60 m, 0.25×10^{-3} m inside diameter, film thickness 0.25×10^{-6} m, Restek, USA). Helium was used as the carrier gas with a flow rate of 1 mL/min. The temperature of the injector was 220 °C, of detector 260 °C, while the initial oven temperature of 130 °C was held for 10 min and then programmed to increase 3 °C min^{-1} to a final oven temperature of 220 °C. The individual fatty acids were identified using fatty acids standard mixtures PUFA-2 and Supelco 37 Component FAME Mix (Sigma–Aldrich). The results for individual fatty acids were expressed as the percentage of total identified fatty acids (in mol %). GC analyses was performed in triplicate for each extractives modality.

Antimicrobial activity

The antimicrobial effect was examined against the following microorganisms: reference strains of Gram-negative bacteria *Escherichia coli* ATCC 25922 (Kwik-stik, Microbiologics Inc.), *Pseudomonas aeruginosa* ATCC 27853 (Kwik-stik, Microbiologics Inc.) and Gram--positive bacteria *Enterococcus faecalis* ATCC 29212 (Kwik-stik, Microbiologics Inc.), *Staphylococcus aureus* ATCC 25923 (Kwik-stik, Microbiologics Inc), as well as the reference strain of *Candida albicans* ATCC 10231 (Kwik-stik, Microbiologics Inc.) and two clinical isolates of *C. albicans*. Gram-negative bacteria can cause serious diseases in humans, especially in immuno-compromised individuals. The cell wall of Gram-negative bacteria is a more extensive and rigid complex than that of Gram-positive species, which is why Gram-negative bacteria species are more resistant. The clinical oral isolates of *C. albicans* were collected from patients diagnosed with prosthetic stomatitis, from the Department of Prosthodontics, School of Dental Medicine, University of Belgrade (Serbia). From the surface of the denture base, a biofilm was obtained using a method of denture sonication described previously.[17] The obtained solution was homogenized and 5×10^{-8} m^3 was plated on CHROM agar *Candida* medium (CHROMagar, Paris, France) and incubated at 37 °C for 48 h. The identification of *Candida* strains was done according to the specific appearance of colonies as defined by the manufacturer.

The antimicrobial activity of petroleum ether and ethanol extracts was assessed using broth microdilution method according to EUCAST.[18] The yeast and bacterial suspensions were prepared in sterile saline and adjusted to 0.5 McFarland standard of turbidity (which corresponds the size of inoculums of 1×10^{12}–5×10^{12} CFU m^{-3}). When testing the bacterial susceptibility, volume of 9×10^{-8} m^3 of dextrose broth (Himedia) and volume of 1×10^{-8} m^3 of each bacterial suspension was added to the wells of a sterile 96-well microtiter plate containing volume of 1×10^{-7} cm^3 of nut and green husk extracts diluted in dextrose broth. When testing yeast susceptibility, volume of 9×10^{-8} m^3 of RPMI 1640 medium (Merck) and volume of 1×10^{-8} m^3 of each fungal suspension was added to the wells of a sterile 96-well microtiter plate already containing volume of 1×10^{-7} m^3 of extract in RPMI 1640 medium. The microplates were then incubated for 24 h at 37 °C. The serial dilutions of nut and green husk extracts were made in the microtiter plate wells. The nut and green husk extracts concentrations of 3.38, 2.75, 1.69 and 1.38 kg m^{-3} were tested.

The minimal inhibitory concentration (*MIC*) was the lowest concentration where microorganism growth was not observed after 24 h. The test for antifungal activity also included positive control (fungi in RPMI 1640 without ethanol and petroleum ether fraction) and negative control (only RPMI 1640 without yeast suspensions). Positive controls were represented with wells containing a bacterial suspension in an appropriate growth medium, as well as a bacterial suspension in an appropriate growth medium with ethanol or petroleum ether in concentration corresponding to the highest used in the broth microdilution assay. In parallel with the examination of the effect of extracts in a given solvent, the effect of the solvent itself (70 % ethanol, petroleum ether) was examined as well. Negative controls were represented with wells containing growth medium and plant extract. All measurements of MIC values were repeated in triplicate.

RESULTS AND DISCUSSION

The total extractive substances of petroleum ether and ethanol extracts

The concentration of total extractive substances in petroleum ether extracts was 0.2 ± 0.02 and 0.25 ± 0.02 kg m^{-3} for nut and green husk, respectively. The concentration of total extractive substances in ethanol extracts was 11.0 ± 1.4 and 13.5 ± 1.5 kg m^{-3} for nut and green husk, respectively.

HPLC analysis of ethanol extracts

The ethanol extracts of *J. nigra* nut and green husk were analyzed by HPLC-PDA. In the both extracts, ellagic acid was the most dominant compound (Fig. 1). The concentration of ellagic acid in ethanol extracts of nut and green husk was $(55.0\pm1.3)\times10^{-3}$ and $(114.1\pm0.5)\times10^{-3}$ kg m^{-3} of extracts, respectively.
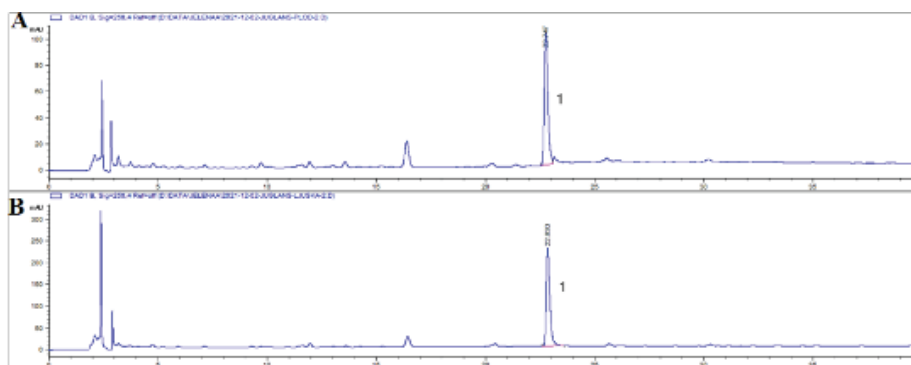
Fig. 1. HPLC chromatogram of *J. nigra* nut (A) and green husk (B) ethanol extracts recordered at 250 nm (1-ellagic acid).

This study showed that *J. nigra* nut is rich in ellagic acid, which is in accordance with previous research.[9] Phenolic profiles of previously reported *J. nigra* kernels[9,10] to some extent differ from phenolic profile of *J. nigra* nut analyzed in this study, probably due to different growth conditions, as well as to the different starting materials and conditions of extraction.[9,10]

Although there is information in the literature regarding *J. nigra* kernel phenolic profile,[8–10] data are missing for green husk. So far, for *J. nigra* green husk the high total phenolic content has been determined by Wenzel and co-workers.[4] Our comparative analysis showed that green husk is generally richer in ellagic acid than nut. Ellagic acid is detected at high concentrations in many berries (strawberries, raspberries, cranberries and grapes), and other known sources of ellagic acid, include walnuts;[19] however, this study points out that *J. nigra* green husk represent a rich source of ellagic acid, as well.

Ellagic acid is a naturally occurring polyphenolic lactone component of some fruits and vegetables.[19,20] It is well known for its antioxidant activity[21] and also possess various pharmacological activities including anti-inflammatory, hepatoprotective, neuroprotective[22] and antiatherogenic,[23] suggesting its potential beneficial health effects.

GC analysis of petroleum ether extracts

Fatty acid compositions were analyzed for petroleum ether extracts of *J. nigra* nut and green husk. Table I lists the fatty acids of two petroleum ether extracts. *J. nigra* nut and green husk containing two saturated fatty acids (SFA), palmitic acid (C16:0) and stearic acid (C18:0), then monounsaturated fatty acids (MUFA) palmitoleic (C16:1n-7), oleic (C18:1n-9), and vaccenic acid (C18:1n-7), as well as polyunsaturated fatty acids (PUFA) linoleic (C18:2n-6), *γ*-linolenic (C18:3n-6) and *α*-linolenic (C18:3n-3) acids.

TABLE I. Fatty acid profile of petroleum ether extracts of *J. nigra* nut and green husk. The results for individual fatty acids were expressed as the percentage of total identified fatty acids (in mol %); SFA – saturated fatty acids; MUFA – monounsaturated fatty acids; PUFA – polyunsaturated fatty acids

Fatty acid		Plant part	
		Nut	Green husk
SFA			
C16:0	Palmitic acid	8.06±0.29	12.45±0.09
C18:0	Stearic acid	3.56±0,19	3.39±0.03
Total SFA		11.66±0.48	15.84±0.12
MUFA			
C16:1(n-7)	Palmitoleic acid	0.23±0.10	0.51±0.03
C18:1(n-7)	Vaccenic acid	2.75±0.22	2.96±0.94
C18:1(n-9)	Oleic acid	41.34±0.31	31.08±1.05
Total MUFA		44.09±0.61	34.04±2.2
PUFA			
C18:2(n-6)	Linoleic acid	36.35±0.57	45.15±0.03
C18:3(n-6)	*γ*-Linolenic acid	0.54±0.09	0.50±0.11
Total n-6 PUFA		36.89±0.66	45.65±0.14
C18:3(n-3)	*α*-Linolenic acid	7.06±0.19	3.96±0.05
Total PUFA		43.95±0.87	49.61±0.19

Among the saturated fatty acids, the concentration of palmitic acid detected in nut was lower than in green husk, while the concentration of stearic acid was similar in nut and green husk of black walnut (Table I). Similar levels of palmitic (7.03 %) and stearic acids (2.75 %) were reported for *J. regia* nut.[24] On the other hand, the percentage of oleic acid in *J. nigra* nut (41.34 %) was significantly higher compared to *J. regia* (14.47 %),[22] making black walnut a rich source of oleic acid.[6] Although the green husk is also rich in MUFA, significantly higher levels were found in the nut (Table I). Oleic acid demonstrates large spectra of biological activities associated with many beneficial health effects. On the cellular level, as a part of membrane phospholipids, oleic acid increases membrane fluidity and transport, stimulates enzymatic activity, and regulates the activity of membrane receptors and signal transduction and transcription of some genes.[25] Numerous epidemiological observations have showed that practicing the Mediterranean diet, rich in oleic acid and nuts, is associated with the decrease of the total cholesterol, low-density lipoprotein cholesterol and triglyceride concentrations in plasma, having thus positive effect on cardiovascular and coronary artery disease.[26] Moreover, it has been showed that Mediterranean diet is positively associated with the bone health, a reduced incidence of cancer, Parkinson's and Alzheimer's diseases, and all-cause mortality.[24,27]

In both *J. nigra* nut and green husk, unsaturated fatty acids content was very high, 84.16 and 88.26 %, respectively. In addition to oleic acid, the nut and particularly green husk are valuable sources of linoleic acid (LA, Table I). In comparison to other walnuts such as *J. regia* (63.15 %),[24] LA was found in considerably lower amounts in *J. nigra* (36.35 %). LA is an essential fatty acid that is indispensable for normal growth and development, and its recommended daily intake is around 10 g day^{-1}. As it can be seen in Table I, α-linolenic (ALA) content of *J. nigra* nuts is significant, 7.06 %. The richest sources of ALA are flaxseed oil (53 %), walnuts (11 %) and canola oil (7 %) as well as rosehip seed oil (about 20 %).[28,29] Accordingly, the consumption of *J. nigra* nuts may have favourable effects on general health.

Other unsaturated fatty acids were also detected: palmitoleic acid, vaccenic acid and γ-linoleic acid, which have a low content (<3 % of total fatty acid). When comparing fatty acids profile of *J. nigra* nut and green husk, it can be concluded that nuts have more favourable composition, with higher levels of oleic acid and ALA, and lower levels of SFA and n-6 PUFA.

Antimicrobial activity petroleum ether and ethanol extracts

The antimicrobial activity of different *J. nigra* nut and green husk extracts was assessed against a diverse range of microorganisms, including both Gram-positive and Gram-negative bacteria, and a yeast *C. albicans*. The ethanol extracts of nut and husk didn't show inhibitory activity against the Gram-negative

and Gram-positive bacteria, whereas petroleum ether extracts of nut and husk didn't show inhibitory activity against any of the tested microorganisms (Table II). Moreover, the ethanol extracts of nut and green husk displayed the ability to inhibit *C. albicans* growth (Table II). The ethanol extract of nut showed *MIC* of 1.38 ± 0.01 kg m^{-3}, while the ethanol extract of green husk showed MIC of 1.69 ± 0.04 kg m^{-3} against reference strain and clinical oral isolate *C. albicans*.

TABLE II. Antimicrobial activity of the extracts of nut and green husk from *J. nigra*

Microorganism	Petroleum ether extract		Ethanol extract	
	Nut	Green husk	Nut	Green husk
Gram-positive bacteria				
S. aureus	–	–	–	–
E. faecalis	–	–	–	–
Gram-negative bacteria				
E. coli	–	–	–	–
P aeruginosa	–	–	–	–
Yeast				
C. albicans	–	–	+	+

The presence of the phenolic compounds in ethanol extracts of nut and husk hints at possible inhibitory effects on *C. albicans* growth. Phenolics, such as gallic acid, ellagic acid, ferulic acid and naringin, have been linked to antimicrobial activity.[10] Recently, the ellagic acid have been reported to show inhibitory effects on *C. albicans*,[20] so ellagic acid present in the ethanol extracts of *J. nigra* could be related to the demonstrated anticandidal activity. Interestingly, the study revealed the contributions of ethanol extracts from nut or green husk to the antifungal activity.

This research showed that the ethanolic extract of *J. nigra* nut and husk exhibits higher anticandidal activity as compared to methanolic extracts of *J. regia*.[30] On the other hand, the ethanol extract of *J. nigra* nut and husk showed less inhibitory effect against the tested oral Candida strains than the ethyl acetate extract of *J. regia* bark.[31] The differences in the *MIC* values obtained in our and previous studied can be explained by different chemical composition of various *Juglans* species and their parts used for antifungal examination.

The ellagic acid has been identified in ethanol extracts of *J. nigra*. The presence of the phenolic compounds in ethanol extracts of nut and husk hints at possible inhibitory effects on *C. albicans* growth. Phenolics, such as gallic acid, ellagic acid, ferulic acid and naringin, have been linked to antimicrobal activity.[10] Recently, the ellagic acid have been reported to show inhibitory effects on *C. albicans*,[32] so ellagic acid present in the ethanol extracts of *J. nigra* could be related to the demonstrated anticandidal activity. A study regarding the mechanism of antifungal activity of ellagic acid showed that this compound inhi-

bits biosynthesis of ergosterol and reduces the activity of membrane sterols.[33] Ergosterol (sterol) is an important component of the fungal membrane responsible for maintaining its stability and fluidity, enzyme activity and transport processes.[34] The inhibitory activity of *J. nigra* nuts and green husk ethanolic extracts originates from the presence of ellagic acid, which contributes to the dysfunction of the fungal membrane. The significance of this study is elucidating the impact of ethanolic extracts from walnut or green husk on the inhibition of clinical oral isolates of *C. albicans*, thus paving the way to the possible use of these extracts in antimicrobial treatment in oral hygiene.

CONCLUSION

The petroleum ether and ethanol extracts of *J. nigra* nut and green husk were chemically analysed and their antimicrobial activity was examined. Ellagic acid was found to be the most dominant phenolic compound in the ethanol extracts of *J. nigra* nut and green husk. Fatty acids analysis identified saturated fatty acids (palmitic acid and stearic acid), monounsaturated fatty acids (palmitoleic, oleic, and vaccenic acid) and polyunsaturated fatty acids (linoleic, γ-linolenic, and α--linolenic acids) in petroleum ether of *J. nigra* nut and green husk. None of the extracts had antimicrobial potency for Gram-positive and Gram-negative bacteria. The petroleum ether extracts didn't show the ability to inhibit *C. albicans* growth, while the ethanol extracts of *J. nigra* nut and green husk showed the ability to inhibit *C. albicans* growth. The obtained results support the possible use of these extracts in the antimicrobial treatment in oral hygiene. In conclusion, the results proved that nut and the green husk of *J. nigra*, considered as by-products, can actually be the raw material for the extraction of components potentially beneficial to human health.

ИЗВОД

ХЕМИЈСКА КАРАКТЕРИЗАЦИЈА И АНТИМИКРОБНА АКТИВНОСТ ОРАШАСТОГ ПЛОДА И ЗЕЛЕНЕ ЉУСКЕ *Juglans nigra* L.

КАТАРИНА М. РАЈКОВИЋ[1], МИЛИЦА ДРОБАЦ[2], ПЕТАР МИЛИЋ[3], ВЕСНА ВУЧИЋ[4], АЛЕКСАНДРА АРСИЋ[4], МИРИЈАНА ПЕРИЋ[5], МИЛЕНА РАДУНОВИЋ[6], САЊА ЈЕРЕМИЋ[7] и ЈЕЛЕНА АРСЕНИЈЕВИЋ[2]

[1]*Техничко-технолошки одсек, Академија васпитачко-медицинских струковних студија, Крушевац,* [2]*Катедра за фармакогнозију, Фармацеутски факултет, Универзитет у Београду, Београд,* [3]*Одсек Ћуприја, Академија васпитачко-медицинских струковних студија, Ћуприја,* [4]*Група за нутритивну биохемију и дијетологију, Институт за медицинска истраживања, Универзитет у Београду, Београд,* [5]*Катедра за протетику, Стоматолошки факултет, Универзитет у Београду, Београд,* [6]*Катедра за микробиологију, Стоматолошки факултет, Универзитет у Београду, Београд и* [7]*Институт за молекуларну генетику и генетичко инжењерство, Универзитет у Београду, Београд*

Juglans nigra (црни орах) као извор биолошки активних једињења се користи у традиционалној медицини. Истраживање биоактивних једињења присутних у црном ораху може довести до шире примене његових производа. Зато ова студија има за циљ да окарактерише орашаст плод и зелену љуску J. nigra на основу хемијске анализе њихових петролетарских и етанолних екстраката, добијених ултразвучним и рефлукс методама екстракције. Антимикробна активност различитих фракција екстракта је тестирана коришћењем Грам-негативних бактерија (*Escherichia coli*, *Pseudomonas aeruginosa*), Грам--позитивних бактерија (*Enterococcus faecalis*, *Staphylococcus aureus*) и квасница (референтни сој и клинички изолати *Candida albicans*). Анализа течном хроматографијом високих перформанси, издвојила је елагинску киселину као најдоминантније једињење у етанолним екстрактима орашастог плода ($(55,0\pm1,3)\times10^{-3}$ kg m^{-3}) и зелене љуске ($(114,1\pm0,5)\times10^{-3}$ g m^{-3}). Неполарна једињења су одређена применом гасне хроматографске анализе петролетарских екстракта. Орашаст плод и зелена љуска садрже две засићене масне киселине, палмитинску (C16:0) и стеаринску киселину (C18:0), затим мононезасићене масне киселине, палмитолеинску (C16:1n-7), олеинску (C18:1n-9) и вакценску киселину (C18:1n-7), као и полинезасићене масне киселине, линолну (C18:2n-6), γ-линоленску (C18:3n-6) и α-линоленску (C18: 3n-3) киселину. Етанолни екстракти орашастог плода и зелене љуске показали су антимикробну активност на сојевима *C. albicans* која је најчешћи узрочник гљивичних инфекција.

(Примљено 10. фебруара, ревидирано 27. фебруара, прихваћено 20. априла 2023)

REFERENCES

1. R. Amarowicz, G. A. Dykes, R. B. Pegg, *Fitoterapia* **79** (2008) 217 (https://doi.org/10.1016/j.fitote.2007.11.019)
2. K. M. Rajković, M. Vasić, M. Drobac, J. Mutić, S. Jeremić, V. Simić, J. Stanković, *Chem. Eng. Res. Des.* **157** (2020) 25 (https://doi.org/10.1016/j.cherd.2020.03.002)
3. J. M. Rorabaugh, A. P. Singh, I. M. Sherrell, M. R. Freeman, N. Vorsa, P. Fitschen, C. Malone, M. A. Maher, T. Wilson, *Food Nutr. Sci.* **2** (2011) 193 (https://doi.org/10.4236/fns.2011.23026)
4. J. Wenzel, S. C. Samaniego, L. Wang, L. Burrows, E. Tucker, N. Dwarshuis, M. Ammerman, A. Zand, *Food Sci. Nutr.* **5** (2017) 223 (https://doi.org/10.1002/fsn3.385)
5. M. Mirjalili, L. Karimi, *J. Chem.* (2013) 375352 (http://dx.doi.org/10.1155/2013/375352)
6. R. S. Camara, V. A. Schlegel, *Int. J. Food Prop.* **19** (2016) 2175 (https://doi.org/10.1080/10942912.2015.1114951)

7. K. V. Ho, Z. Lei, L. W. Sumner, M. V. Coggeshall, H. Y. Hsieh, G. C. Stewart, C. H. Lin, *Metabolites* **29** (2018) 8 (https://doi.org/10.3390/metabo8040058)

8. K. V. Ho, A. Roy, S. Foote, P. H. Vo, N. Lall, C. H. Lin, *Molecules* **25** (2020) 4516 (https://doi.org/10.3390/molecules25194516)

9. D. C. Vu, P. H. Vo, M. V. Coggeshall, C. H. Lin, *Food Chem.* **66** (2018) 4503 (https://doi.org/10.1021/acs.jafc.8b01181)

10. D. C. Vu, T. H. D. Nguyenb, T. L. Hoc, *RSC Adv.* **10** (2020) 33378 (https://doi.org/10.1039/D0RA05714B)

11. J. N. Ndukauba, I. A. Olawuni, D. C. Okafor, R. O. Enwereuzoh, M. Ojukwu, *Int. J. Life Sci.* **4** (2015) 58 (https://doi.org/10.13140/RG.2.2.27483.67360)

12. S. Cosmulescu, I. Trandafir, G. Achim, M. Botu, A. Baciu, M. Gruia, *Hort. Agrobot. Cluj* **38** (2010) 53 (https://doi.org/10.15835/nbha3814624)

13. A. Jahanban-Esfahlan, A. Ostadrahimi, M. Tabibiazar, R. A. Amarowicz, *Int. J. Mol. Sci.* **20** (2019) 3920 (https://doi.org/10.3390/ijms20163920)

14. A. Salejda, U. Janiewicz, M. Korzeniowska, J. Kolniak-Ostek, K. Grazyna, *LWT-Food Sci. Tech.* **65** (2016) 751 (https://doi.org/10.1016/j.lwt.2015.08.069)

15. B. Shi, W. Zhang, X. Li, X. Pan, *Int. J. Food Prop.* **20** (2018) 1094 (https://doi.org/10.1080/10942912.2017.1381706)

16. C. Glaser, H. Demmelmair, B. Koletzko *J. Lipid. Res.* **51** (2010) 216 (https://doi.org/10.1194/jlr.D000547)

17. M. Perić, M. Radunović, M. Pekmezović, J. Marinković, R. Živković V. Arsić Arsenijević, *J. Prosthodont.* **28** (2017) 580 (https://doi.org/10.1111/jopr.12610)

18. J. L .Rodriquez-Tudela, J. P. Donnelly, M. C. Arendrup, S. Arikan, F. Barchiesi, J. Bille, E. Chryssanthou, M. Cuenca-Estrella, E. Dannaoui, D. Denning, W. Fegeler, P. Gaustad, C. Lass-Flörl, C. Moore, M. Richardson, A. Schmalreck, A. Velegraki, P. Verweij, *Clin. Microbiol. Infect.* **14** (2008) 982 (https://doi.org/10.1111/j.1469-0691.2008.02086.x)

19. D. A. Vattem, K. Shetty, *J. Food Biochem.* **29** (2005) 234 (https://doi.org/10.1111/j.1745-4514.2005.00031.x)

20. A. D. G. Sampaio, A. V. L. Gontijo, H. M. Araujo, C. Y. Koga-Ito, *Antimicrob. Agents Chemother.* **26** (2018) 62 (https://doi.org/10.1128/AAC.01716-18)

21. S. Alfei, B. Marengo G. Zuccari, *Antioxidants* **9** (2020) 707 (https://doi.org/10.3390/antiox9080707)

22. J. L. Ríos, R. M. Giner, M. Marín, M. A. Carmen Recio, *Planta Medica* **84** (2018) 1068 (https://doi.org/10.1055/a-0633-9492)

23. Z. Papoutsi, E. Kassi, I. Chinou, M. Halabalaki, L. A. Skaltsounis, P. Moutsatsou, *Brit. J. Nutr.* **99** (2008) 715 (https://doi.org/10.1017/S0007114507837421)

24. A. Arsic, M. Takic, M. Kojadinovic, S. Petrovic, M. Paunovic, V. Vucic, D. Ristic Medic, *Can. J. Physiol. Pharmacol.* **99** (2021) 64 (https://doi.org/10.1139/cjpp-2020-0317)

25. A. Arsić, A. Stojanović, M. Mikić, *Ser. J. Exp. Clin. Res.* **20** (2019) 3 (https://doi.org/10.1515/sjecr-2017-0077)

26. D. Ristic-Medic, M. Kovacic, M. Takic, A. Arsic, S. Petrovic, M. Paunovic, V. Vucic, *Nutrients* **13** (2021) 15 (https://doi.org/10.3390/nu13010015)

27. A. Arsic, in *The Mediterranean Diet, An Evidence-based Approach*, V. R. Preedy, R. R. Watson, Eds., Academic Press, An Imprint Elsevier, 2020, pp. 267–274, ISBN: 9780128195789, 2020 (https://doi.org/10.1016/B978-0-12-818649-7.00024-2)

28. V. Vucic, J. Tepsic, A. Arsic, T. Popovic, J. Debeljak-Martacic, M. Glibetic, *Acta Alimentaria* **41** (2012) 343 (https://doi.org/10.1556/AAlim.41.2012.3.6)

29. S.M. Milic, D.M. Kostic, S.P. Milić, M.V. Vučić, C.A. Arsić, B.V. Veljković, O.S. Stamenković, *Chem. Eng. Technol.* **43** (2020) 1 (https://doi.org/10.1002/ceat.201900689)

30. A. Naseri, A. Fata, S. A. A. Shamsian, *Int. J. Med. Res. Health Sci.* **5** (2016) 72 (https://www.ijmrhs.com/medical-research/in-vitro-anticandidal-effects-of-aqueous-and-methanolic-extracts-of-walnut-juglansregia-tree-fruit-peel-in-comparision-w.pdf)

31. E. Noumi, M. Snoussi, H. Hajlaoui, E. Valentin, A. Bakhrouf, *Eur. J. Clin. Microbiol. Infect. Dis.* **29** (2010) 81 (https://doi.org/10.1007/s10096-009-0824-3)

32. A. D. G. Sampaio, A. V. L. Gontijo, H. M. Araujo, C. Y. Koga-Ito, *Agents Chemother.* **26** (2018) 62:e01716-18 (https://doi.org/10.1128/AAC.01716-18)

33. Z. J. Li, X. G. G. Dawuti, S. Aibai, *Phytother. Res.* **29** (2015) 1019 (https://doi.org/10.1002/ptr.5340)

34. I. S. Mysiakina, N. S. Funtikova, *Mikrobiology* **76** (2007) 5 (https://doi.org/10.1134/S0026261707010018).

Comparative study of chemical composition and the antimutagenic activity of propolis extracts obtained by means of various solvents

PINAR G. RASGELE[1]*, NISA SIPAHI[2] and GULDEN YILMAZ[3]

[1]*Duzce University, Faculty of Agriculture, Department of Biosystems Engineering, Duzce, Turkey, [2]Duzce University, Traditional and Complementary Medicine Application and Research Center, Duzce, Turkey and [3]Trakya University, Faculty of Science, Department of Biology, Balkan Campus, 22030, Edirne, Turkey*

Abstract: The present study is aimed to evaluate the chemical characterization and antimutagenic potential of propolis extracted in three different solvents (ethanol, polyethylene glycol and water). The chemical properties of different extracts of propolis were identified using HPLC-DAD and LC–MS/MS and polyethylene glycol extract of propolis were found to be richer than the ethanolic and water extracts of propolis considering chemical composition. In addition, the antimutagenic activities of propolis extracts were determined using Ames assay. The concentrations of 3, 1.5 and 0.75 mg plate^{-1} of ethanolic and polyethylene glycol extracts, as well as 0.3, 0.15 и 0.075 mg plate^{-1} of water extract of propolis were used as active materials. Propolis extracted in three different solvents indicated strong antimutagenic activity against both 4-nitro--*o*-phenylendiamine and sodium azide mutagens in the *Salmonella typhimurium* TA98 and 100 strains at all concentrations. Ethanolic extract of propolis had the highest inhibition rates for both bacterial strains and these rates were 98.94 and 97.37 % for TA98 and TA100, respectively. The inhibition rates of polyethylene glycol extract of propolis ranged from 68.27 to 98.94%. Moreover, it was determined that water extract of propolis had the lowest inhibition rates, which were 56.86 and 55.35% for TA98 and TA100, respectively. The toxicological safety of natural products such as propolis has gained great importance due to extensive usage.

Keywords: HPLC-DAD; ames assay; genotoxicity test; *Salmonella typhimurium*.

INTRODUCTION

Propolis is a mixture of substances synthesized by combining the resin that bees collect from buds, exudates and other parts of plants with their own saliva

---

615

enzymes, wax and bees use it to protect the hive.[1] Although the content of propolis has a different chemical composition according to the country, region and plant variety, similar action mechanisms such as antibacterial, antifungal, antiviral, antiparasitic, anti-inflammatory, antiproliferative and antioxidant activity have been defined.[1]

The content of propolis varies according to the plant species used by the bees, the plant components collected, the harvesting season, the climate, the diet of the bees and the genetic differences in the queen bee. Chemical standardization is very difficult due to the wide variation in the chemical mix depending on the source of propolis.[2] It is also important to use suitable solvents in the extraction of propolis due to impurities such as wax, pollen and dead bees. Common solvents used for the extraction of propolis are ethanol, methanol and water in different concentrations. The solvents used during the extraction can affect the activity of propolis because different solvents dissolve and remove different compounds. Since most substances in the composition of propolis are lipophilic and lipophilic compounds are soluble in ethanol, ethanol has been the commonly used solvent for extracting propolis.[3] In addition, it has been known that flavonoids and phenolic acids are obtained by the extraction of propolis with different solvents such as methanol, acetone, chloroform, propylene glycol and especially water.[4] Medical and food technology processes are almost always carried out with ethanol or aqueous extracts. In addition, glycol extracts can be used for many cosmetic applications that improve dissolution in water-based emulsions.[5,6]

Many powerful chromatographic methods are used to determine and measure biologically active substances in complex mixtures such as propolis. HPLC, high performance thin layer chromatography (HPTLC), nuclear magnetic resonance (NMR), thin layer chromatography (TLC), gas chromatography (GC) and capillary electrophoresis (CE) are some of these methods.[7] Today, against the standardization of propolis, high-performance liquid chromatography with photodiode-array detection (HPLC-DAD) is one of the most widely used methods for the separation and quantification of phenolic compounds of propolis, thanks to its very high separation efficiency.[8]

The Ames test is one of the short-term test systems used to detect mutagens/ /antimutagens because it provides standard and reliable results.[9] The Ames *Salmonella* test is also accepted as a viable test by international organizations such as the Organization for Economic Co-operation and Development, International Conference on Harmonisation, the Japanese Ministry of Health and Welfare and the United States Environmental Protection Agency: Health Effects Test Guidelines International Workshop on the Standardization of Genotoxicity Test Procedures, and is one of the recommended tests to observe the mutagenicity/antimutagenicity of chemicals. Therefore, the aim of this study was to compare

chemical compositions of propolis extracted in three different solvents and to investigate the antimutagenic potential of them by Salmonella back mutation test.

EXPERIMENTAL

Chemicals

For the preparation of propolis extracts, ethanol (96.0 %) and polyethylene glycol 400 were purchased from Sigma Aldrich and Zag Chemistry®, respectively. For HPLC-DAD, caffeic acid (≥98.0 %), quercetin (≥95.0 %), apigenin (≥95.0 %), kaempferol (≥90.0 %), chrysin (≥97.0 %) and caffeic acid phenyl ester (≥97.0 %) were used as standards (Sigma Aldrich). For antimutagenicity assay, D-biotin, L-histidine, top agar, 4-nitro-*o*-phenylenediamine (NPD) and sodium azide (NaN₃) were bought at Sigma Aldrich. Nutrient agar was obtained from Merck.

Collection of propolis samples and preparation of extracts

Raw propolis samples was collected from Düzce (Yığılca) situated in Western Black Sea Region of Türkiye; latitude: 40° 57′ 28″ N, longitude: 31° 27′ 15″ E, in 2020 were kept in the freezer (–20 °C) until analysis. Raw propolis taken from the same hive was divided into 3 parts and used for different extraction.

Raw propolis samples were extracted in Duzce University, Traditional and Complementary Medicine Application and Research Center, Duzce, Türkiye. Briefly, for the ethanolic extract of propolis (EEP), a sample (50 g) was crushed into small pieces in a blender, extracted with 500 ml 96 % ethanol for 48 h, filtered and evaporated to dryness in a vacuum evaporator (Labfreeez®, China) at 40 °C. The resultant resinous product was added to 70 % ethanol.

For polyethylene glycol extract of propolis (PEGEP), preparation processes were as in the EEP and then dissolved in 60 % PEG400 (Zag Chemistry®, Türkiye).

For the water extract of propolis (WEP), 50 g of propolis was shaken (Allsheng® OS--200) in 500 ml distilled water for 10 days at room temperature at 1400 rpm and filtered. An orbital shaker was used for all process.

High-performance liquid chromatography with photodiode-array detection

The chemical characterizations of different extracts of propolis were identified by in--house method using HPLC-DAD at Duzce University, Scientific and Technological Research Application and Research Center Laboratory. HPLC-DAD analyzes (254 and 325 nm) were performed in HPLC (Shimadzu LC20A®) instrument with PDA detector. The HPLC conditions used in the study of Çakır *et al*.[10] were modified. Mobile phase (A) and acetonitrile (B) (HPLC grade, Isolab®) gradients containing 2 % acetic acid were applied on the C18 column (250mm×4.6mm×5um, Inertsil). In 20 μL injection volume, at 30 °C column temperature at 1.0 ml min⁻¹ flow rate, initial volumes are 75 % of mobile phase A and 25 % of mobile phase B and programmed as A mobile phase 25 % and B mobile phase 75 % in 25 min linearly. The method was completed at 30 min and each reading was carried out under these conditions.

Liquid chromatography–mass/mass spectrometry (LC–MS/MS)

The samples were analyzed at Trakya University, Technology Research and Development Application and Research Center (TÜTAGEM) with triple quadrupole performance using liquid chromatography–mass/mass spectrometry (LC–MS/MS). In the analysis process, first of all, the certified standard compounds were prepared at 5 points between 5–100 ng/ml concentrations and a calibration curve was created. In this method, the emergence of the compounds in the chromatogram at a certain time interval, the ratios of parent ions and confirm-

ation ions are compared with the ratios of fragmented ions obtained from the matrix spike. The area of the peaks obtained as a result of the analysis is plotted against the concentration of the added standard in the sample. Thus, substance determination is made with high sensitivity and accuracy. Two different sample preparation processes were applied for the analysis of phenolic compounds.

Hydrolysis method

100 µl of the sample was added to 900 µl of the extraction solution (79 % ultrapure water + 20 % methanol + 1 % formic acid) and was vortexed for 30 s and then kept for 10 min in an ultrasonic bath at 45 °C. Then the sample was centrifuged at 9000 rpm for 5 min and the clear filtrate was poured into glass vials for analysis.

Acidic hydrolysis method

200 µl of 2 M HCl solution was added to 100 µl sample, vortexed for 30 s, and kept in an ultrasonic bath at 90 °C for 40 min. Then, 700 µl of extraction solution (79 % ultrapure water + 20 % methanol + 1 % formic acid) was added. The samples were centrifuged at 9000 rpm for 5 min and the clear filtrate was poured into insert glass vials for injection.

Analyzes of phenolic compounds were performed with Agilent 1260 infinity liquid chromatography, Agilent 6460 Triple Quadrupole MS/MS system (Jet Stream Electrospray ion source). Mobile phase A: 5 mM ammonium acetate in ultra pure water; mobile phase B: 50 % acetonitrile, 49 % methanol, 1 % acetic acid by volume; column: Agilent Zorbax SB-C8 3.0 mm×150 mm×3.5 µm.

Determination of toxicity

In order to determine the cytotoxic concentrations, 48, 24, 12, 6, 3, 1.5 and 0.75 mg plate[-1] concentrations of EEP and PEGEP and 4.8, 2.4, 1.2, 0.6, 0.3, 0.15 and 0.075 mg plate[-1] concentrations of WEP were prepared according to Dean *et al.*[11] with minor modifications. Propolis extracts (100 µl) and bacterial culture (100 µl) were added to tubes containing top agar, the mixture was shaken well. It was spilled into Nutrient Agar plates and spread rapidly. Plates were incubated at 37 °C for 24 h. Based on the results obtained, non-cytotoxic concentrations were determined as 3, 1.5 and 0.75 mg plate[-1] concentrations for EEP and PEGEP; 0.3, 0.15 and 0.075 mg plate[-1] concentrations for WEP.

Test strains

S. tpyhimurium TA98 strain, which is widely used to detect frame shift mutation and TA100 strain, which is widely used to detect point mutation, were provided by EBPI Bio-Detection Products (Mississauga, ON, Canada) and the genotypes of the test strains were checked for histidine requirement, biotin requirement, rfa mutation, uvrB mutation.[12]

4-Nitro-*o*-phenylendiamine-NPD and sodium azide were used as positive controls for *S. typhimurium* TA98 and TA100 strains, respectively, in the absence of S9 mix.[13]

Evaluation of antimutagenicity assay

For the antimutagenicity assay, the bacterial culture (100 µl), the test substance (100 µl), and the positive mutagens (100 µl) were added to top agar (3 ml) containing of histidine/biotin (0.30 ml) and they were spread homogeneously on Minimal Glucose Agar plates. After the incubation (48–72 h at 37 °C) the revertant colonies were scored on the plates for each sample.

The value of the propolis extracts to inhibit the effect of positive mutagens was evaluated between 0 and 100 %. Three plates were used for each variable in each experiment, and each experiment was repeated two times. The results obtained were evaluated using the % inhibition formula:

$$I = 100\left[1-(a-b)/(c-b)\right] \tag{1}$$

a: number of returned colonies in petri dishes with propolis extract, mutagen and bacteria, b: number of colonies returning spontaneously, c: number of colonies in petri dishes with mutagen.

To quantify antimutagenic effects by propolis extracts, the classification was made according to inhibition rates and according to this, antimutagenic effect is defined as: <20 %, negative; 20–40 %, moderate; >40 %, strong.[14]

Statistical analysis

The data were analyzed using SPSS 20 for Windows (SPSS Inc., Chicago, IL, USA) and the results obtained were expressed as the mean±standard deviation (*SD*). The Kruskal–Wallis test was carried out followed by the Mann–Whitney U-test to compare the statistical significance of the differences between the treated and control groups. The dose response relationship was determined using the Pearson correlation analysis. $P < 0.05$ was considered significant.

RESULTS AND DISCUSSION

For the HPLC-DAD method, the amounts of the phenolic compounds were given in Table I. According to the results, chrysin (901.9 and 1371.0) and caffeic acid phenyl ester (CAPE, 1980.8 and 3196.1) were seen dominantly in EEP and PEGEP, respectively. PEGEP was found to be richer than the EEP and WEP in terms of phenolic compounds. The HPLC-DAD chromatograms of standard phenolic compounds are given in Fig. S-1 of the Supplementary material to this paper. There are many compounds that have not been identified as a result of the huge and different amounts of compounds within the propolis samples. While caffeic acid, quercetin and chrysin were determined in WEP, apigenin, kaempferol and CAPE were additionally detected in the EEP and PEGEP.

TABLE I. Chemical compositions (content in ppm) of different extracts of propolis by HPLC--DAD; ND: not determined

Compound	EEP	PEGEP	WEP
Caffeic acid	208.1	314.6	112.6
Quercetin	24.2	38.2	1.5
Apigenin	12.8	28.7	ND
Kaempferol	35.3	66.0	ND
Chrysin	901.9	1371.0	7.7
Caffeic acid phenyl ester	1980.8	3196.1	ND

For the LC–MS/MS method, the amounts of the phenolic compounds were given in the Supplementary material (Tables S-I and S-II of the Supplementary material).

The phenolic compounds of EEP, PEGEP and WEP were detected using LC–MS/MS hydrolysis and acid-hydrolysis methods using thirty-three phenolic standards. Of the 33 investigated phenolic compounds (Tables S-I and S-II), 22 were measured in the samples. In the hydrolysis method, when the concentrations

of phenolic compounds obtained in the EEP, PEGEP and WEP were evaluated, the phenolic compounds detected in the highest concentration were caffeic acid (1.74 mg/ml) and transferullic acid (0.64 mg/ml) for EEP; caffeic acid (3.95 mg/ml) and chlorogenic acid (0.23 mg/ml) for PEGEP; caffeic acid (1.06 mg/ml) and transferullic acid (0.07 mg/ml) for WEP.

In the acid hydrolysis method, when the concentrations of phenolic compounds obtained in the EEP, PEGEP and WEP were evaluated, the phenolic compounds detected in the highest concentration were caffeic acid (2.45 mg/ml) and transferullic acid (0.46 mg/ml) for EEP; caffeic acid (4.53 mg/ml) and transferullic acid (0.20 mg/ml) for PEGEP; caffeic acid (1.26 mg/ml) and protocatechuic acid (0.07 mg/ml) for WEP. In the results obtained from both methods, it can be said that caffeic acid and transferullic acid are the major components for all three solvents and there is no big difference between these two methods.

When the results were compared considering solvents, it was seen that the PEGEP had the richest content and this result was consistent with the result obtained by the HPLC-DAD method.

For the antimutagenicity assay, three different concentrations of EEP, PEGEP and WEP were used as material. The obtained results were showed in Table II. It was determined that the all of extracts of propolis had a strong antimutagenic effect at all concentrations on *S. typhimurium* TA 98 and 100 strains.

TABLE II. Antimutagenic effects as revertant colonies number of different concentrations of different propolis extracts on *S. typhimurium* TA98 and TA100 strains; NPD: 4-nitro-*o*-phenylendiamine

| Group | Concentration mg/plate | Strain | | | |
| | | *S. typhimurium* TA98 | | *S. typhimurium* TA100 | |
		Mean±*SD*	Inh. rate, %	Mean±*SD*	Inh. rate, %
Negative control	–	38.16±12.89	–	141.40±76.08	–
NPD	0.02	527.60±198.26	–	–	–
NaN$_3$	0.02	–	–	1625.60±993.14	–
EEP	3	63.33±4.93	94.86	541.00±470.53	73.07
	1.5	54.00±2.64	96.76	299.66±118.50	89.33
	0.75	43.33±3.51	98.94	180.66±100.50	97.35
PEGEP	3	119.00±64.37	83.48	612.33±75.63	68.27
	1.5	95.33±17.50	88.31	459.66±61.50	78.55
	0.75	43.33±11.37	98.94	340.00±37.24	86.61
WEP	0.3	249.33±50.52	56.86	804.00±96.50	55.35
	0.15	182.33±39.24	70.54	628.66±95.10	67.16
	0.075	121.66±36.74	82.94	456.33±27.39	78.78

EEP, PEGEP and WEP indicated strong antimutagenic activity against both 4-nitro-*o*-phenylendiamine and NaN$_3$ mutagens in the *S. typhimurium* TA98 and 100 strains at all concentrations. EEP had the highest inhibition rates for both bacterial strains and these rates were 98.94 and 97.37 % for TA98 and TA100,

respectively. Moreover, it was determined that WEP had the lowest inhibition rates, which were 56.86 and 55.35 % for TA98 and TA100, respectively (Fig. 1). However, it is thought that this low level in WEP may be due to the lower concentrations used than the others.
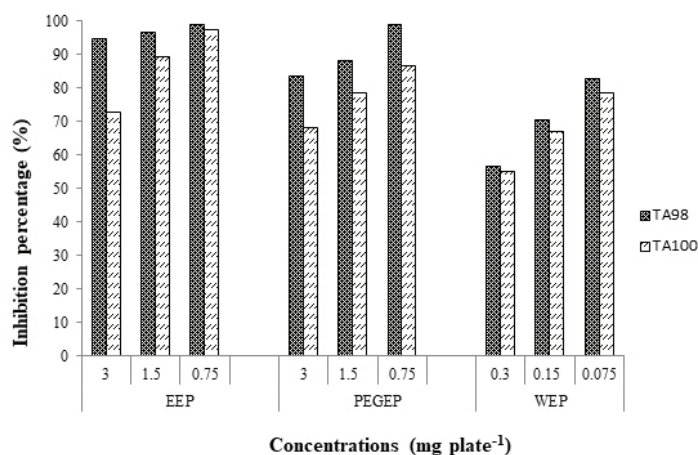
Fig. 1. The value of inhibition (%) of different concentrations of different propolis extracts on *S. typhimurium* TA98 and TA100.

The relationship between concentrations of EEP, PEGEP and WEP and the percentage of inhibition was evaluated by Pearson correlation test. It was observed that the percentage of inhibition significantly increased as the propolis concentrations decreased in *S. typhimurium* TA98 and TA100 strains (in *S. typhimurium* TA98 and TA100: $R^2 = 1$, P≤0.05 for EEP, PEGEP and WEP) (Fig. 2).

In the present study, the chemical compositions of propolis extracts were analyzed by HPLC-DAD and LC–MS/MS. PEGEP were found to be richer than the EEP and WEP in terms of chemical composition. The chemical characterization of many different extracts of propolis collected from different regions using many different methods (HPLC, GC–MS, LC–MS/MS, *etc.*) has been previously studied by many different researchers.[15–17] Furthermore, there are also many studies conducted with propolis collected from the Yığılca district of Düzce (Türkiye). Sevim *et al.*[18] determined by HPLC–UV method that EEP is rich in *p*-coumaric acid, ferulic acid, chrysin and pinocembrin components. Donmez *et al.*[19] investigated the volatile components of propolis in different solvents by LC–MS/MS and GC–MS–UV methods. It has been reported that the richest extract in terms of volatile component content is EEP. Ozdal *et al.*[20] reported that EEP has a rich content in their studies using the LC–MS/MS method. Rasgele and Kekecoglu[21] investigated the content of EEP with HPLC-DAD and they reported that biochanin, gallic acid, CAPE, pinostrobin and pinobankstin compounds were dominant. According to these data obtained from previous studies, propolis

Ethanolic Extract of Propolis (EEP)

$$y = 0,1362x^2 + 1,4983x + 93,223$$
$$R^2 = 1$$

$$y = -4,12x^2 + 28,62x + 48,57$$
$$R^2 = 1$$

TA98 — Polinom. (TA98) TA100 ·········· Polinom. (TA100)

Concentrations (mg plate⁻¹)

Polyethylene Glycol Extract of Propolis (PEGEP)

$$y = 2,8945x^2 - 3,848x + 84,438$$
$$R^2 = 1$$

$$y = -1,1117x^2 + 13,621x + 55,761$$
$$R^2 = 1$$

TA98 — Polinom. (TA98) TA100 ·········· Polinom. (TA100)

Concentrations (mg plate⁻¹)

Water Extract of Propolis (WEP)

$$y = -0,647x^2 + 15,63x + 41,872$$
$$R^2 = 1$$

$$y = -0,095x^2 + 12,095x + 43,35$$
$$R^2 = 1$$

TA98 — Polinom. (TA98) TA100 ·········· Polinom. (TA100)

Concentrations (mg plate⁻¹)

Fig. 2. Relationship between concentrations and inhibition rate (%) of test bacterial strains after exposure to different solvents of propolis.

has remarkable component richness in terms of content. The reasons for this diversity may be the region where propolis is collected, plant flora, bee race and solvent. When the results obtained from our study are discussed with others from literature, it can be noticed that although a diode array detector is used with the HPLCA-DAD method, the number of identified components is relatively low due to the peak overlap and the absence of compounds that do not absorb UV light.[22]

The Ames test is a useful method standardized in the 1970s for the mutagenicity of chemical compounds. It has also been used in the mutagenicity and antimutagenic effects of medicinal plants and natural products. However, due to the difficulty of working with natural products, there may be some technical problems and therefore sensitive and new guidelines are needed by regulatory agencies,[23] because the antimutagenic effect of natural extracts is a very important issue. Natural antimutagens can act against various mutagenic substances. On the other hand, antitumor effects of some compounds with antimutagenic effects have also been reported. Therefore, the search for antimutagenic compounds also represents a rapidly expanding field of cancer research. Therefore, it is very important to investigate both natural and synthetic antimutagens.[24] Especially in recent years, the preference of natural products such as propolis as a preservative in foods increases the importance of this. In general, it is desired to replace chemical compounds with active natural compounds.

Propolis is a complex bee product and contains very rich bioactive substances.[25] In this study, it is supposed that the antimutagenic effect of propolis is due to its rich phenol content,[26] because phenolics can act against mutagens through both intracellular and extracellular mechanisms.[27]

In the present study, EEP, PEGEP and WEP showed strong antimutagenic activity, being similar to the result obtained by many researchers using Ames assay. Varanda *et al.*[28] indicated that the ethanolic extract of propolis inhibited mutagenic potentials of mutagens in the *S. typhimurium* TA102, TA100 and TA98 strains. Jeng *et al.*[29] reported that the ethanolic extract of propolis showed an inhibitory effect against 4-nitro-*o*-phenylenediamine, 1-nitropyrene , 2-amino--3-methylimidazo[4,5-*f*]quinoline and benzo[*a*]pyrene mutagens on the *S. typhimurium* TA98 test system. Fu *et al.*[30] stated the antimutagenic effect of alcoholic propolis in the Ames assay *S. typhimurium* TA98 and TA100 strains, in which propolis inhibited the mutagenic activity of 2-aminofluorene and daunomycin. Moreno *et al.*[31] reported that extracts of propolis inhibited the effects of isoquinoline and 4-nitro-*o*-phenylenediamine mutagens in *S. typhimurium* TA98 and TA100 strains. Bayram *et al.*[32] observed that the ethanolic extract of propolis showed antigenotoxic effects against NaN_3, 9-aminoacridine and *N*-methyl-*N'*--nitro-*N*-nitrosoguanidine mutagens on *S. typhimurium* TA1535, TA1537 and *E. coli* WP2uvrA test strains.

Many antimutagenicity studies of propolis extracts, which were studied with different test systems, are also consistent with the results of our study. For example; Fu *et al.*[30] stated the antimutagenic effect of refined peanut oil in the micronucleus and chromosome aberration assays in mice, in which propolis inhibited the mutagenic activity of mitomycin and cyclophosphamide. Similarly, Lima *et al.*[33] reported that the aqueous extract of propolis had antimutagenic activity against DNA damage induced by 1,2-dimethylhydrazine in rats by aberrant crypt foci and comet methods. Also, Roberto *et al.*[34] reported that the ethanolic extract of propolis was not mutagenic and genotoxic in rat hepatoma cell lines, on the contrary, it caused a decrease in DNA damage in mutagen-treated groups. The researchers indicated that mechanisms of action of propolis might be related to either suppression of the mutagenic effects or antioxidant potentials of the components of propolis. It is thought that the antioxidant potential of propolis is due to its chemical components. The content of propolis varies according to the flora, harvest time, bee breed, etc., so it is one of the natural products that are very difficult to standardize.

CONCLUSION

Our study confirms the previous knowledge about the chemical composition of propolis. Chemically important and effectively bioactive components have been identified. Natural sources such as propolis remain an important component in drug development. Although propolis is used in traditional and complementary medicine, pharmacology and cosmetic industries, it is important to determine its antimutagenic potential in different solvents and more comprehensive studies are needed.

SUPPLEMENTARY MATERIAL

Additional data and information are available electronically at the pages of journal website: https://www.shd-pub.org.rs/index.php/JSCS/article/view/12280, or from the corresponding author on request.

И З В О Д

УПОРЕЂИВАЊЕ ХЕМИЈСКОГ САСТАВА И АНТИМУТАГЕНЕ АКТИВНОСТИ ЕКСТРАКАТА ПРОПОЛИСА ДОБИЈЕНИХ ПРИМЕНОМ РАЗЛИЧИТИХ РАСТВАРАЧА

PINAR G. RASGELE[1], NISA SIPAHI[2] и GULDEN YILMAZ[3]

[1]Duzce University, Faculty of Agriculture, Department of Biosystems Engineering, Duzce, Turkey, [2]Duzce University, Traditional and Complementary Medicine Application and Research Center, Duzce, Turkey u [3]Trakya University, Faculty of Science, Department of Biology, Balkan Campus, 22030, Edirne, Turkey

Циљ студије је било испитивање хемијског састава и антимутагеног потенцијала прополиса екстрахованог применом три различита растварача (етанол, полиетилен гликол и вода). Идентификација хемијских састојака екстраката прополиса је изведена применом HPLC-DAD и LC–MS/MS метода. Већи број састојака је нађен у полиетилен-гликолном, него у етанолном и воденом екстракту. Антимутагена активност екстраката прополиса је одређена Ејмсовим (Ames) тестом. Као активни материјал су коришћени

екстракти прополиса у три концентрације: 3; 1,5 и 0,75 mg по плочи, у случају етанолног и полиетиленгликолног екстракта, односно 0,3; 0,15 и 0,075 mg по плочи, у случају воденог екстракта. Екстракти прополиса у сва три растварача и у свим тестираним концентрацијама су испољили јаку антимутагену активност када су бактеријски сојеви *Salmonella typhimurium* TA98 и TA100 изложени дејству мутагена 4-нитро-*o*-фенилендиамина и натријум азида. Највећи инхибиторни ефекат је имао етанолни екстракт прополиса, на оба соја бактерија, 98,94 и 97,37 % за TA98, односно TA100. Инхибиторни ефекат полиетиленгликолног екстракта је био од 68,27 до 98,94 %, док је ефекат воденог екстракта био најслабији, 56,86 и 55,35 % за сој TA98, односно TA100. Природни производи, као што је прополис, имају велики значај јер су токсиколошки безбедни за употребу.

REFERENCES

1. I. Przybyłek, T. M. Karpinski, *Mol.* **24** (2019) 2047 (https://doi.org/10.3390/molecules24112047)
2. D. Kasote, V. Bankova, A. M. Viljoen, *Phytochem. Rev.* **1** (2022) 25 (https://doi.org/10.1007/s11101-022-09816-1)
3. M. Jug, M. Z. Koncic, I. Kosalec, *LWT Food Sci. Technol.* **57** (2014) 530 (https://doi.org/10.1016/j.lwt.2014.02.006)
4. R. D. Vargas-Sánchez, A. M. Mendoza-Wilson, G. R. Torrescano-Urrutia, A. Sánchez-Escalante, *Comput. Theor. Chem.* **1066** (2015) 7 (https://doi.org/10.1016/j.comptc.2015.05.003)
5. A. F. N. Ramos, J. L. Miranda, *J. Venom Anim. Toxins Incl. Trop. Dis.* **13** (2007) 697 (https://doi.org/10.1590/S1678-91992007000400002)
6. J. M. Sforcin, *Phytother. Res.* **30** (2016) 894 (https://doi.org/10.1002/ptr.5605)
7. M. L. F. Bittencourt, P. R. Ribeiro, R. L.P. Franco, H. W. M. Hilhorst, R. D. de Castro, L. G. Fernandez, *Food Res. Int.* **76** (2015) 449 (https://doi.org/10.1016/j.foodres.2015.07.008)
8. J. M. Sforcin, V. Bankova, *J. Ethnopharmacol.* **133** (2011) 253 (https://doi.org/10.1016/j.jep.2010.10.032)
9. F. I. Abdullaev, L. Riveron-Negrete, H. Caballero-Orgeta, J. M. Hernandez, I. Perez-Lopez, R. Pereda-Miranda, J. J. Espinosa-Aguirre, *Toxicol. In Vitro* **17** (2003) 731 (https://doi.org/10.1016/s0887-2333(03)00098-5)
10. E. H. Çakır, Y. Şirin, S. Kolaylı, Z. Can, *J. Apither. Nat.* **1** (2018) 13 (https://dergipark.org.tr/en/download/article-file/449611)
11. B. J. Dean, T. M. Brooks, G. Hodsonwalker, D. H. Hutson, *Mutat. Res.* **153** (1985) 57 (https://doi.org/10.1016/0165-1110(85)90005-3)
12. K. Mortelmans, E. Zeiger, *Mutat. Res.* **455** (2000) 29 (https:/doi.org/10.1016/s0027-5107(00)00064-6)
13. D. M. Maron, B. N. Ames, *Mutat. Res.* **113** (1983) 173 (https://doi.org/10.1016/0165-1161(83)90010-9)
14. P. S. Negi, G. K. Jayaprakasha, B. S. Jena, *Food Chem.* **80** (2003) 393 (https://doi.org/10.1016/S0308-8146(02)00279-0)
15. I. Sofrenić, J. Ljujić, K. Simić, S. Ivanović, J. S. Jeremić, A. Ćirić, M. Soković, B. Anđelković, *J. Serb. Chem. Soc.* **86** (2021) 1205 (https://doi.org/10.2298/JSC210812086S)

16. M. Arslan, Y. Sevgiler, C. Guven, Z. T. Murathan, N. Erbil, D. Yildirim, M. Buyukleyla, S. Karadas, R. Celik, E. Rencuzogullari, *Arh. Hig. Rada. Toksikol.* **72** (2021) 53 (https://doi.org/10.2478/aiht-2021-72-3492)

17. A. Sorucu, H. H. Oruc, *J. Food Measur. Character.* **13** (2019) 2461 (https://doi.org/10.1007/s11694-019-00166-9)

18. E. Sevim, A. Bozdeveci, M. Pinarbaş, M. Kekeçoğlu, R. Akpinar, M. Keskin, S. Kolayli, S. A. Karaoğlu, *U. Bee J.* **21** (2021) 177 (https://doi.org/10.31467/uluaricilik.976536)

19. M. Donmez, S. Karadeniz, T. Yoldas, G. Aydin, P. Karagul, O. Aksu, P. G. Rasgele, IJTCMR **1** (2020) 137 (https://dergipark.org.tr/en/download/article-file/1407649)

20. T. Ozdal, F. D. Ceylan, N. Eroglu, M. Kaplan, E. O. Olgun, E. Capanoglu, *Food Res. Internat.* **122** (2019) 528 (https://doi.org/10.1016/j.foodres.2019.05.028)

21. P. G. Rasgele, M. Kekecoglu, *J. Apither. Nat.* **1** (2018) 20 (https://dergipark.org.tr/en/download/article-file/562828)

22. R. Chang, D. Piló-Veloso, S. A. L. Morais, E. A. Nascimento, *Brazilian J. Pharmacogn.* **18** (2008) 549 (https://doi.org/10.1590/S0102-695X2008000400009)

23. F. G. da Silva Dantas, P. F. de Castilho, A. A. de Almeida-Apolonio, R. P. de Araújo, K. M. P. de Oliveira, *Mutat. Res./Reviews Mutat. Res.* **786** (2020) 108338 (https://doi.org/10.1016/j.mrrev.2020.108338)

24. K. Słoczyńska, B. Powroźnik, E. Pękala, A. M. Waszkielewicz, *J. Appl. Genetics* **55** (2014) 273 (https://doi.org/10.1007/s13353-014-0198-9)

25. M. M. Nichitoi, A. M. Josceanu, R. D. Isopescu, G. O. Isopencu, E. I. Geana, C. T. Ciucure, V. Lavric, *Sci. Rep.* **11** (2021) 1 (https://doi.org/10.1038/s41598-021-97130-9)

26. D. López-Romero, J. A. Izquierdo-Vega, J. A. Morales-González, E. Madrigal-Bujaidar, G. Chamorro-Cevallos, M. Sánchez-Gutiérrez, G. Betanzos-Cabrera, I. Alvarez-Gonzalez, A. Morales-González, E. Madrigal-Santillán, *Nutrients* **10** (2018) 1954 (https://doi.org/10.3390/nu10121954)

27. M. Majidinia, A. Bishayee, B. Yousefi, *DNA Repair* **82** (2019) 102679 (https://doi.org/10.1016/j.dnarep.2019.102679)

28. E. A. Varanda, R. Monti, D. C. Tavares, *Teratogen. Carcinogen. Mutagen.* **19** (1999) 403 (https://doi.org/10.1002/(SICI)1520-6866(1999)19:6<403::AID-TCM4>3.0.CO;2-2)

29. S. N. Jeng, M. K. Shih, C. M. Kao, T. Z. Liu, S. C. Chen, *Food Chem. Toxicol.* **38** (2000) 893 (https://doi.org/10.1016/s0278-6915(00)00081-8)

30. J. Y. Fu, Y. Xia, Y. Y. Zheng, *Biomed. Environ. Sci.* **17** (2004) 469 (https://www.besjournal.com/en/article/id/ef7d9720-e640-4de1-b0aa-8829172e2920)

31. M. I. N. Moreno, I. C. Zampini, R. M. Ordóñez, G. S. Jaime, M. A. Vattuone, M. I. Isla, *J. Agric. Food Chem.* **53** (2005) 8957 (https://doi.org/10.1021/jf0513359)

32. N. E. Bayram, M. Karadayi, M. Gulluce, S. Bayram, K. Sorkun, G. C. Oz, M. N. Aydogan, T. Y. Koc, B. Alaylar, B. Salih, *Mellifera* **15** (2015) 29 (https://dergipark.org.tr/en/pub/mellifera/issue/17834/186991)

33. R. O. A. Lima, A. P. Bazo, R. A. Said, J. M. Sforcin, V. Bankova, B. R. Darros, D. M. F. Salvadori, *Environ. Mol. Mutagen.* **45** (2005) 8 (https://doi.org/10.1002/em.20082)

34. M. M. Roberto, S. T. Matsumoto, C. M. Jamal, O. Malaspina, M. A. Marin-Morales, *Toxicol. In Vitro* **33** (2016) 9 (https://doi.org/10.1016/j.tiv.2016.02.005).

Comparative study of chemical composition and the antimutagenic activity of propolis extracts obtained by means of various solvents

PINAR G. RASGELE[1]*, NISA SIPAHI[2] and GULDEN YILMAZ[3]

[1]Duzce University, Faculty of Agriculture, Department of Biosystems Engineering, Duzce, Turkey, [2]Duzce University, Traditional and Complementary Medicine Application and Research Center, Duzce, Turkey and [3]Trakya University, Faculty of Science, Department of Biology, Balkan Campus, 22030, Edirne, Turkey

＊ Corresponding author. E-mail: pinargocrasgele@gmail.com
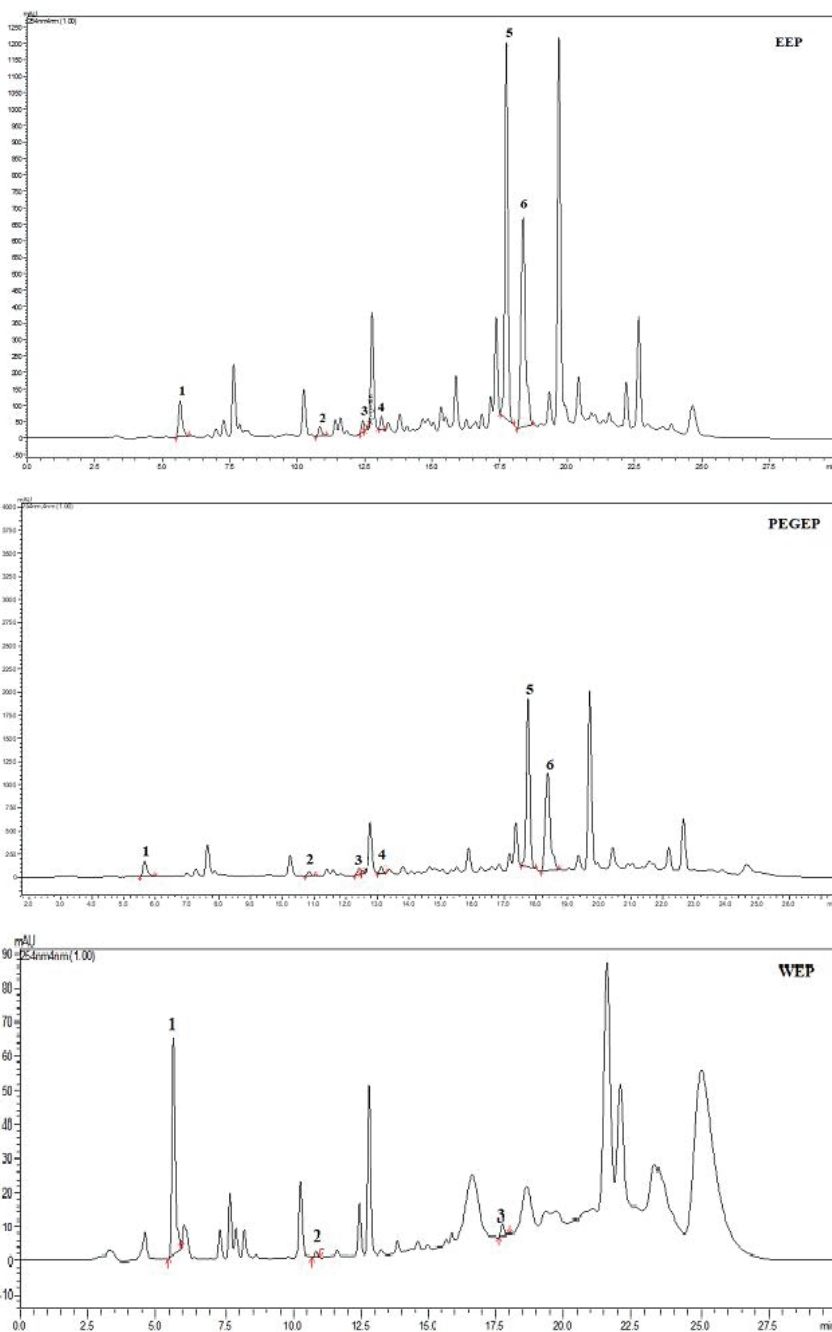
Fig. S-1. Chromatograms of different propolis extracts EEP, PEGEP and WEP with identified marker compound. (1) cafeic acid; (2) quercetin; (3) apigenin; (4) kaempferol; (5) chrysin; (6) caffeic acid phenyl ester.

Table S-I. Chemical compositions of different extracts of propolis by LC-MS/MS

| | Hydrolysis method | | | | | |
| | EEP | | PEGEP | | WEP | |
Compounds	RT	Conc (ng/ml)	RT	Conc (ng/ml)	RT	Conc (ng/ml)
Gallic Acid	1.669	6089.82	1.685	6372.29	1.694	**7863.34**
Protocatechuic Acid	1.822	16942.81	1.822	15454.19	1.813	**39990.99**
2,5-Dihydroxybenzoic ac.	2.175	255.23	2.175	**369.86**	2.158	196.24
Syringic Acid	3.166	0.00	3.807	0.00	3.925	0.00
Caffeic Acid	3.731	1741671.45	3.740	**3950734.23**	3.706	1065005.09
Chlorogenic Acid	3.660	21752.79	3.677	**228606.63**	3.711	2670.34
Salicyclic Acid	3.750	456.41	3.767	450.16	3.767	**526.15**
Catechin	3.863	40.07	3.829	**445.56**	3.821	118.50
Hesperidin	3.978	**192.34**	3.953	192.20	3.860	2.75
Verbascoside	4.096	0.00	3.919	0.00	3.944	0.00
Rutin	3.970	**602.18**	3.936	574.56	3.953	7.75
2-Hydroxytranscinnamic ac.	4.020	0.00	3.986	0.00	4.003	0.00
p-Coumaric Acid	4.019	**280024.06**	3.985	121966.77	3.994	53546.57
Sinapic Acid	3.890	0.00	3.899	0.00	4.000	0.00
Naringin	4.038	0.00	3.877	0.00	3.903	0.00
Trans Ferrulic Acid	4.061	**636401.30**	4.052	250267.13	4.061	73149.18
Ethyl Gallate	4.069	24.64	4.145	0.53	4.103	2.15
Oleuropein	4.055	0.00	4.123	0.00	4.097	0.00
Phlorizin	4.114	**30.14**	4.148	14.31	4.165	0.99
Indole-3-Acetic Acid	4.458	0.00	4.458	0.00	4.483	0.00
Myricetin	4.166	0.00	4.191	0.00	4.183	0.00
Resveratrol	4.389	**55.65**	4.355	52.88	4.389	0.00
Aloin A	4.233	0.00	4.258	0.00	4.182	0.00
Propyl Gallate	4.136	0.00	3.713	0.00	4.000	0.00
Quercetin	4.268	**1402.40**	4.268	1231.89	4.268	266.20
Lutolein	4.302	170.91	4.311	**199.58**	4.302	32.62
Abscisic Acid	4.304	174.71	4.312	**182.13**	4.312	152.30
Naringenin	4.395	2010.29	4.395	2094.61	4.395	**2426.36**
Kaempferol	4.362	862.92	4.353	**924.16**	4.328	362.76
Isorhamnetin	4.327	3320.89	4.327	**3387.57**	4.327	724.52
Genistein	4.631	**92.75**	4.631	89.23	4.590	52.05
Apigenin	4.439	146.03	4.438	**155.96**	4.438	45.80
Jasmonic Acid	4.423	0.00	4.390	0.00	4.423	0.00

EEP: Ethanolic extract of propolis; PEGEP: Polyethylene glycol extract of propolis; WEP: Water extract of propolis; RT: Retention time; Conc: Concentration

Table S-II. Chemical compositions of different extracts of propolis by LC-MS/MS

	Acidic hydrolysis method					
	EEP		PEGEP		WEP	
Compounds	**RT**	**Conc (ng/ml)**	**RT**	**Conc (ng/ml)**	**RT**	**Conc (ng/ml)**
Gallic Acid	1.694	51135.74	1.694	52561.86	1.694	**56182.52**
Protocatechuic Acid	1.839	34490.72	1.830	35940.28	1.830	**65688.17**
2,5-Dihydroxybenzoic Ac.	2.192	125.78	2.184	**162.90**	2.184	75.53
Syringic Acid	3.892	0.00	3.209	0.00	3.292	0.00
Caffeic Acid	3.740	2449797.25	3.757	**4526984.01**	3.706	1263642.70
Chlorogenic Acid	3.677	12085.21	3.685	**65752.41**	3.719	3968.67
Salicyclic Acid	3.767	230.58	3.733	29.78	3.767	**471.65**
Catechin	3.888	41.98	3.838	182.14	3.838	**220.90**
Hesperidin	3.987	41.45	3.970	**58.77**	4.037	2.63
Verbascoside	4.113	0.00	4.333	0.00	3.927	0.00
Rutin	3.978	**179.01**	3.961	156.02	3.987	9.28
2-Hydroxytranscinnamic ac.	4.028	0.00	3.994	0.00	4.003	0.00
p-Coumaric Acid	4.028	**218816.83**	3.994	91937.97	4.002	46524.13
Sinapic Acid	4.490	0.00	4.178	0.00	3.594	0.00
Naringin	3.996	0.00	3.962	0.00	4.063	0.00
Trans Ferrulic Acid	4.061	**460120.78**	4.069	196675.58	4.061	58382.57
Ethyl Gallate	4.086	**36.61**	4.162	1.09	4.120	2.93
Oleuropein	4.123	0.00	4.199	0.00	3.895	0.00
Phlorizin	4.131	**9.41**	4.123	3.23	4.199	0.00
Indole-3-Acetic Acid	4.467	0.00	4.467	0.00	4.483	0.00
Myricetin	3.930	226.90	3.930	111.63	3.955	29.97
Resveratrol	4.380	87.62	4.406	**121.10**	4.448	55.22
Aloin A	4.233	0.00	4.191	0.00	4.199	0.00
Propyl Gallate	4.212	0.00	3.773	0.00	4.077	0.00
Quercetin	4.285	**931.10**	4.285	732.08	4.268	276.60
Lutolein	4.319	**169.78**	4.319	165.64	4.311	52.59
Abscisic Acid	4.304	100.17	4.312	**135.74**	4.329	72.39
Naringenin	4.404	**3499.25**	4.404	3187.08	4.395	2158.61
Kaempferol	4.379	**799.68**	4.379	784.50	4.319	340.09
Isorhamnetin	4.335	**3616.81**	4.335	3367.07	4.327	871.79
Genistein	4.623	121.96	4.623	**180.38**	4.598	61.16
Apigenin	4.438	192.93	4.438	**193.18**	4.447	61.06
Jasmonic Acid	4.449	0.00	4.466	0.00	4.423	0.00

EEP: Ethanolic extract of propolis; PEGEP: Polyethylene glycol extract of propolis; WEP: Water extract of propolis; RT: Retention time; Conc: Concentration

Physicochemical properties of the heterogeneous system Li$_2$CO$_3$–Na$_2$CO$_3$–K$_2$CO$_3$/MgO

IRINA D. ZAKIRYANOVA*, ELENA V. NIKOLAEVA and IRAIDA V. KORZUN

Institute of High-Temperature Electrochemistry, 20 Akademicheskaya Street, 620066 Yekaterinburg, Russia

Abstract: The structure, conductivity, melting points and caloric melting effects of the (Li$_2$CO$_3$–Na$_2$CO$_3$–K$_2$CO$_3$)$_{eut}$ melt/MgO nanopowder heterogeneous system with MgO concentration up to 70 vol. % have been investigated. A wide variety of methods (DSC, XRD, BET, high resolution scanning electron microscope, AC impedance method, IR and Raman spectroscopy) were used to evaluate samples and research. It is revealed that at the values of effective thickness of the salt phase interlayer between MgO particles below 100 nm there is an abrupt decrease in the melting points of the salt and the normalized phase transition enthalpy of the heterogeneous system. The activation energy of the electrical conductivity rises as the values of effective thickness of the melt phase interlayer between MgO particles decreases. The study established the lack of any chemical interaction between MgO and carbonate melt at 400–600 °C. *In situ* Raman spectroscopy of the (Li$_2$CO$_3$–Na$_2$CO$_3$–K$_2$CO$_3$)$_{eut}$ melt/MgO nanopowder systems revealed the solvation of solid particles by salt-melt ions.

Keywords: molten carbonate; composite; conductivity; melting points.

INTRODUCTION

To find the optimal operating medium for the carbonate fuel cells (MCFC), the reliable physicochemical properties of heterogeneous systems based on the molten alkali metal carbonates are demanded.[1]

Molten alkali metal carbonates are chemically aggressive towards the construction materials. This fact limits their wide industrial application. Electrochemical cells with porous ceramic matrices filled with molten alkali metals carbonates are usually chosen for industrial usage.[1–4] Currently fuel cells based on binary Li/K or Li/Na molten carbonates with the γ-LiAlO$_2$ matrix are used. The operating temperature of such element is 650 °C.

627

The usage of the carbonate fuel cells is considered to be economically feasible in the case of at least 40000 h operation. The instability of the γ-LiAlO$_2$ phase under operation conditions is one of the major causes of the fuel cell degradation. At the temperatures above 700 °C the γ-LiAlO$_2$ modification transfers to the α-LiAlO$_2$ phase. However, with the inevitable in the MCFC operations presence of CO$_2$, this transfer takes place at the operation temperatures. The α-LiAlO$_2$ phase is seen to be more stable than γ-LiAlO$_2$ phase both in Li/K and Li/Na molten carbonates at 650 °C in CO$_2$ atmosphere.[5]

The resulting α-LiAlO$_2$ has a larger particle size than γ-LiAlO$_2$. Therefore, pore size in the matrix increase, and the mechanical strength degrade up to destruction. During the fuel cell operation the electrical conductivity decrease, and the operational performance degrade.[5]

These problems motivate the search of the materials that chemically inert to molten alkali metal carbonates and could be an alternative to γ-LiAlO$_2$.

We have previously studied the structure, conductivity and caloric melting effects of the (Li$_2$CO$_3$–Na$_2$CO$_3$–K$_2$CO$_3$)$_{eut}$ melt/α-Al$_2$O$_3$ nanopowder heterogeneous systems.[6–8] Raman spectroscopy and XRD analysis established the lack of any chemical interaction between α-Al$_2$O$_3$ and carbonate melt at 400–550 °C.

Previous articles[9–11] reported the results of the research on physicochemical properties of heterogeneous systems (Li$_2$CO$_3$–K$_2$CO$_3$)$_{eut}$ melt/CeO$_2$ (or α-Al$_2$O$_3$) and Li$_2$CO$_3$ melt/MgO, in which the liquid phase concentration in the studied systems is within the interval of 5 to 40 vol. %. The decrease in the relative melting enthalpy and growth of the electrical conductivity activation energy, at small liquid phase concentrations, were determined. The electrical conductivity of a Li$_2$CO$_3$ melt in a MgO matrix was compared with that in a γ-LiAlO$_2$ matrix and shown to be better.[10] Authors[10] did not prove this fact and their explanation is limited to broad terms about the influence of the solid phase on the melt conductivity.

Magnesium oxide has a stable cubic crystalline lattice (*Fm3m*) up to the melting point at 2825 °C and it is considered to be one of the most accessible and well-studied materials.

The present work is aimed at the study of the physicochemical properties of the (Li$_2$CO$_3$–Na$_2$CO$_3$–K$_2$CO$_3$)$_{eut}$ melt/MgO nanopowder heterogeneous system in order to evaluate the capability of this magnesia to be used as the filling material of the MCFC matrix. We focused on the study of the electrolyte conductivity, which is one of the most important characteristics of the fuel cell operation, as well as on the study of the melting point and melting enthalpy of the salt phase in heterogeneous systems. Raman spectroscopy allowed us to obtain *in situ* data on the peculiarities of the interparticle interaction and behavior of the CO$_3^{2-}$ in the presence of the MgO nanopowder.

EXPERIMENTAL

Methods

The analysis of the phase composition of the initial salt and the frozen samples after high temperature experiments was performed using an automated X-ray diffractometer Rigaku D/MAX-2200VL/PC (Japan). The average size of the crystallites (areas of the coherent scattering) of the MgO powder was assessed using the Scherrer equation[12] and the data on the half width of diffraction peaks obtained by a diffractometer Shimadzu XRD-7000 (Japan). A certified silicon powder was used as a reference standard that denoted the instrumental input into the peak width. The samples certification on the amount of admixtures was performed using the IR absorption spectroscopy method by the IR-Fourier spectrometer Tensor 27 (Bruker, Germany). The specific surface area of the MgO powders was determined using the BET method by a SORBI (Meta, Russian Federation) device. The morphology of MgO powder was investigated by SEM (Tescan Mira 3 LMU, Czech Republic).

The melting points and the thermal effects were measured using a synchronous thermal analyzer STA 449C Jupiter (NETZSCH, Germany). The measurements were performed in pure argon atmosphere (99.998 %) at the sample heating rate of 10 K/min (Pt–Rh crucibles). The error of the phase transitions temperature measurements did not exceed 1 K. The differential scanning calorimetry (DSC) measurements of the heterogeneous system provided reproducible results, and the data on the second and the following heating of the samples were used for analysis.

Electrical resistance of heterogeneous systems, contain up to 50 vol. % of MgO, was determined *via* godograph of the impedance. AC impedance was measured under Ar atmosphere with the impedancemeter Z-1500J (Elins, Russian Federation) in a frequency range 20 Hz–1.5 MHz using platinum (Pt) electrodes. Specific electrical conductivity was calculated according to the equation: $\sigma = K/R$, where K is the cell constant (cm^{-1}), and R is the ohmic resistance of electrolyte (Ohm). The cell constant was determined using the electrical conductivity values of molten KNO$_3$. The cell was standardized according to the melt with the known values of electrical conductivity under the same conditions as at the experiments on the determination of the electrical resistance of the systems under study, *i.e.*, at the fixed immersion depth of the electrode into the melt, at the same interelectrode distance and in the same temperature range. At least three parallel measurements were made for each series of experiments.

Raman spectra of high temperature heterogeneous systems with MgO concentrations 23 and 70 vol. %, were recorded by a fiber optic spectrometric complex Ava-Raman (Avantes, Netherlands), which includes a source of monochromatic laser emission (50 mW, λ = 532 nm, 180° registration scheme). The spectrometer is equipped with a notch-filter, which limits intense Rayleigh scattering in the region of 150 cm^{-1}. The determination error of the wave numbers was 1 cm^{-1}. An original high temperature optic attachment was developed and successfully tested previously at the *in situ* analysis of interaction between barium oxide or lead oxide and molten alkali metal chlorides.[13,14] In this work the attachment was used to record spectra of the heterogeneous systems. A platinum crucible of the 20 mm height and 12 mm diameter was used as a container for the heterogeneous systems under study. The spectra were recorded at the temperatures above the melting point of carbonate eutectic (398 °C) in air atmosphere. The spectral characterizations are reproducible both in a series of experiments and in heating-cooling modes for the desired composition of a heterogeneous system. The presence of any interaction products of the container material (Pt) and the heterogeneous systems under study has not been detected by the XRD analysis of the frozen fusions.

Preparation and certification of the samples

Chemically pure grade Li_2CO_3, Na_2CO_3 and K_2CO_3 ("Vekton", St. Petersburg, Russian Federation) were preliminary dehydrated under vacuum at stepwise temperature growth and melted in argon atmosphere.

The carbonate eutectic mixture $(Li_2CO_3–Na_2CO_3–K_2CO_3)_{eut}$ (43.5, 31.5 and 25.0 mol %, respectively) was prepared by fusion of the weighted portions of the salts. The salts were thoroughly mixed, dried at reduced pressure at 200 °C for 1 h to remove traces of adsorbed H_2O, heated in a CO_2 atmosphere, and held for 5 h at 800 °C to obtain homogeneous molten mixture. The frozen eutectic carbonate mixture was examined by DSC analysis. The melting point (T_m = 398 °C) and the melting enthalpy (ΔH_{eut} = 277 J/g) of eutectic composition are in agreement with the published data.[15]

MgO powder (analytically pure, "Chimreaktivsnab," Ufa, Russian Federation) was confirmed to be a single phase using XRD and IR spectroscopy. The IR spectrum of MgO showed a strong broad band in the range 400–700 cm^{-1} that corresponded to Mg–O vibrations. There are no any vibration bands inherent to adsorbed water or hydroxyl groups. Magnesium oxide of different dispersity was used: average crystallites size of 95 nm and specific surface area (S) of 9.4±0.1 m^2/g; and crystallite size of 25 nm and S = 15.0±0.1 m^2/g. The morphology of MgO powder investigated by SEM is shown in Fig. 1.
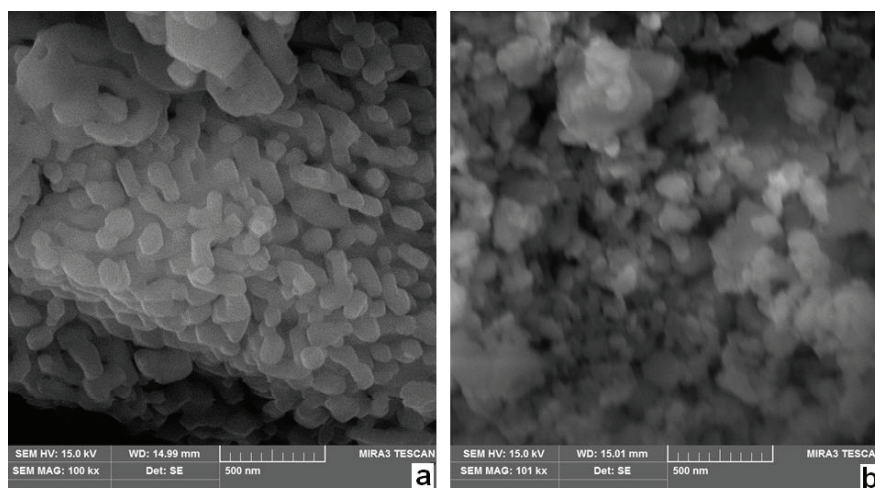
Fig. 1. The morphology of MgO powder (S = 9.4 m^2/g – a; S = 15.0 m^2/g – b).

The required amounts of carbonate eutectic and MgO were ground in an agate mortar and loaded into the instrument high-temperature accessory. The lack of any sedimentation of finely dispersed powders in molten $(Li_2CO_3–Na_2CO_3–K_2CO_3)_{eut}$ in a course of measurements was shown earlier.[8]

To analyze the changes of the physicochemical properties of the heterogeneous systems containing solid particles of different morphology with different geometrical parameters (specific surface area, crystallites average size) we used the approach suggested earlier.[11] The effective thickness (d) of the salt phase interlayer between MgO particles was taken into account. Parameter d was calculated according to the ratio:

$$d = \frac{V_{eut}}{Sm_{MgO}} \qquad (1)$$

where V$_{eut}$ is the salt composition volume and m$_{MgO}$ is the MgO weight.

<div align="center">RESULTS AND DISCUSSION</div>

DSC studies

DSC curves of the (Li$_2$CO$_3$–Na$_2$CO$_3$–K$_2$CO$_3$)$_{eut}$/MgO nanopowder hetero-geneous systems with MgO concentrations up to 70 vol. % are depicted in Fig. 2. It was found that the melting point T_m and melting enthalpy ΔH reduced with an increase of the MgO nanopowder content in the system. This fact accounts for the influence of the salt – oxide interphase boundary on the thermodynamic parameters of ionic salt.
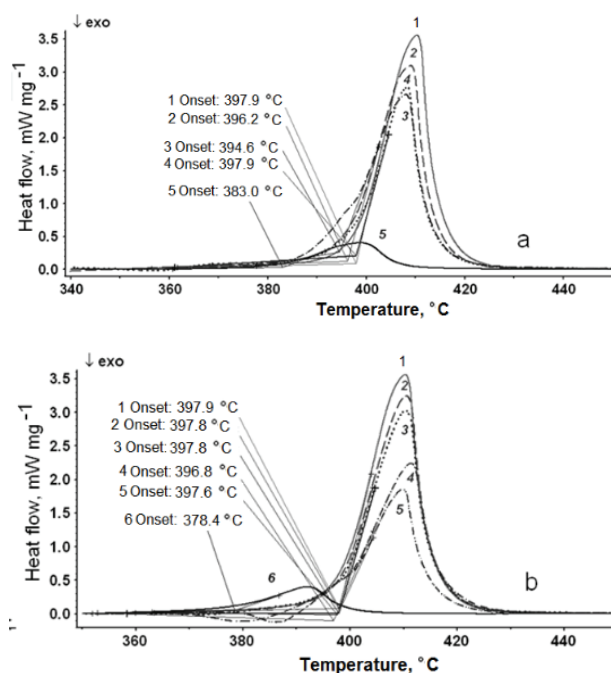
Fig. 2. DSC curves of the (Li$_2$CO$_3$–Na$_2$CO$_3$–K$_2$CO$_3$)$_{eut}$/MgO heterogeneous systems, MgO (vol. %): 1 – 0; 2 – 4.8; 3 – 11.1; 4 – 29.7; 5 – 70.1; S = 9.4 m^2/g – a; 1 – 0; 2 - 4.9; 3 – 8.9; 4 – 19.1; 5 – 28.6; 6 – 68.8; S = 15.0 m^2/g – b.

Fig. 3 demonstrates the dependences of obtained melting points (T_m) and normalized melting enthalpies (ΔH_{norm}) on the effective thickness d. Here ΔH_{norm} defined as $\Delta H_{norm} = \Delta H/\Delta H_{eut}$. From Fig. 3 we see that at d less than 100 nm, both the T_m and ΔH_{norm} of the salt phase in the heterogeneous system decreased drastically.
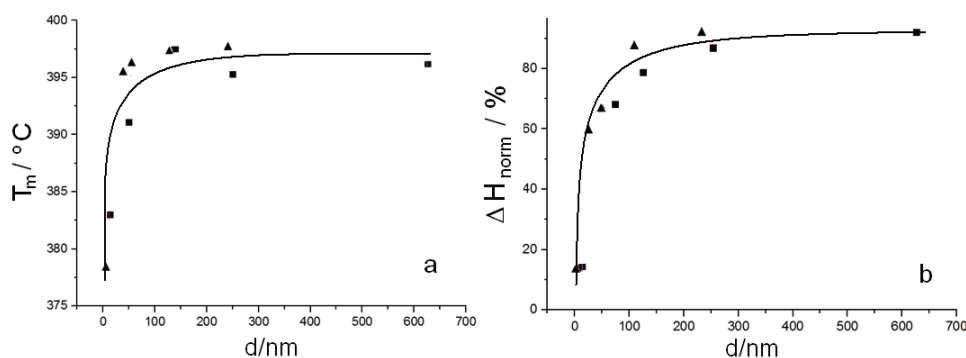
Fig. 3. Melting points (a) and the normalized melting enthalpies (b) of the salt phase in the heterogeneous system $(Li_2CO_3–Na_2CO_3–K_2CO_3)_{eut}/MgO$ ($S = 9.4$ m^2/g (squares), $S = 15.0$ m^2/g (triangles)).

At the temperatures below T_m the studied heterogeneous system may be analyzed as a nanocomposite,[16] which is composed of the alkali metal carbonates matrix and MgO powder filler. The interphase boundaries are known to contribute to the crystal defectiveness, which causes changes in thermodynamic parameters of phase transitions. In particular, the values of melting points and melting enthalpy provide information on the crystal disorder in near of melting temperature.[16] A drastic decrease of the T_m and ΔH_{norm} of the ionic salt in nanocomposite (Fig. 3) may be associated with the increase in defects concentration in the alkali metals carbonates crystalline lattice. It is important to note, that the effect does not depend on morphology and size of MgO particle, but only on effective thickness of the salt phase interlayer between MgO particles, which emphasizes its versatility to describe the physicochemical properties of composites ionic salt––oxide filler.

Electrical conductivity

The next stage of our work was devoted to the determination of the specific electrical conductivity of the $(Li_2CO_3–Na_2CO_3–K_2CO_3)_{eut}/MgO$ heterogeneous system with the magnesium oxide concentration within the interval of 0 to 50 vol. %. The obtained experimental results are presented in Fig. 4a. In all cases the conductivity decreases with an increase of the solid content. Thus the specific conductivity reduces at the order of magnitude when volume fraction of MgO is equal 40 vol. %. The temperature dependence of the specific electrical conductivity, σ, can be approximated by linear equation as follows:

$$\ln \sigma = -E_a/RT + A \qquad (2)$$

where E_a is the activation energy, R is the universal gas constant, A is the constant. The obtained dependencies are shown in Fig. 4b. Therefore, the values of E_a can be calculated, and in Fig. 5 presented the dependences of E_a on the effective

thickness of the carbonate melt interlayer between MgO particles (d). From Fig. 5 we see that at d less than 100 nm the activation energy of the specific electrical conductivity increase drastically. Returning to the data on T_m and ΔH_{norm}, it may be suggested that in $(Li_2CO_3–Na_2CO_3–K_2CO_3)_{eut}$/MgO heterogeneous system $d = 100$ nm is the boundary thickness of the salt phase between MgO particles, and for lesser values d the properties change significantly.
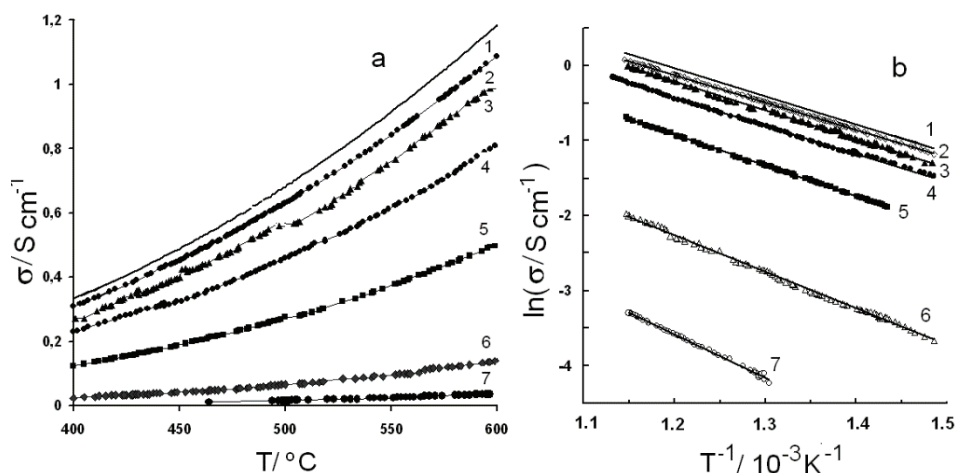
Fig. 4. Temperature dependences of the specific electric conductivity of the $(Li_2CO_3–Na_2CO_3–K_2CO_3)_{eut}$/MgO heterogeneous systems, MgO (vol. %): 1 – 0; 2 – 4.93; 3 – 9.90; 4 – 19.44; 5 – 29.45; 6 – 39.38; 7 – 49.52.
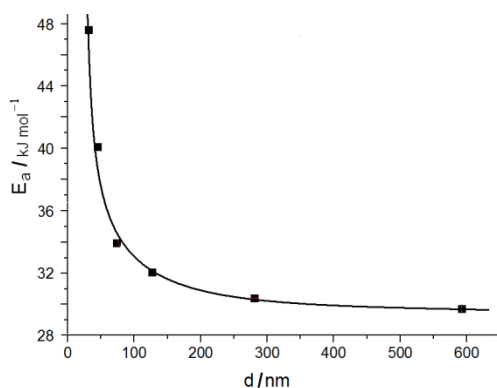
Fig. 5. Variation of the activation energy of the electrical conductivity with the effective average thickness of liquid phase for $(Li_2CO_3–Na_2CO_3–K_2CO_3)_{eut}$/MgO heterogeneous system.

The obtained data demonstrate that the charge transfer process near the solid phase particles surface is hindered and that there is an interaction between a disperse filler (solid MgO particles) and dispersing medium (molten carbonate eutectic). To specify the nature of this interaction we used the Raman spectroscopy.

Raman spectra

Raman spectra of molten $(Li_2CO_3–Na_2CO_3–K_2CO_3)_{eut}$ and $(Li_2CO_3–Na_2CO_3–K_2CO_3)_{eut}$ melt/MgO heterogeneous system with the magnesium oxide concentration up to 70 vol. % were qualitatively similar. Fig. 6 shows a typical spectrum of the $(Li_2CO_3–Na_2CO_3–K_2CO_3)_{eut}$ melt/MgO heterogeneous system. According to the selection rule, crystals of the *Fm3m* symmetry, such as magnesium oxide, have no the vibrational bands in the Raman spectra.
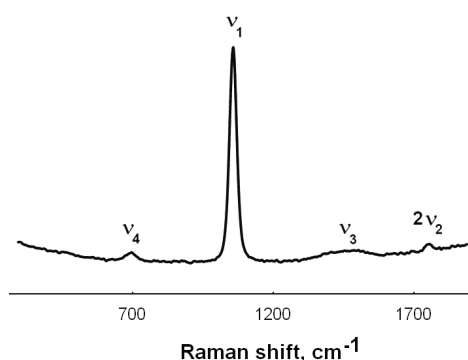
Fig. 6. Raman spectrum of the $(Li_2CO_3–Na_2CO_3–K_2CO_3)_{eut}$ melt/MgO heterogeneous system, 500 °C.

A strong band corresponding to fully symmetric stretching vibration ν_1 of CO_3^{2-} was observed at 1065 cm^{-1}. A weak band for bending vibration ν_4 near 700 cm^{-1}; a broad split band with maxima at 1390 and 1495 cm^{-1} for asymmetric stretching vibration ν_3; and overtone $2\nu_2$ near 1760 cm^{-1} of CO_3^{2-} were observed. Splitting of the ν_3 band into two components indicated that the symmetry of the CO_3^{2-} – anion reduced from D_{3h} to C_{2v}.[17] We found no bands point to the chemical interaction of magnesium oxide and $(Li_2CO_3–Na_2CO_3–K_2CO_3)_{eut}$ melt even with the long-term (4–5 h) exposure of $(Li_2CO_3–Na_2CO_3–K_2CO_3)_{eut}$ melt/MgO systems at 400–600 °C.

The XRD of the $(Li_2CO_3-Na_2CO_3-K_2CO_3)_{eut}$/MgO heterogeneous system after the high-temperature spectral experiments demonstrated the presence of $(Li_2CO_3–Na_2CO_3–K_2CO_3)_{euc}$ salt and MgO phases (Fig. 7).

However, we noticed a difference in the profiles of the vibration band ν_1 of the $(Li_2CO_3–Na_2CO_3–K_2CO_3)_{eut}$ melt and $(Li_2CO_3–Na_2CO_3–K_2CO_3)_{eut}$ melt/MgO heterogeneous systems: for molten $(Li_2CO_3–Na_2CO_3–K_2CO_3)_{eut}$ it was found to be symmetrical and to be well described by the Gaussian function (Fig. 8 (1)), while for $(Li_2CO_3–Na_2CO_3–K_2CO_3)_{eut}$ melt/MgO heterogeneous system ν_1 band profile is asymmetric because of the appearance of the additional high-frequency compound (Fig. 8, band C). In addition, under isothermal conditions the relative intensity of the high-frequency component (Fig. 8, band C) in the ν_1 band profile increases as the oxide phase specific surface area increase (Fig. 8 (2, 3)).
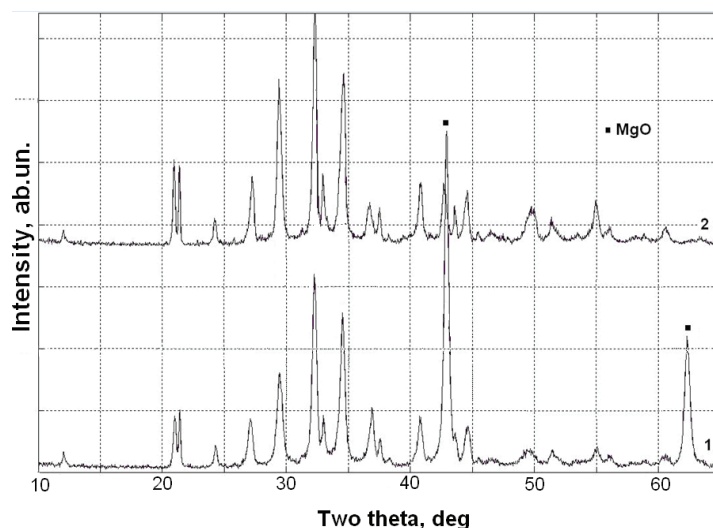
Fig. 7. XRD analysis (20 °C) of the (Li$_2$CO$_3$–Na$_2$CO$_3$–K$_2$CO$_3$)$_{euc}$/MgO heterogeneous system, MgO (vol. %): 1 – 70; 2 – 0.
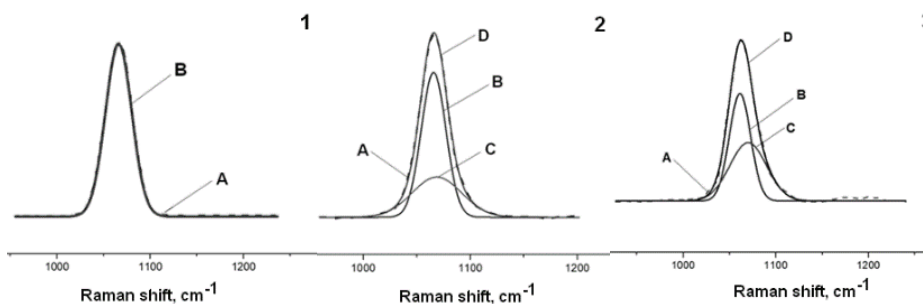
Fig. 8. Envelope of CO$_3^{2-}$ vibrational band ν$_1$ in the Raman spectrum of (Li$_2$CO$_3$–Na$_2$CO$_3$–K$_2$CO$_3$)$_{euc}$ melt at 500 °C: experimental spectrum (A) and Gaussian approximation (B) of band – 1; envelope of the ν$_1$ band for (Li$_2$CO$_3$–Na$_2$CO$_3$–K$_2$CO$_3$)$_{eut}$ melt/MgO system, 70 vol. % MgO, S = 9.4 m^2/g – 2; S = 15.0 m^2/g – 3: experimental spectrum (A), Gaussian deconvolution components (B, C), and additive curve of B and C (D).

Previously was shown[18] that strong low-frequency component of the ν$_1$ band (Fig. 8, band B) for the disperse system (Li$_2$CO$_3$–Na$_2$CO$_3$–K$_2$CO$_3$)$_{eut}$ melt/MgO nanopowder is the ν$_1$ band of the carbonate ion in melt bulk, while a high-frequency component in the ν$_1$ band profile (Fig. 8, band C) associated with the CO$_3^{2-}$, adsorbed at the solid phase particle surface.[18,19] That is why the relative intensity of the high-frequency component in the ν$_1$ band increases as the oxide phase specific surface area increase (Fig. 8 – 2, 3).

Salt anions adsorbed on nanopowder-particle surfaces formed solvate shells that should have considerably affected the physicochemical properties of the

high-temperature disperse system $(Li_2CO_3–Na_2CO_3–K_2CO_3)_{eut}$ melt/MgO nano-powder. In particular, solvation of salt melt ions on the developed interface of solid phase particles hinders the process of electric charge transfer. Therefore, the a significant increase of the activation energy of electrical conductivity for the $(Li_2CO_3–Na_2CO_3–K_2CO_3)_{eut}$ melt/MgO nanopowder systems may be explained by the process of molten salt ions adsorption at the surface of the MgO solid phase particles.

CONCLUSION

DSC, AC impedance method and Raman spectroscopy were used to study the structure, conductivity and caloric melting effects of the $(Li_2CO_3–Na_2CO_3–K_2CO_3)_{eut}$ melt/MgO heterogeneous systems.

The data on the thermodynamic parameters of composite systems with MgO concentration up to 70 vol. % has been obtained by the DSC method. The ano-malous decrease in the melting point and normalized melting enthalpy were obs-erved at the values of effective thickness of the salt interlayer between the oxide particles below than 100 nm. The fall in the melting point from 398 to 378 °C and a normalized enthalpy of melting by 75 % was found.

The specific electrical conductivity of the heterogeneous systems based on the molten carbonate eutectic and finely MgO powder in the temperature range of 400–600 °C and magnesium oxide concentration up to 50 vol. % has been inves-tigated. A significant increase in the activation energy of electrical conductivity from 30 to 48 kJ/mol was found when the thickness of the carbonate melt inter-layer between magnesia particles became less than 100 nm.

The appearance of an additional vibrational band of the carbonate at 1075 cm^{-1} was found in the Raman spectrum of the heterogeneous system. The band is shifted by 10 cm^{-1} to higher frequencies compared to the vibrational band of the carbonate anion in the melt bulk. This is due to the Coulomb interaction of the carbonate anion and the Mg^{2+} in the surface layer of the magnesium oxide par-ticles.

The data obtained by the *in situ* Raman spectroscopy method proved that the peculiarities of the electrical conductivity of the molten $(Li_2CO_3–Na_2CO_3–K_2CO_3)_{eut}$/MgO heterogeneous system are caused by the electrolyte ions ads-orption at the surface of the solid phase particles.

ИЗВОД

ФИЗИЧКОХЕМИЈСКЕ ОСОБИНЕ ХЕТЕРОГЕНОГ СИСТЕМА $Li_2CO_3–Na_2CO_3–K_2CO_3$/MgO

IRINA D. ZAKIRYANOVA, ELENA V. NIKOLAEVA и IRAIDA V. KORZUN

Institute of High-Temperature Electrochemistry, 20 Akademicheskaya Street, 620066 Yekaterinburg, Russia

Истражена је структура, проводност, тачке топљења и калоријски ефекти топљења хетерогене смеше растопа $(Li_2CO_3–Na_2CO_3–K_2CO_3)_{eut}$ и MgO нанопраха са концентра-

цијом MgO до 70 % запремине. За карактеризацију узорака коришћен је широк спектар метода (DSC, XRD, BET, скенирајући електронски микроскоп високе резолуције, AC импеданција, IC и Раманска спектроскопија). Показано је да постоји нагли пад вредности тачака топљења соли и нормализоване енталпије фазног прелаза хетерогеног система када је ефективна дебљина међуслоја соли између MgO честица мања од 100 nm. Енергија активације електричне проводљивости се повећава са смањењем ефективне дебљине међуслоја фазе растопа између MgO честица. Истраживање је показало да не постоји хемијска интеракција између MgO и карбонатног растопа при температурама од 400–600 °C. *In situ* Раманска спектроскопија система растоп (Li$_2$CO$_3$–Na$_2$CO$_3$–K$_2$CO$_3$)$_{eut}$//MgO нано-прах је показала солвацију чврстих честица јонима растопљених соли.

REFERENCES

1. R. Remick, D. Wheeler, *Molten Carbonate and Phosphoric Acid Stationary Fuel Cells: Overview and Gap Analysis*, National Renewable Energy Laboratory, Golden, CO, 2010 (https://www.nrel.gov/docs/fy10osti/49072.pdf)
2. M.W. Breiter, in *Electrochemical Processes in Fuel Cells,* Ed. M. Becke-Goehring, Springer, Berlin, 1969, p. 217 (https://doi.org/10.1007/978-3-642-46155-2_13)
3. S. Scaccia, *J. Mol. Liquids* **116** (2005) 67 (https://doi.org/10.1016/j.molliq.2004.07.078)
4. A. Kulkarni, S. Giddey, *J. Solid State Electrochem.* **16** (2012) 3123 (https://doi.org/10.1007/s10008-012-1771-y)
5. E. Antolini, *Ceram. Int.* **39** (2013) 3463 (https://doi.org/10.1016/j.ceramint.2012.10.236)
6. Zakir'yanova, I. Korzun, V. Khokhlov, V. Dokutovich, E. Nikolaeva, B. Antonov, *Russ. J. Appl. Chem.* **89** (2016) 1066 (https://doi.org/10.1134/S1070427216070041)
7. V. Dokutovich, V. Khokhlov, I. Zakir'yanova, *Int. J. Heat Mass Trans.* **119** (2018) 365 (https://doi.org/10.1016/j.ijheatmasstransfer.2017.11.132)
8. E. Nikolaeva, A. Bovet, I. Zakiryanova, *Zeitschrift Naturforsch., A* **73** (2018) 79 (https://doi.org/10.1515/zna-2017-0222)
9. M. Mizuhata, T. Ohashi, A. Béléké, *Int. J. Hydrogen Energy* **37** (2012) 19407 (https://doi.org/10.1016/j.ijhydene.2011.09.109)
10. M. Mizuhata, Y. Harada, G. Cha, A. Béléké, S. Deki, *J. Electrochem. Soc.* **151** (2004) 179 (https://doi.org/10.1149/1.1688798)
11. M. Mizuhata, A. Béléké, H. Watanabe, Y. Harada, S. Deki, *Electrochim. Acta* **53** (2007) 71 (https://doi.org/10.1016/j.electacta.2007.06.020)
12. R. Jenkins, R. Snyder, *Introduction to X-ray Powder Diffractometry*, John Wiley & Sons, New York, 1996 (https://doi.org/10.1002/9781118520994)
13. I. Zakir`yanova, E. Nikolaeva, A. Bove, *J. Appl. Spectrosc.* **81** (2015) 919 (https://doi.org/10.1007/s10812-015-0029-8)
14. I. Zakir′yanova, P. Arkhipov, D. Zakir′yanov, *J. Appl. Spectrosc.* **82** (2016) 920 (https://doi.org/10.1007/s10812-016-0205-5)
15. G. J. Janz, *J. Phys. Chem. Ref. Data* **17** (1988) 3 (https://srd.nist.gov/JPCRD/jpcrdS2Vol17.pdf)
16. A. Ulihin, N. Uvarov, *ECS Trans.* **16** (2009) 445 (https://doi.org/10.1149/1.3242260)
17. K. Nakamoto, *Infrared and Raman Spectra of Inorganic and Coordination Compounds: Part A: Theory and Applications in Inorganic Chemistry,* John Wiley & Sons, New York, 2009 (https://doi.org/10.1002/9780470405840)

18. I. D. Zakir′yanova, *J. Appl. Spectr*., **85** (2018) 611 (https://doi.org/10.1007/s10812-018-0694-5)
19. Béléké, M. Mizuhata, S. Deki. *Vibr. Spectrosc.* **40** (2006) 66 (https://doi.org/10.1016/j.vibspec.2005.07.002).

Use of aliphatic thiols for on-site derivatization and gas chromatographic identification of Adamsite

TOMAS ROZSYPAL*

Nuclear, Biological and Chemical Defence Institute, University of Defence, Vita Nejedleho 691, 68203 Vyskov, Czech Republic

Abstract: The report describes the development of methods for rapid and simple identification of Adamsite in mobile laboratory conditions using a field gas chromatograph coupled with mass spectrometer. Adamsite is a chemical warfare agent with unique properties that cannot be analysed without conversion to a volatile derivative. Derivatization procedures with 5 aliphatic thiols (ethanethiol, 1-propanethiol, 2-propanethiol, 1-butanethiol and 1-hexanethiol) were developed and compared. The retention characteristics of the derivatization products, peak characteristics and the formation of unwanted artifacts in the chromatograms were monitored. The influence of the reaction media and the time dependence of the reaction were also objects of interest. Other investigated parameters were the optimal reaction temperature and the volume of the derivatization agent. Mass spectra of newly created substances that are not yet included in the chemical weapons related databases were recorded. With optimal reagents (1-butanethiol and 1-hexanethiol), the calibration procedures for analyte determination were subsequently developed, and the methods were verified during the Adamsite identification test in selected environmental and urban matrices.

Keywords: mobile laboratory; chemical weapons; mass spectrometry; dumped organoarsenical.

INTRODUCTION

After the end of World War II, the states disposed large quantities of chemical weapons arsenals by dumping them into seas, oceans and rivers in various places. A lot of exact locations are not known to this day and represent significant ecological problems.[1] Munitions with arsenic chemical warfare agents (CWAs), lewisite, Adamsite, Clark I and Clark II and arsenic oil were also dumped.[2] Arsenic substances can gradually break down into various degradation

---

639

products, often very toxic.[3] Complete spontaneous decomposition of arsenic CWAs in water is expected to take more than 100 years, but for Adamsite it may take even longer.[4]

Adamsite (5-chloro-5,10-dihydrophenarsazine, DM) is an irritating and vomiting CWA, its aerosols irritate the upper respiratory system causing breathing difficulties, pain in the lungs and strong salivation. Despite its practical insolubility in water (0.064 g L^{-1}), its concentration in some dump sites is equal to the acute toxicity values of some aquatic organisms.[5] Death has been reported with excessive exposure.[6] The literature reports poor solubility even in organic solvents. The boiling point is unusually high (410 °C). Its low volatility predetermines it for use in aerosol form. Due to the very stable structure, the compound is relatively inert. It is able to last in water for many years without significant degradation. It is one of the most effective and at the same time one of the cheapest CWAs.[7]

There are a number of methods for the analysis of DM and other arsenic CWAs using adsorption on green phosphorene nanotubes,[8] liquid chromatography (LC),[9,10] handheld Raman spectrometry[11] or vapour-sampling direct gas chromatography/mass spectrometry (GC/MS).[12] However, these methods are either unsuitable for use in mobile laboratory tasks or do not reach the parameters for the required level of identification. Military mobile laboratories have specific tasks and must identify contaminants in samples on-site in a relatively short time. The groups follow NATO documentation, namely STANAG 4632[13] and AEP--66.[14] According to these documents, the mobile laboratory should be able to identify chemical substances at the so-called confirmed level. Preferably, chromatography with mass spectrometry is required to meet this criterion. Due to the time-consuming nature of the procedure (6 h for the process of acceptance of the crude sample to the presentation of the analysis protocol and issuance of recommendations), the supporting technique is GC/MS and the procedures must be reasonably rapid. Field devices are often used, which are rugged for transport, but do not reach the parameters of benchtop devices. The amount and volume of other equipment is also limited, especially by the dimensions of the laboratory, which is mostly located in a deployable container.

Some arsenic CWAs have been analysed in the past by GC without derivatization. However, this is not possible with DM due to its very low vapour pressure and other disadvantages (low linearity of the method at low concentrations due to adsorption in the injection port).[15] Derivatization by pyrolytic ethylation or bromination was proposed.[16] The substitution of chlorine atoms bound to arsenic in CWA by alkanethiols has been also reported.[17] The thiolation of arsenic CWAs is used in antidote therapy.[18] Another method for diphenylarsenic compounds was based on derivatization using *n*-propanethiol at ambient temperature or 60 °C and 20 min.[19] Muir *et al*.[20] used 1-butanethiol and 3,4-disulf-

anyltoluene, but analysed air samples after thermal desorption, which cannot be applied to DM. Using the Clark I substance as an example, ethanethiol and 1-propanethiol were compared. The latter was a more suitable agent.[21] Tornes *et al.*[22] tested water samples containing DM. They derivatized with 1-propanethiol, 1,3--propanedithiol and 3,4-disulfanyltoluene in dichloromethane. The best results were obtained with 1-propanethiol. Other authors also lean towards the same agent.[23]

The aim of the research was the development and the optimization of a simple procedure for the identification of DM by GC/MS, which will be applicable in the conditions of a mobile laboratory.

EXPERIMENTAL

Chemicals

5-chloro-5,10-dihydrofenarsazine (DM) 95 % was produced by Military Repair Facility Zemianske Kostolany (Slovakia). Tributyl phosphate 99 % (Sigma Aldrich) was used as the internal standard. As reaction media, acetonitrile (MECN) gradient grade (Sigma Aldrich), dichloromethane (DCM), hexane (HEX) (both reagent grade ACS, Scharlau, Germany), ethyl acetate (ETAC) for HPLC and acetone (ACON) rectapur (both VWR Chemicals, USA) were used. As thiol reagents, ethanethiol 97 %, 1-propanethiol 99 %, 2-propanethiol 97 %, 1-butanethiol 99 % and 1-hexanethiol 99 % (all Sigma Aldrich) were used. The column was calibrated by the alkanes solution C7-C30 1000 µg mL^{-1} in hexane (all Sigma Aldrich, Germany).

Equipment

GC/MS was conducted using mobile GC/MS system EM 640 (electron ionization, 70 eV, quadrupole mass filter, *m/z* 50–550). The injection was splitless, HP-5MS column (25 m×0.32 mm×1.0 µm) was used. Carrier gas was nitrogen (30 ml/min flowrate).

For the acquisition and evaluation of the data, software packages m.a.c.s. LabStar and Bruker DataAnalysis (all Bruker, Germany) were used. After analysis, the data were exported and interpreted in the automated mass spectral deconvolution and identification system (Tobias Kind, Germany). GC program was: start at 40 °C (1 min hold) – 10 °C min^{-1} gradient until 280 °C (10 min hold). Total time was 35 min.

GC with flame ionization detector (GC/FID) Trace 1310 (Thermo Scientific, USA) was used to verify the retention characteristics. The column was TG-5MS, 30 m×0.32 mm×0.50 µm (Thermo Scientific, USA). The temperature program was set identically as for GC/MS analytical method described in previous paragraph. The injection port was set at 250 °C, the injection proceeded in split mode (1:20 ratio). A constant flow rate of 1.5 mL min^{-1} of carrier gas (He) was applied to the column. The detector temperature was 280 °C. FID gases were set at flow rate of 350 mL min^{-1} (air) and 40 mL min^{-1} (H$_2$). All gases were of 5.0 purity. Furthermore, make-up gas (N$_2$) was introduced into the system in a volume of mL min^{-1}. Chromeleon 7 software (Thermo Scientific, USA) was used for data acquisition and interpretation.

Manual injections were performed in the volume of 2 µL. Microlitre syringes (Hamilton, USA) were used for injection. TriPlus RSH autosampler (Thermo Scientific, USA) was used for GC/FID automatic injections. Ultrasonic bath Sonorex Digitec (Bandelin, Germany) was used to homogenize solutions and for extractions. Multi Reax automatic shaker (Heidolph, Germany) was also used for extractions. For temperature control during reactions, HD-4 thermostat (Julabo, Germany) was used.

As environmental and urban matrices were used distilled water, sea sand pure (Lachema, Czech Republic), Arenosol Epieutric soil (Czech University of Life Sciences Prague, Czech Republic), 4 mm Planibel Clearlite soda-lime-silica glass (AGC Glass Europe, Belgium), road concrete curb MONO (BEST, Czech Republic) and spruce deck Standard (Rettenmeier, Slovakia).

Derivatization procedure

Table I lists some parameters of the tested thiols, especially with regard to possible reaction temperatures and storage conditions. It is evident that, especially in the case of ethanethiol, it is necessary to follow certain requirements. Pentanethiol was evaluated as an unsuitable reagent for field conditions due to the necessity of its storage under inert gas. Therefore, the reagent was excluded from the experiments.

TABLE I. Characteristics of thiol compounds used for Adamsite derivatization

Thiol	Abbreviation	CAS	Boiling point, °C	Storage conditions	Odor
Ethanethiol	EtSH	75-08-1	35	2 to 8 °C	Skunk
1-Propanethiol	1-ProSH	107-03-9	67–68	Cool, ventilated place	Cabbage
2-Propanethiol	2-ProSH	75-33-2	52	Ventilated place	Skunk
1-Butanethiol	BuSH	109-79-5	97–99	Cool, ventilated place	Skunk
1-Hexanethiol	HeSH	111-31-9	151	Ventilated place	Asphalt

The literature does not offer many solvents that dissolve the tested analyte well. As media for reactions between DM and thiols, 4 polar aprotic solvents were used, which were verified to dissolve DM in the used concentration – MECN (dielectric constant 37.5), ACON (20.3), DCM (8.9), ETAC (6.0).

As first thiol, BuSH was chosen, which is used in mobile laboratories for the identification of lewisites. Several aspects that influence the derivatization of DM by BuSH have been investigated. Different solvents, the effect of temperature on the course of the reaction and the time dependence of the reaction were tested. A solution of DM in the appropriate solvent (MECN, DCM, ETAC, ACON) with a concentration of 2 mg mL^{-1} was prepared. This solution was spiked with an internal standard (tributyl phosphate, 200 nL mL^{-1}). This substance was present in the solution due to mobile GC/MS and hand injections error propagation reduction. 50 µL of BuSH was added to this 1 ml solution. Subsequently, sonication was performed for sample homogenization (2 min). Furthermore, the reaction was monitored at different temperatures – 25 and 60 °C (MECN), 25 and 35 °C (DCM), 25 and 50 °C (ETAC), 25 °C (ACON). The kinetics of the reaction was monitored in the range of 15–180 min. The maximum reaction time of 180 min was chosen for the application reasons. Mobile laboratories are intended for rapid identification of substances in samples. A longer derivatization time would thus be difficult to implement in practice. Chromatograms were always compared to a blank created under identical conditions without the presence of analyte.

In the case of 1-ProSH and HeSH, the same procedure was followed as for BuSH and the same solvents were measured. In the case of 2-ProSH, the reaction in MECN at 60 °C was not observed. In the case of EtSH, due to its high volatility, the reactions were only monitored under mild conditions (25 and 35 °C).

Reaction temperature and reagent volume

Since DCM and ACON are low-boiling solvents, the effect of temperature on the course of the reaction was monitored in MECN and ETAC using BuSH as the derivatizing reagent.

DM solutions were prepared in the appropriate solvent (with spiked internal standard) at concentration of 2 mg mL^{-1}. Then, 50 µL of BuSH was added to a volume of 1 mL of solution. The reaction took place at different temperatures (25–70 °C) and was terminated in each case after 60 min.

The optimal volume of thiol was verified in a similar way. DM solutions were prepared in DCM as described above. BuSH or HeSH in a volume of 10–100 µL was added to the solutions. The reaction took place at 35 °C and was terminated after 60 min.

Calibration curves

Using thiols with longer alkane chains (BuSH, HeSH), the calibration dependences of the response of the DM derivatized signal on the analyte concentration were developed. DM concentrations were chosen to be 0.2; 1.0 and 2.0 mg mL^{-1} in DCM spiked with internal standard. Due to the low reproducibility of the results of the mobile GC/MS system when the device is turned off and on, the calibration curve was always recreated at the beginning of the measurement day to check its stability.

Adamsite identification in environmental and urban matrices

Water, sand, soil, glass, concrete and pre-treated wood were used as sample matrices for recovery tests. The water in a volume of 100 mL was contaminated with the analyte to a final concentration of 2 mg mL^{-1}. Five ml were then sampled and subsequently extracted with 5 mL of DCM (spiked with internal standard) for 10 min by vortexing (1000 rpm). The theoretical maximum yield should thus have been 2 mg mL^{-1} in the tested solution (upper point of the calibration curve). The other matrices were contaminated with 20 mg of DM in a weight of 5 g. Each sample was placed in a sampling vial and 10 mL of DCM with internal standard was added. The extraction took place by ultrasonication for 10 min. The matrices were also contaminated with DM in DCM solution. The resulting mass of contaminant per sample was kept the same as in previous case. The samples were allowed to free evaporate the solvent for 30 min before extraction. Each sample was created and analysed 3 times.

RESULTS AND DISCUSSION

The reaction of 5-chloro-5,10-dihydrophenarsazine (and other arsenic compounds with an As–Cl bond) with thiols is a nucleophilic substitution that proceeds according to the scheme shown in Fig. 1. The chlorine atom is replaced by an R–S– group and the chlorine atom is cleaved off and forms hydrochloric acid. It is advisable (in some cases necessary) to store thiols in the cold to reduce volatility – these are very malodorous substances. Thus, storage in a refrigerated desiccator is recommended.
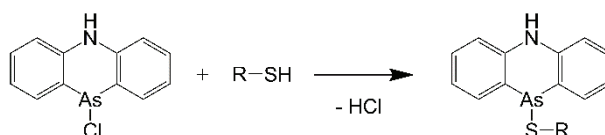

Fig. 1. Thiolation of Adamsite.

Derivatization by ethanthiol

Ethanethiol is a relatively unsuitable reagent due to its very high volatility and strong resistant odour, which can be detected even in trace concentrations.

The following substances were recorded when the reaction was performed in DCM: At retention time (*RT*) 7.94 min (retention index, *RI*, 929) diethyl disulphide was identified. Other signals corresponded to the internal standard tributyl phosphate (*RT* 18.27 min, *RI* 1659) and a double peak of derivatized DM – 5--ethylthio-5,10-dihydrophenarsazine (*RT* 25.78 min, *RI* 2457 and *RT* 26.65 min, *RI* 2545). In addition, the identified DM was characterized by a low signal-to--noise (*S/N*) ratio. In ACON, the peak of diethyl disulphide was very intense, in addition, 2 more EtSH related products were recorded at *RT* 5.37 min (*RI* 787) and *RT* 11.44 min (*RI* 1139). Increasing the reaction time rose the intensity of these artifacts in the chromatogram. Inappropriate results were also noted in ETAC. In the case of all solvents, the signal of the derivatized analyte increased with the extension of the monitored reaction time, and the maximum was not reached after 180 min. Table II lists the most represented fragments of mass spectra of DM derivatives using different thiols.

TABLE II. Retention indexes (RI) and the most abundant fragment ions of thiolated Adamsite using different thiols (the first most abundant fragment ion was used for quantification).

Parameter	EtSH	1-ProSH	2-ProSH	BuSH	HeSH
RI	2457, 2545	2613	2563	2706	2985
Relative abundance	166 (99.9)	242 (99.9)	242 (99.9)	242 (99.9)	64 (99.9)
of fragment ions, %	63 (64.2)	167 (31.5)	241 (74.7)	56 (36.3)	50 (94.0)
	113 (57.0)	166 (25.8)	59 (62.3)	167 (32.7)	55 (82.3)
	167 (57.0)	140 (15.5)	76 (61.3)	166 (28.4)	87 (58.7)
	241 (49.9)	243 (12.3)	63 (51.5)	55 (28.3)	241 (47.0)
Molecular ion	303	317	317	331	359

Derivatization by 1-propanethiol

In DCM, in addition to the internal standard, peaks were found at 11.15 min (*RI* 1117), which corresponded to dipropyl disulphide, and at 27.50 min (*RI* 2613), which corresponded to 1-ProSH derivative of DM, 5-propylthio-5,10--dihydrophenarsazine. After 60 min of reaction, the chromatographic background before the DM derivative started to rise, so that the identification was complicated. In the case of 1-ProSH, however, MECN was an unsuitable solvent. Before the DM derivative peak, the background began to increase significantly, a large broad peak was formed, which made quantification difficult. In addition to the previously mentioned substances, a peak of 1,3-bis(propylthio)propane (*RT* 30.86 min; *RI* 1915) was noted in the chromatograms. In the case of reactions in ETAC, the chromatogram was not clear, in the *RT* interval 22–27 min a significant increase in the background was recorded, and at 13.51 min (*RI* 1278) there was a 1-ProSH related product. The reagent is preferred by a number of authors[19,21–23] for the derivatization of organoarsenic toxic substances. However, apparently it is not possible to use 1-ProSH for the field GC/MS identification of DM.

Derivatization by 2-propanethiol

2-ProSH is the more volatile isomer of 1-ProSH. A peak identifying the oxidized reagent, bis(1-methylethyl)disulfide (*RT* 9.74 min, *RI* 1033) was noted in MECN. Furthermore, there were other artifacts in the chromatogram that would make identification in field conditions difficult. Derivatized DM, 5-(1--methyl)ethylthio-5,10-dihydrophenarsazine, was noted at *RT* 26.84 min (*RI* 2563). However, it was associated with a peak at *RT* 25.83 min (*RI* 2462) that was again related to DM. Moreover, from *RT* 23 min an increase in noise was evident and the results were unsuitable for identification. This phenomenon was then enormous in the environment of ETAC. DCM could be determined as the best reaction medium, no remaining characteristic of previous solvents were found in the extract. Again, the derivatized DM was noted in the double peak, but this could probably be a shortcoming of 2-ProSH itself. As the temperature increased from 25 to 35 °C, the chromatographic background became more intense. The disulphide of the original thiol was not found in DCM.

Derivatization by 1-butanethiol

During the reaction in MECN at a temperature of 60 °C, 4 peaks were recorded in the chromatogram – 14.12 min (*RI* 1320) corresponded to dibutyl disulphide, which was formed by the oxidation of BuSH. Peak intensity increased with temperature, as well as with reaction time. The peak at *RT* 18.27 min (*RI* 1659) corresponded to tributyl phosphate (internal standard), the peak at 23.48 min (*RI* 2179) was identified as tributyl arsenotrithiolite, which is a BuSH derivative of arsenic trichloride, probably a decomposition product of DM. The BuSH derivative of DM, 5-butylthio-5,10-dihydrophenarsazine, was recorded at 28.81 min (*RI* 2706).

Tributyl arsenotrithiolite was not found upon changing the solvent, nor upon derivatization in MECN at 25 °C. In the case of the latter conditions, further in DCM at 25 and 35 °C, only 3 peaks corresponding to the analyte, internal standard and disulphide were recorded. In ETAC (at 25 and 50 °C) the mixture of recorded substances was extended by 2 BuSH related products (*RT* 10.80 min, *RI* 1094 and *RT* 16.05 min, *RI* 1475). Fig. 2 illustrates the mass spectra of the BuSH derivative of DM alongside all other newly identified derivatization products using additional thiols.

Derivatization by 1-hexanethiol

Due to its highest mass, HeSH had high retention and was recorded in the chromatograms (in MECN *RT* 8.32 min, *RI* 949). Due to its high concentration in the solution, the acquisition of mass spectra in subsequent measurements was started 10 min after injection. Dihexyl disulphide, a HeSH oxidation product, was also found in MECN at 18.96 min (*RI* 1730). The 5-hexylthio-5,10-dihydrophen-

arsazine was found at *RT* 32.19 (*RI* 2985), which is a relatively high value for field analysis. Significant peak broadening was associated with this high retention of substance in the column. In addition, an increased chromatographic background was noted in the region of *RT* 26–28 min. When the temperature increased from 25 to 50 °C, additional artifacts arose (a significant peak at *RT* 23.41 min, *RI* 2194, which came from HeSH related product) and the noise was significant from the 15th min. The broad HeSH peak of the DM derivative was encountered in all tested solvents. The best results in terms of number of artifacts and noise level were recorded using DCM (25 and 35 °C) and MECN at 25 °C. Several other interfering peaks were found in ACON, at 12.73 min (*RI* 1225), 14.83 min (*RI* 1379), 21.02 min (*RI* 1933), 22.09 min (*RI* 2045) and 22.99 min (*RI* 2146). In all cases, these were HeSH related products.

Fig. 2 illustrates the chromatograms obtained after thiolation of DM in DCM at 35 °C using different thiols. The reaction time was 60 min.
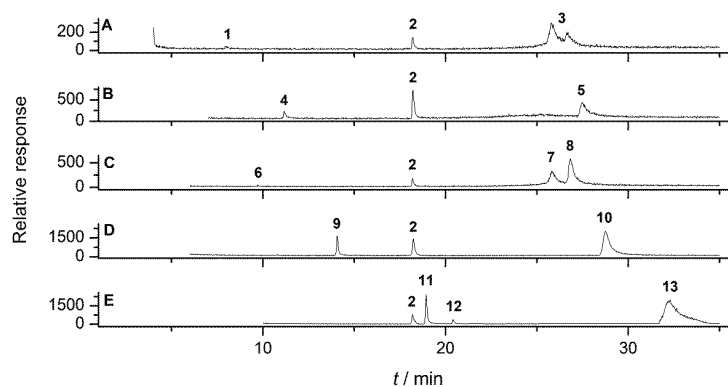
Fig. 2. Chromatograms after direct injection of the reaction mixtures: Adamsite + EtSH (A), 1-ProSH (B), 2-ProSH (C), BuSH (D) and HeSH (E). The reactions were performed in dichloromethane. Peaks correspond to: diethyl disulfide (1), tributyl phosphate internal standard (2), 5-ethylthio-5,10-dihydrophenarsazine double peak (3), dipropyl disulfide (4), 5-propylthio-5,10-dihydrophenarsazine (5), bis(1-methylethyl)disulfide (6), 5-(1-methyl)-ethylthio-5,10-dihydrophenarsazine related product (7), 5-(1-methyl)ethylthio-5,10-dihydrophenarsazine (8), dibutyl disulfide (9), 5-butylthio-5,10-dihydrophenarsazine (10), dihexyl disulfide (11), HeSH related product (12), 5-hexylthio-5,10-dihydrophenarsazine (13).

Fig. 3 illustrates the comparison of the best methods for each thiol in the kinetic curves. *S*/*N* ratios and peak area ratios of derivatized DM and internal standard were taken into account during the selection. In terms of signal intensity, the hexanethio- derivatives of the investigated substance dominate significantly. It should also be mentioned that when short thiols are used, the reaction must be prolonged to maximize the yield, while for longer thiols (BuSH, HeSH) 60 min of reaction is sufficient and prolonging the reaction no longer leads to an increase in the concentration of the reaction products. The DCM environment,

when using shorter thiols (EtSH, 1-ProSH, 2-ProSH), caused product decomposition after 60 min.
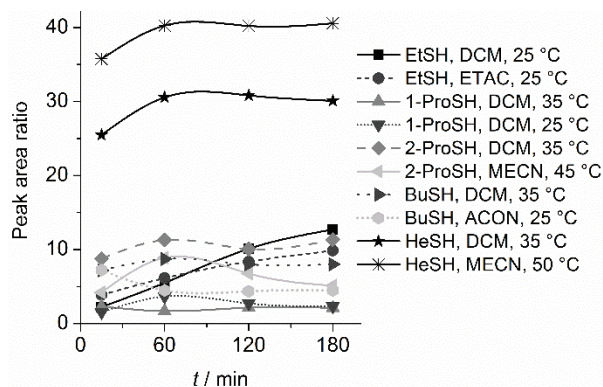
Fig. 3. Kinetics of reactions of Adamsite with derivatizing agents in different media.

Optimal reaction temperature

Fig. 4 illustrates monitoring the effect of the reaction temperature on the intensity of the resulting signal of the derivatized analyte. The results are displayed as a percentage change when the ratio of the peak areas of DM/internal standard at room temperature equals 100 %. Increasing the temperature to 35 °C resulted in a ratio increase of 5 % (ETAC) and 14 % (MECN). A further temperature increase of 10 °C only led to an increase in the ratio of 3 % (ETAC) and 2 % (MECN). The intensity difference between 25 and 65 °C is 9 % (ETAC) and 17 % (MECN). The optimal temperature for thiolation of DM is 35 °C and the reaction takes place smoothly even at room temperature.

Reagent volume

The testing of the optimal volume of the derivatization reagent was carried out in the range of 10 to 100 µL (1 to 10 % of the total volume of the reaction mixture), which are reasonable values to avoid unnecessarily large consumption.
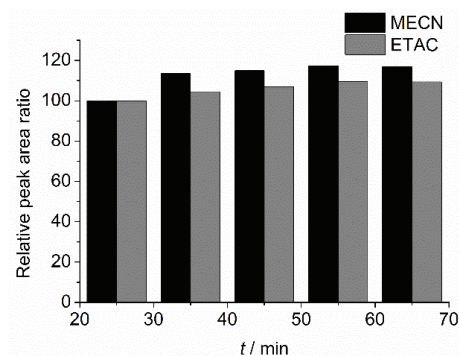
Fig 4. Effect of reaction temperature on the signal intensity of derivatized Adamsite in acetonitrile (MECN) and ethyl acetate (ETAC).

The results (Fig. 5) are displayed as the relative peak area ratio between the derivatized analyte and the internal standard, where the value of the ratio for a thiol volume of 50 µL was marked as 100 %. Under these conditions, increasing the reagent volume from 10 to 50 µL resulted in the rise of the relative ratio value from 35 to 100 % (BuSH) and from 29 to 100 % (HeSH). A two-fold increase in the volume of the reagent to 100 µL then only led to the rise of the monitored value by 19 % (BuSH) and 27 % (HeSH), respectively. Increasing the volume thus no longer leads to a linear increase in the signal. In addition, it is demonstrated that the derivatization by HeSH is more sensitive to increasing the volume of the reagent.
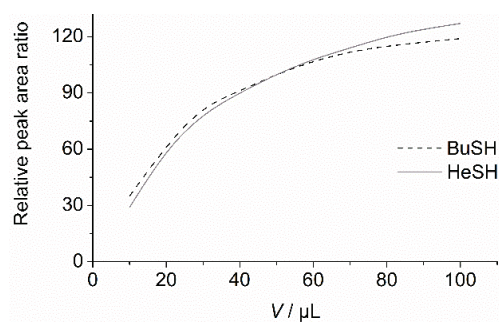
Fig 5. Effect of the volume of the derivatization reagent (BuSH and HeSH) on the signal intensity of the derivatized analyte.

Application of the methods in the identification of Adamsite in matrices

Table III documents the parameters of the calibration curves using BuSH and HeSH as derivatization reagents, the reaction was carried out in DCM at 35 °C (35 °C for EtSH) and was terminated after 60 min. The reproducibility of the measurements was increased using the internal standard. Switching the mobile GC/MS system off and on again led to error propagation, and therefore three-point calibration curves were always created at the beginning of the measurement day, reducing the *RSD* of repeat measurements from 35 to 15 %. The detection limit of the methods was determined according to the calibration curve for the *S/N* ratio of the derivatized analyte equal to 3. Relatively high limits of detection are associated with the low reactivity of the substance and its high molecular weight and the parameters of the mobile GC/MS system. The linearity of the methods was verified in the range of 0.2–4.0 mg mL^{-1}. The parameter is documented in Fig. 6 that illustrates the linearity when the curve was created three times on different measurement days. It demonstrates that linearity was maintained even though curve shifts occurred.

TABLE III. Calibration curves parameters

Thiol	Coefficient of determination	*RSD* / %	Detection limit, mg mL^{-1}
BuSH	0.993	16	0.10±0.02
HeSH	0.994	14	0.05±0.01
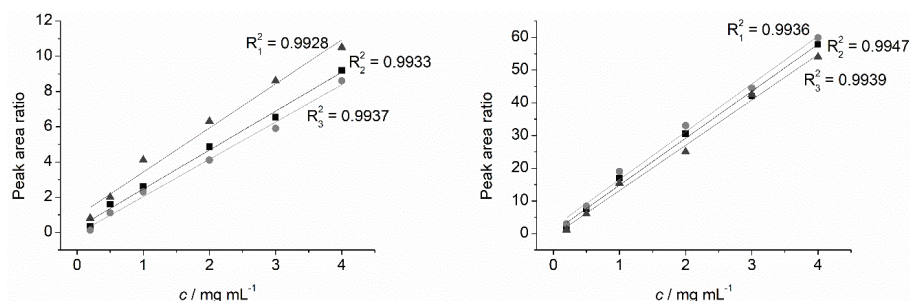
Fig. 6. Linearity of derivatization reaction of Adamsite by BuSH (left) and HeSH (right).

Table IV demonstrates the use of the above methods for DM identification in environmental and urban matrices. The results demonstrate that neat DM can be extracted from samples more efficiently than in the case of a matrix contamination by DM solution. It is more evident with porous matrices. This is due to the greater penetration of the contaminant into the depth of the matrix when using a liquid solution. In the case of water, the organic DM sample was not tested. No significant difference in efficiency value was noted when HeSH was used instead of BuSH as the derivatizing reagent. None of the matrices caused unwanted interference in the area of analyte retention. Both methods were assured to be valid for the 6 sample matrices tested.

TABLE IV. Adamsite recovery as BuSH and HeSH derivatives from different matrices after contamination with neat analyte (E_{neat}) and analyte dissolved in dichloromethane (E_{sol}). The results are given as efficiency value when derivatized by BuSH / by HeSH

Sample	E_{neat} / %	E_{sol} / %	Sample	E_{neat} / %	E_{sol} / %
Water	82 / 85	–	Glass	92/88	90/93
Soil	76 / 75	45 / 51	Concrete	70/74	35/29
Sea sand	80 / 81	62 / 58	Wood	75/70	38/31

Fig. 7 illustrates the applicability of DM derivatization via HeSH after extraction from the most problematic matrix in terms of chromatographic back-
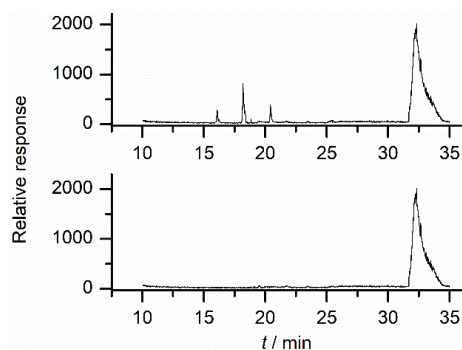
Fig. 7. Comparison of chromatogram after extraction of Adamsite from soil and subsequent derivatization with HeSH (top) and chromatogram of the same measurement after background subtraction (bottom).

ground – soil. The mobile GC/MS did not have the ability to perform automatic background subtraction. However, after data export and external subtraction, it can be seen that only the derivatized analyte peak is visible in the chromatogram after the hiding of background effects. A disadvantage of the used mobile GC//MS system is also the fact that when the experiment is repeated, the mass spectra are not identical in the area of ions with lower abundance. The first 5 fragment ions were always the same (Table II).

CONCLUSION

It has been shown that Adamsite, which in its neat form has very unsuitable analytical properties, can be analysed by gas chromatography. All investigated aliphatic thiols are able to convert the substance into a more volatile derivative by nucleophilic substitution. Due to the large weight of the Adamsite molecule, the derivatives have considerable retention in the standard HP-5 column, and with the growing alkane chain of the reagent, it is necessary to adjust (especially prolong) the chromatographic method. Aromatic thiols would thus be inappropriate reagents for field analysis.

The best results in terms of the signal intensity and the associated characteristics (detection limit, S/N ratio) were achieved using HeSH. However, the substance was significantly retained by the column (RI 2985) and the peak was broad.

A high RI is associated with the length of the method, which must be at least 35 min. However, the derivative was recorded with a significantly higher resulting signal even after 15 min of derivatization. For other reagents (BuSH comes into consideration), it is recommended to extend the derivatization time to 60 min.

И З В О Д

УПОТРЕБА АЛИФАТИЧНИХ ТИОЛА ЗА *ON-SITE* ДЕРИВАТИЗАЦИЈУ И ИДЕНТИФИКАЦИЈУ АДАМСИТА ГАСНОМ ХРОМАТОГРАФИЈОМ

TOMAS ROZSYPAL

Nuclear, Biological and Chemical Defence Institute, University of Defence, Vita Nejedleho 691, 68203 Vyskov, Czech Republic

У овом раду је описан развој методе за брзу и једноставну идентификацију Адамсита у мобилној лабораторији, применом гасне хроматографије са масеном спектрометријом. Адамсит је хемијски бојни агенс са јединственим особинама да се не може анализирати без конверзије у испарљив дериват. Развијена је и упоређена дериватизација са пет алифатичних тиола (етантиол, 1-пропантиол, 2-пропантиол, 1-бутантиол и 1-хексантиол). Праћене су ретенционе карактеристике деривата, карактеристике пикова главних једињења и нежељених пикова на хроматограмима. Праћени су такође и утицај реакционог медијума и време реакције. Испитивани су оптимална реакциона температура и запремина реагенса за дериватизацију. Снимљени су масени спектри новоформираних деривата, који се још увек не налазе у базама података хемијских бојних супстанци. Калибрација потребна за одређивање је изведена са оптималним реагенсима (1-

-бутантиол и 1-хексантиол) и метода је верификована тестом идентификације Адамсита у одабраним матрицама из природне и околине и урбане околине.

REFERENCES

1. J. Beldowski, M. Brenner, K. K. Lehtonen, *Mar. Environ. Res.* **162** (2020) 105189 (https://doi.org/10.1016/j.marenvres.2020.105189)
2. H. Sanderson, P. Fauser, M. Thomsen, P. B. Sorensen, *J. Hazard. Mater.* **154** (2008) 846 (https://doi.org/10.1016/j.jhazmat.2008.05.059)
3. L. Polak-Juszczak, J. Szlinder Richert, *Chemosphere* **284** (2021) 131326 (https://doi.org/10.1016/j.chemosphere.2021.131326)
4. F. Francken, A. M. Hafez, *Mar. Technol. Soc. J.* **43** (2009) 52 (https://doi.org/10.4031/MTSJ.43.4.3)
5. M. Czub, J. Nawala, S. Popiel, *Aquat. Toxicol.* **230** (2021) 105693 (https://doi.org/10.1016/j.aquatox.2020.105693)
6. B. Radke, L. Jewell, S. Piketh, J. Namiesnik, *Crit. Rev. Environ. Sci.* **44** (2014) 1525 (https://doi.org/10.1080/10643389.2013.782170)
7. S. Franke, *Lehrbuch der Militärchemie: Band 1*, Militärverlag der Deutschen Demokratischen Republik, Berlin, 1977
8. V. Nagarajan, R. Chandiramouli, *Chem. Phys.* **535** (2020) 110782 (https://doi.org/10.1016/j.chemphys.2020.110782)
9. E. W. J. Hooijschuur, C. E. Kientz, U. A. T. Brinkman, *J. Chromatogr., A* **982** (2002) 17 (https://doi.org/10.1016/S0021-9673(02)01426-7)
10. K. Kinoshita, A. Noguchi, K. Ishii, A. Tamaoka, T. Ochi, T. Kaise, *J. Chromatogr., B* **867** (2008) 179 (https://doi.org/10.1016/j.jchromb.2008.03.033)
11. T. Kondo, R. Hashimoto, Y. Ohrui, R. Sekioka, T. Nogami, F. Muta, Y. Seto, *Forensic Sci. Int.* **291** (2018) 23 (https://doi.org/10.1016/j.forsciint.2018.07.032)
12. H. Nagashima, T. Kondo, T. Nagoya, T. Ikeda, N. Kurimata, S. Unoke, Y. Seto, *J. Chromatogr., A* **1406** (2015) 279 (https://doi.org/10.1016/j.chroma.2015.06.011)
13. STANAG 4632: *Deployable NBC Analytical Laboratory* (2005)
14. AEP-66: *NATO handbook for sampling and identification of biological, chemical and radiological agents (SIBCRA)* (2015)
15. S. Hanaoka, K. Nomura, T. Wada, *J. Chromatogr., A* **1101** (2006) 268 (https://doi.org/10.1016/j.chroma.2005.10.028)
16. K. Schoene, H. J. Bruckert, H. Jürling, J. Steinhanses, *J. Chromatogr., A* **719** (1996) 401 (https://doi.org/10.1016/0021-9673(95)00751-2)
17. R. Haas, *Environ. Sci. Pollut. Res.* **5** (1998) 2 (https://doi.org/10.1007/BF02986365)
18. L. I. Szekeres, B. Gyurcsik, T. Kiss, Z. Kele, A. Jancsó, *Inorg. Chem.* **57** (2018) 7191 (https://doi.org/10.1021/acs.inorgchem.8b00894)
19. S. Hanaoka, E. Nagasawa, K. Nomura, M. Yamazawa, M.Ishizaki, *Appl. Organomet. Chem.* **19** (2005) 265 (https://doi.org/10.1002/aoc.790)
20. B. Muir, S. Quick, B. J. Slater, D. B. Cooper, M. C. Moran, C. M. Timperley, W. A. Carrick, C. K. Burnell, *J. Chromatogr., A* **1068** (2005) 315 (https://doi.org/10.1016/j.chroma.2005.01.094)
21. R. Haas, A. Krippendorf, *Environ. Sci. Pollut. Res.* **4** (1997) 123 (https://doi.org/10.1007/BF02986314)

22. J. Tornes, A. Opstad, B. Johnsen, *Sci. Total Environ.* **356** (2006) 235 (https://doi.org/10.1016/j.scitotenv.2005.03.031)
23. H. Niemikoski, M. Söderström, H. Kijlunen, A. Östin, P. Vanninen, *Anal. Chem.* **92** (2020) 4891 (https://doi.org/10.1021/acs.analchem.9b04681).

Use of Jamun seed (*Syzyum cumini*) biochar for the removal of Fuchsin dye from aqueous solution

DIVYA KOSALE, CHANDRAKANT THAKUR and VINOD KUMAR SINGH*

Department of Chemical Engineering, National Institute of Technology Raipur, Raipur 492010, Chhattisgarh, India

Abstract: The textile, leather, paint and other industries discharge lots of dyes in their effluent which can cause major impact to environment and human life. Therefore, it becomes necessary to eliminate the dye from the effluent before its discharge and reuse. Several procedures for the removal and inactivation of dyes have been proposed over past, but the adsorption has gained popularity due to its efficiency and operational ease. Use of the biochars as an adsorbent is gaining attention due to their low cost, availability and high adsorption capability. The current study focuses on the removal of basic Fuchsin (BF) dye by adsorption using Jamun (*Syzyum cumini*) seed powder biochar as an adsorbent. The biochar was characterized through various analyses such as: XRD, EDS, FTIR, TGA and SEM. Adsorption was studied by varying the parameters such as pH, contact duration, temperature, adsorbent dose, and temperature. Further, the isotherm, kinetic and thermodynamic studies were also performed to understand the adsorption mechanism. The maximum adsorption capacity for BF dye was found with Jamun seed biochar produced at 500 °C. The study reveals that the biochar manufactured from Jamun seed power has a significant potential for the elimination of BF dye from wastewater.

Keywords: adsorption; pyrolysis; TGA; isotherm; kinetics; thermodynamics.

INTRODUCTION

The cosmetics, textiles, paper, pharmaceuticals and leather industries consume enormous quantities of dyes and chemicals during the processing of raw materials and the making of different products. Accordingly, they generate large volumes of dyes-containing liquid effluents which need to be treated for the removal of dyes prior to their disposal, as the untreated waste water may impart toxicity to aquatic life and damage the quality of receiving water bodies and environment.[1] There are different treatment techniques which have been used for

---

* Corresponding author. E-mail: vksingh.che@nitrr.ac.in

the reduction of dye such as advanced oxidation, ozonation, adsorption, coagulation/flocculation, aerobic and anaerobic degradation, membrane filtration, *etc*.[2–5] Each technique is having its own advantages and drawbacks but the adsorption has got a lot of attention because of its operational ease, low cost, flexibility, design simplicity, efficiency and profitability.[6]

India's textile sector consumes almost 80% of the overall production of 130,000 tons of dyestuff,[7] which include non-biodegradable dye in the concentrations ranging from 1 to 2500 mg L^{-1}.[8] There are about 100,000 commercially available dyes[9] and basic Fuchsin (BF) dye is one of widely used dye in the textile sector. Due to its toxicity the BF dye can cause several health issues such as skin infection, nausea irritation, vomiting and diarrhoea, damages organs like spleen, thyroid and liver. Also, its inhalation can result in respiratory irritation.[10] BF dye is also known by the name basic violet 14, chemically known as triaminotriphenylmethane ($C_{20}H_{20}ClN_3$). It is the combination of three dyes namely, pararosaniline, rosaniline and Magenta II.[11] BF dye is commonly used for colouring of textile and leather products.[12]

There are many researchers who have worked on BF dye removal through adsorption process using different types of adsorbents such as bottom ash, deoiled soya, graphite oxide, polymer nanocomposite, kola nut pod carbon, eggshell and euryale ferox salisbury seed shell, *etc*.[10,13–17] Among these adsorbents biomass has gained major attention of the researchers due to its easy availability and low cost. The biochar derived from the biomass of *Syzygium cumini* has been selected as an adsorbent for this study. *Syzygium cumini* is locally known as Jamun (black plum). India produces around 15.4 % of the total world production of Jamun (approximately 13.5 million tons) and its rank is second. Maharashtra is the main producer of Jamun followed by Uttar Pradesh, Tamil Nadu, Gujarat and Assam.[18] Large quantity of Jamun seeds are discarded into open area as waste. The aim of this study is to use these seeds to prepare biochar for the degradation of BF dye from the aqueous solution. No previous studies were found using Jamun seed powder biochar (JSPB) as an adsorbent for the BF dye removal. That is why JSPB was selected as an adsorbent for the reduction of BF dye through batch adsorption process. The Jamun seed powder (JSP) and JSPB were characterized using various techniques like scanning electron microscopy (SEM), X-ray diffraction (XRD), Fourier transform infrared spectroscopy (FTIR), energy dispersive X-ray spectroscopy (EDS) and thermal gravimetric analysis (TGA); the batch adsorption experiments were conducted by varying different parameters. The linear and non-linear form of Langmuir, Freundlich and Temkin isotherm models were applied to understand the mechanism of adsorption process. Kinetic study for this process was done using pseudo 1st and pseudo 2nd order kinetic models. The behaviour of the adsorption process was determined by a thermodynamic study.

EXPERIMENTAL

Materials

BF dye was purchased from Titan Biotech Ltd., Bhiwadi, Rajasthan, India. Its chemical structure is given in Fig. 1.[19] Dried Jamun fruits were purchased from the local market. NaOH and HCl were purchased from Sigma–Aldrich, India, and used for pH adjustment of the dye solution. Distilled water was used for the preparation of all dye solutions.
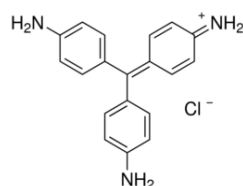
Fig. 1. Structure of basic Fuchsin dye.

Preparation of adsorbent

Dried Jamun fruits were soaked in water for 48 hrs followed by its peeling for seed separation. The seeds were dried in the hot air oven at the temperature 383 K for 36 h and broken down into small pieces using mortar pestle. The pieces of the seeds were ground using mixer grinder followed by screening to get the powder having an average particle size of 49 μm. The screening operation was completed by using 300 and 350 mesh British standard sieve (BSS). JSP was pyrolyzed in a pit type furnace reactor (S. D. Scientific, Kolkata make) at 773 K for 60 min. The resultant Jamun seed powder biochar (JSPB) was taken out from the reactor and kept in air tight container at room temperature for further experiments.

Preparation of adsorbate

A dye solution of 1000 mg L^{-1} was prepared by dissolving the 1mg of BF dye in the 1000 mL of distilled water. The stock solution was then diluted to the desired concentrations of 100, 75, 50, 25, 12.5, 6.25 and 3.125 mg L^{-1}. pH was tuned to the desired value using 0.1 M NaOH and 0.1 M HCl solution. λ_{max} of 548 nm was the maximum absorbance wavelength and hence used as the basis for all the experiments to evaluate the BF dye concentration.

Characterizations of JSP and JSPB

JSP, JSPB before adsorption and JSPB after adsorption were characterised using different techniques. SEM (Zeiss EVO 18) and field emission scanning electron microscopy (FESEM, Carl Zeiss Uhr FESEM model Gemini SEM 500 KMAT) were used for the morphological study and the presence of different elements was found using EDS (INCA 250 EDS). XRD technique was used to find out the structure (crystalline or amorphous) of the samples. FTIR (Alfa, Bruker, Germany) spectroscopy was performed with IR-Affinity-1, Shimadzu, to find the functional groups in the sample by recording the spectra between the frequency ranges of 400–4000 cm^{-1}. The thermal behaviour of the JSP sample was studied by TGA (Setaram Labsys EVO) in the temperature range of 30–850 °C.

Batch adsorption experiment

The adsorption experiments were conducted by varying different parameters to examine the adsorption characteristics of JSPB for the removal of BF dye from synthetic solution. For batch process, 100 mL of the dye solution (3–100 mg L^{-1}) with a 0.1–1.0 g of JSPB was taken in the conical flask and shaken in the orbital shaker at 95±5 rpm for time 15–120 min, at pH 2.03–10.02, and temperature 298–338 K. After shaking, the suspensions were filtered and the

BF dye concentration in the supernatant solution was measured with the help of UV–Vis spectrophotometer (LabIndia 3092). The absorbance values at specified wavelength (λ_{max} of 548 nm) of the samples were recorded, and the equivalent dye concentration value was obtained from the calibration graph. The adsorption capacity, q_e, and the percentage of dye removal, R, were calculated using following equations, respectively:[20]

$$q_e = \frac{(c_i - c_f)V}{m} \tag{1}$$

$$R = 100\frac{c_i - c_f}{c_i} \tag{2}$$

where V = volume of BF dye solution (mL), c_i = initial BF dye concentration (mg L^{-1}), m = = mass of JSBP (g) and c_f = final concentration of BF dye at equilibrium (mg L^{-1}).

RESULTS AND DISCUSSION

Characterizations of JSP and JSPB

The surface characteristics and morphological features of JSP before adsorption and JSPB after adsorption were determined by the SEM analysis and the images are shown in Fig. 2. The image of raw sample of JSP shows uneven structures with less porous surface whereas the image of JSPB shows porous structures developed during the pyrolysis. After the adsorption of BF dye, the surface of JSPB became comparatively smooth as the pores get filled up with molecules of dye. The elemental composition (% weight basis) of JSP and JSPB before adsorption was determined by the EDS analysis and the results are given in Table I. The JSP surface contains various elements such as carbon, oxygen, nitrogen, silicon, sulphur and potassium. After the pyrolysis, the weight percentage of some of these elements (carbon, silicon and potassium) in the JSPB surface increased and that of oxygen decreased. Also, the presence of new elements like iron and manganese has been observed. The increased percentage of the elements and the addition of new elements may result in the improvement of the adsorption capacity of JSPB.
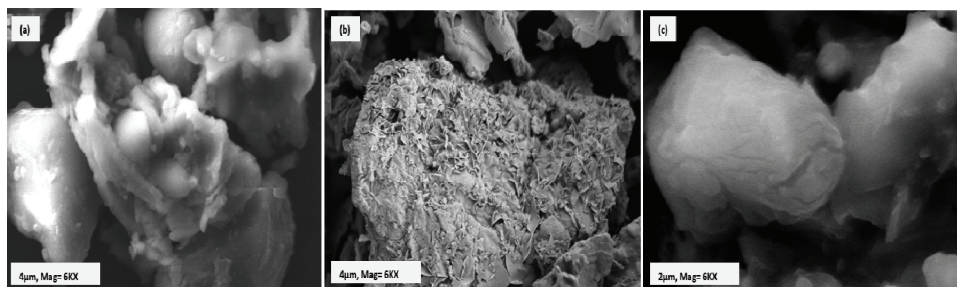
Fig. 2. SEM image of: a) raw JSP 2, b) JSPB before adsorption and c) JSPB after adsorption.

The XRD spectra for raw JSP, JSPB before adsorption and JSPB after adsorption are presented in Fig. 3a. The graph of raw JSP shows non-crystalline

peak with low intensity at an angle of 26.70°, whereas the graph for JSPB has more peaks with slightly increased intensities at the angles 26.70, 31.51, 50.08 and 59.98°. It clearly indicates the semi-crystalline nature of JSPB surface which will favour the adsorption process. After the adsorption, the peak at an angle of 26.70° is slightly decreased and some peaks have disappeared, which confirms the successful adsorption of BF dye on JSPB surface.[21]

TABLE I. EDS analysis of JSP and JSPB

No.	Raw JSP		JSPB	
	Element	Weight, %	Element	Weight, %
1	C	18.08	C	40.20
2	O	71.61	O	47.98
3	N	6.23	Mg	1.76
4	Si	1.54	Si	4.51
5	S	0.07	K	3.76
6	K	1.79	Fe	1.78
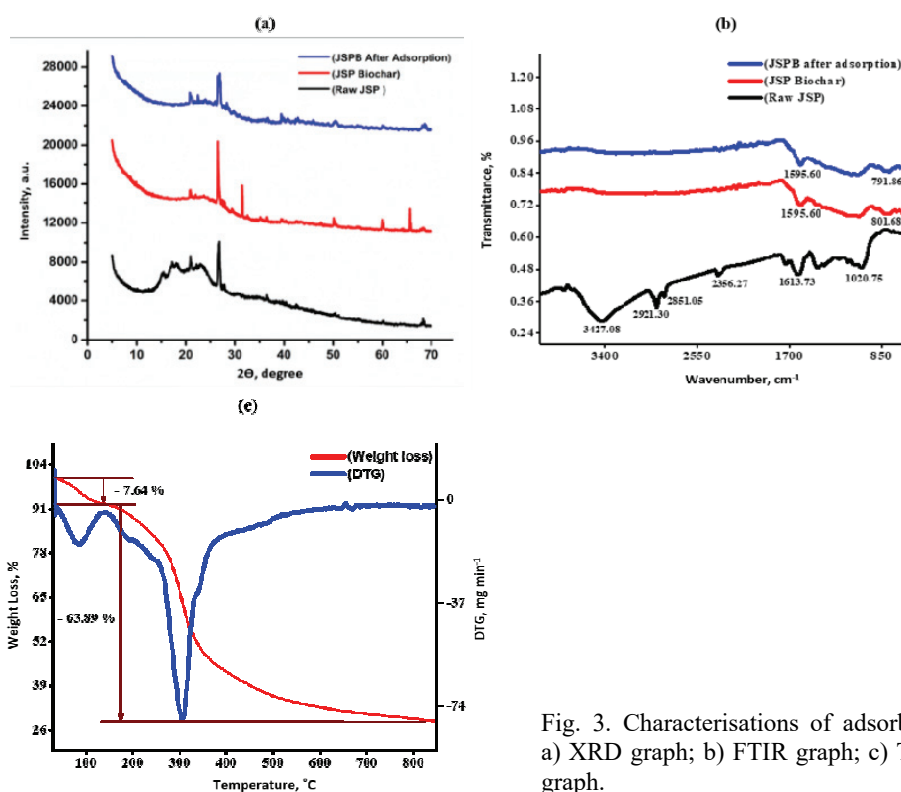
Fig. 3. Characterisations of adsorbent; a) XRD graph; b) FTIR graph; c) TGA graph.

FTIR spectra of raw JSP, JSPB before adsorption and JSPB after adsorption between 400–4000 cm^{-1} are shown in Fig. 3b. The raw JSP shows a broad-band

around 3427 cm^{-1} indicating O–H stretching (alcohol group). Also, this peak shows the presence of cellulosic components. The band at 2921.30 cm^{-1} confirms the presence of alkyl groups which is the indication of asymmetric C–H band alkyl groups (methyl and methylene group). The band around 2851.05 cm^{-1}, is attributed to H–C=O; C–H stretching vibrations of alkanes groups, whereas the band 2356.27 cm^{-1} is assigned to the amino related component (–N–H component).[22] The band 1613.73 cm^{-1} (C=C ring stretching) corresponds to aromatic compounds. Aliphatic ether C–O and alcohol (C–O stretching) components were confirmed by the peak of 1020.75 cm^{-1}. After pyrolyzing the sample all strong peaks like hexagonal, alkyl and alkanes groups disappeared, whereas aromatic groups are still visible. The shallow peaks were observed in both the samples of JSPB before adsorption and JSPB after adsorption, at the band 1595.60 and 801.68–791.96 cm^{-1}, which can be assigned to aromatic group (C=C ring stretching) and 2 adjacent H deformation, respectively.[23] These functional groups may assist in the adsorption of dye molecules on the surface of JSPB.

TGA analysis of raw JSP was performed in the temperature range 30–850 °C. Two weight-loss peaks were found which are shown in Fig. 3c. The first peak was observed with a weight loss of 7.64 % below 100 °C, which indicates the dissociation of water molecules from the JSP biomass. The reduction of hemicellulose, cellulose and lignin from the sample was detected by the second peak in the temperature range of 200–300 °C with a maximum weight loss of 63.89 %. After 300–400 °C, the sample began to deform, and at higher temperatures the peak seemed almost flat and it was decomposed before its reached 850 °C. This is the sign of complete pyrolyzation of JSP biomass. Therefore, 500 °C is considered for pyrolysis process.[24]

Batch adsorption study with effect of various parameters

Effect of concentration. The dye removal in the adsorption study is strongly influenced by the initial dye concentration. The initial concentrations of BF dye were varied from 3–100 mg L^{-1} at pH 8.01, dosage 0.6 g, contact time 75 min, and the temperature 318 K. The effect of initial dye concentration on the removal has been shown in Fig 4a. It is clear from the plot that the sorption of dye is increasing from 54 to 97% (adsorption capacity increasing from 0.1–8 mg g^{-1}) with the solution concentration. The reason for this may be due to the availability of more dye molecules for the limited binding sites on the adsorbent surface accounts for the rise in BF adsorption.[25,26] On the other hand, higher initial dye concentration causes an increase in surface use of the adsorbent because of the enhanced contact between adsorbate and adsorbent. The same trend was also observed by Bessashia *et al.* for BF dye.[27] The maximum removal efficiency was found to be 97 % with the concentration of 100 mg L^{-1}.
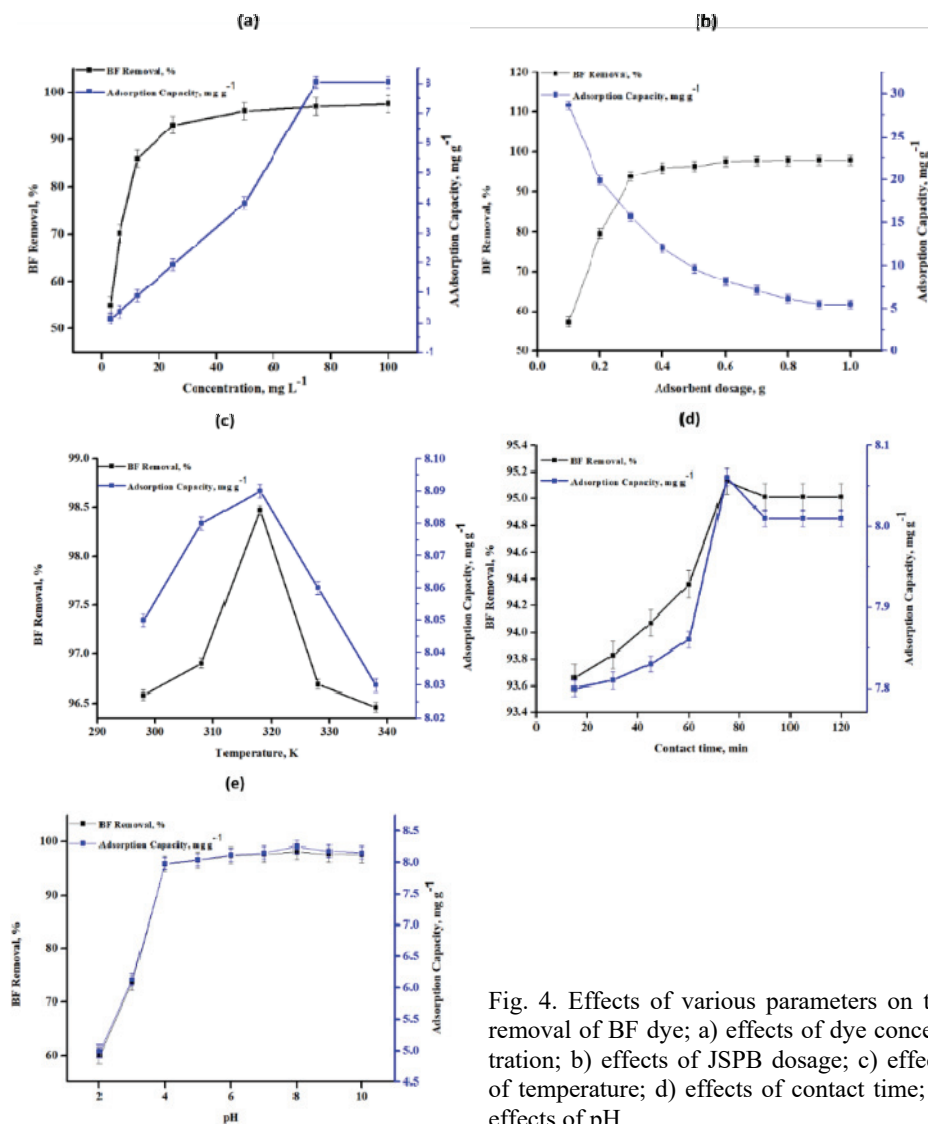
Fig. 4. Effects of various parameters on the removal of BF dye; a) effects of dye concentration; b) effects of JSPB dosage; c) effects of temperature; d) effects of contact time; e) effects of pH.

Effect of adsorbent dosage. The JSPB dosages were varied from 0.1 to 1 g in the amount of liquid 50 ml for each sample at the optimum parameters of contact time 75 min, temperature 318 K and pH 8.01 (Fig. 4b). With the increasing adsorbent dose (0.1 to 1.0 g), the removal percentage is also increasing (55.54– –95.56 %) initially (up to 0.6 g), but no significant change occurs later on. This is due to the fact that the dye molecules have occupied the available surface. On the other hand, as the adsorbent dose increases from 0.1 to 1.0 g, the adsorption capacity decreases dramatically from 28.67 to 5.18 mg g^{-1}. As the JSPB dose inc-

reases, the adsorbent particles continually aggregate or agglomerate. Thus, the surface area per unit weight of the adsorbent is reduced, and the diffusion route length increases. This results in a continuous loss of adsorption capacity. For further experiments, 0.6 g of the adsorbent dose was finalised because of its benefits and drawbacks in terms of removal efficiency and adsorption capacity.[28]

Effect of pH. The pH study was performed at the optimum parameters as adsorbent dosage 0.6 g, temperature 318 K, concentration 100 mg L^{-1} and time 75 min. The percentage removal was observed to be increasing with pH from 2.03–10.02 (increasing adsorption capacity 4–8 mg g^{-1}) as shown in Fig. 4e. This trend can be understood from the fact that at lower pH, the concentration of H$^+$ in a solution remains higher, which will lead to the protonation of active sites of the adsorbent. Since the BF dye is also positively charged, there will be a repulsive force between the adsorbent and adsorbate resulting in less adsorption. At higher pH, H$^+$ concentration is lower and hence higher percentage removal can be obtained.[29]

Effect of contact time. Completion of the process within a short time is extremely important for industrial applications, in terms of cost-effectiveness and efficiency. The influence of contact time (15–120 min) on the uptake dye solution is shown in Fig. 4d. While performing this experiment other parameters were kept constant (pH 8.01, concentration 100 mg L^{-1}, temperature 318 K and dosage 0.6 g). These results show that the adsorption of dye increases with contact time (removal of 93–95 %, adsorption capacity 6–8 mg g^{-1}) and it remains constant after the equilibrium time of 75 min. This may be because of the availability of more active sites initially on JSBP for the dyes and also due to the rate at which the BF dye solution is transferred from the exterior to the interior sites of the JSPB particles, which controls the uptake rate as the surface adsorption sites become exhausted.[30]

Effect of temperature. The effect of temperature is another significant physicochemical process parameter because the temperature changes the adsorption capacity of the adsorbent. The temperature effect on BF dye removal was studied at the optimum conditions of pH 8.01, contact time 75 min, dosage 0.6 g and concentration 100 mg L^{-1}, Fig. 4c. As the percentage removal of dye increased from 96.58–98.47 % with the increase in temperature from 298 K–318 K, the process shows the endothermic behaviour. With the further temperature rise the removal is decreasing in the temperature range 318 K–338 K, which indicates the exothermic nature of the process. Thus, the temperature study shows the change in nature of the process from endothermic to exothermic. This may be due to the decrease of the quantity of the dye molecules and the active sites on the adsorbent with increasing temperature. Also, the swelling of internal surface of JSPB and the increasing mobility of dye ions at higher temperatures leads to poor adsorption capacity of the adsorbent. This pattern was also observed by Abdus *et al.*[31,32]

Isotherms, kinetics and thermodynamic study

Isotherm study. The relationship between adsorption capacity and equilibrium concentration is well understood by the adsorption isotherm models. The graph plotted between the solid phase and liquid phase concentration of the JSPB illustrates the equilibrium adsorption isotherms. The linear and nonlinear form of Langmuir, Freundlich and Temkin isotherms were used to describe the experimental data of adsorption for this study. For the analysis of adsorption isotherms, the experiments were conducted at pH 8.01 by adding a 0.6 g of JSPB with 50 ml of BF dye solution and by varying concentrations from 12.5 to 100 mg L^{-1}. JSPB was separated from the solution after 75 min and the concentration of BF dye was estimated using UV spectrophotometer. The experimental and calculated data are summarized in Table II for all the three isotherms.[11,33]

TABLE II. Freundlich, Langmuir and Temkin constants of linear and nonlinear isotherms for adsorption of dye

Isotherm	Constant	Temperature , K		
		303	308	328
Langmuir	q_m / mg g^{-1}	5.45	50.25	14.89
	K_L / L mg^{-1}	0.67	0.05	0.23
	R^2 (Linear)	0.93	0.94	0.92
	R^2 (Non-linear)	0.88	0.85	0.85
	R_L	0.02	0.15	0.05
Freundlich	n	0.09	0.10	0.11
	K_f / L g^{-1}	0.002	0.006	0.021
	R^2 (Linear)	0.88	0.88	0.87
	R^2 (Non-linear)	0.99	0.91	0.84
Temkin	A_T / L mg^{-1}	0.57	0.58	0.36
	B_T / J mol^{-1}	37.7	31.8	30.2
	R^2 (Linear)	0.99	0.99	0.99
	R^2 (Non-linear)	0.99	0.99	0.99

The Langmuir isotherm is applicable for homogeneous adsorption process, in which there is no contact between the adsorbed molecules due to the monolayer adsorption. Nonlinear and linear form of Langmuir equations are given as:

$$q_e = \frac{q_m K_L c_e}{1 + K_L c_e} \tag{3}$$

$$\frac{1}{q_e} = \frac{1}{K_L q_m} \frac{1}{c_e} + \frac{1}{q_m} \tag{4}$$

where q_m is the maximum adsorption capacity (mg g^{-1}), q_e denotes equilibrium adsorption capacity (mg g^{-1}) and c_e is concentration of BF dye solution at equilibrium (mg L^{-1}). The plots of linear and shows low value of the R^2, which

indicates that the given adsorption data is not suitable for Langmuir isotherm. The separation factor (R_L) of this isotherm is represented as:

$$R_L = \frac{1}{1 + K_L c_i} \tag{4}$$

where c_i and K_L are the initial concentration and Langmuir constant, respectively. The positive value of R_L ($0 < R_L < 1$), shows the feasibility of process.

Freundlich isotherm is valid for multilayer adsorption and the heterogeneous nature of the process. The non-linear and linear form of Freundlich equations are:

$$q_e = K_f c_e^{\frac{1}{n}} \tag{6}$$

$$\log q_e = \log K_f + \frac{1}{n} \log c_e \tag{7}$$

where the adsorption capacity is measured by intercept $\log K_f$ (Freundlich constant) and the adsorption intensity is represented by the slope $1/n$. The linear and non-linear plots were used to calculate the values of K_f and n. The value of n is 0.11 which is less than 1, and therefore indicates poor adsorption and suggests that the adsorption data does not fit to this isotherm.

The Temkin isotherm model assumes that the heat of adsorption of all molecules in the layer decreases linearly with coverage due to the adsorbate–adsorbent repulsions. It also implies that adsorption occurs as a result of a homogenous binding energy distribution.[11] The Temkin non-linear and linear equation can be given as:

$$q_e = \frac{RT}{B_T} \ln \left(A_T c_e \right) \tag{8}$$

$$q_e = B_T \ln A_T + B_T \ln c_e \tag{9}$$

$$B_T = \frac{RT}{b} \tag{10}$$

where R = universal gas constant (8.314 J mol^{-1} K^{-1}), T (K) = absolute temperature, A_T (L mg^{-1}) = equilibrium binding constant, B_T = heat of adsorption, B = = Temkin constant (J mol^{-1}).

The higher values of R^2 for both the nonlinear and linear form of this model suggest that the Temkin isotherm is the most favourable for the adsorption data. Positive value of B_T is a sign of the exothermic nature of the process.

Kinetic study. Efficiency, mechanism and potential rate controlling step (including mass transfer and chemical reaction) of the adsorption process were determined by the kinetic study. The necessary time for the adsorption kinetics was determined by conducting the experiment in the orbital shaker for a period of 15––75 min (concentrations 25–100 mg L^{-1} at pH 8.01, dosage 0.6 g, and the tempe-

rature 318 K). The samples were taken out from the shaker at an interval of 15 min. Data obtained from the kinetic experiments were evaluated for both linear and nonlinear form of pseudo 1st and pseudo 2nd order and are summarised in Table III.[34,35]

Pseudo-first-order kinetic model is used to describe the kinetics of many adsorption systems. The nonlinear and linear equations for this model are expressed as follows:

$$q_t = q_e \left(1 - e^{-K_1 t}\right) \tag{11}$$

$$\ln\left(q_e - q_t\right) = \ln\left(K_1 q_e\right) - K_1 t \tag{12}$$

where K_1 = rate constant of pseudo 1st (L min^{-1}), q_t = adsorption capacity at time t (mg g^{-1}).

TABLE III. Linear and non-linear kinetic parameters for BF dye adsorption

c / mg L^{-1}	$q_{e,exp}$ mg g^{-1}	Pseudo 1st order				Pseudo 2nd order			
		$q_{e,cal}$ mg g^{-1}	K_1	R^2 (Linear)	R^2 (Nonlinear)	$q_{e,cal}$ mg g^{-1}	K_1	R^2 (Linear)	R^2 (Nonlinear)
12.5	0.899	0.463	–0.0002	0.86	0.80	0.913	0.665	0.99	0.97
25	1.956	0.230	–0.0003	0.85	0.94	1.945	4.735	1	0.94
50	4.019	0.446	–0.0004	0.83	0.81	3.980	1.062	1	0.92
100	8.029	0.517	–0.0001	0.49	0.88	8.019	0.182	0.99	0.99

The values of K_1 and q_e were calculated from the slopes and intercepts of the plot between $ln(q_e–q_t)$ and time. On the basis of lower correlation coefficients, it is confirmed that the adsorption of BF dye on JSPB does not involve pseudo first order kinetics.

Pseudo 2nd order kinetic model stated that the rate of occupation of adsorption sites is proportional to the square of number of unoccupied sites. The non-linear equation of this model is given below:

$$\frac{dq_t}{dt} = K_2 \left(q_e - q_t\right)^2 \tag{13}$$

$$\frac{1}{q_t} = \frac{1}{K_2 q_e^2} + \frac{1}{q_e} t \tag{14}$$

where K_2 = pseudo 2nd order rate constant (g mg^{-1} min^{-1}).

The values of K_2 and R^2 show the continuous increasing trend for liner pseudo 2nd order, which confirms the suitability of this model for the adsorption of BF dye on the JSPB, but the nonlinear pseudo 2nd order does not fit with this process as R^2 has lower value comparatively.

Thermodynamic study. This study was conducted by shaking the 50 mL of the synthetic BF dye solution in the concentration range 25–100 mg L^{-1} for different temperatures (308–328 K) at the optimum process conditions of pH 8.01,

contact time 75 min, dosage 0.6 g and concentration 100 mg L^{-1} in the orbital shaker. At the end of shaking (after reaching equilibrium time), the flasks were withdrawn, solutions were filtered and the filtrates were analysed for the content of dye in the final solution using UV spectrophotometer. To know about the nature of the process, the thermodynamic parameters like Gibbs energy (ΔG^0), enthalpy (ΔH^0) and entropy (ΔS^0) changes were evaluated (Table IV).

The values of ΔH^0 and ΔS^0 were estimated from the plot of ln K_c *vs.* 1/*T*. The negative value of ΔH^0 signify the exothermic nature of the process. The negative values of ΔG^0 show that the dye adsorption was spontaneous. The positive value of ΔS^0 points toward the increase in randomness due to interaction between adsorbent and dye molecules.

TABLE IV. Thermodynamic parameter for BF dye adsorption

Concentration mg L^{-1}	ΔH^0 kJ mol^{-1}	ΔS^0 J k^{-1} mol^{-1}	ΔG^0 / kJ mol^{-1}		
			308 K	318 K	328 K
25	−19.86	06.74	−0.093	−0.142	−0.228
50	−45.51	20.34	−1.709	−2.018	−2.112
75	−04.14	10.19	−2.721	−2.822	−2.924
100	−26.73	19.11	−3.215	−3.402	−3.597

Comparison study

The comparison study of obtained result with the reported results in literature are given in Table V. JSPB shows higher adsorption capacity compared to the reported data (Gupta *et al.*,[10] Quin *et al.*,[13] Kaith *et al.*,[37] Nwodika *et al.*[15]), while other adsorbents show higher adsorption capacity (Guan *et al.*;[38] Wang *et al.*[39]) as they have used expensive chemicals to fabricate the adsorbent materials.

TABLE V. Comparison of adsorption capacity for BF dye removal with other literature data

Adsorbent	Adsorption capacity, mg g^{-1}	Reference
Polymeric nanocomposite	0.439	Kaith *et al.*[37]
Graphite oxide	1.830	Quin *et al.*[13]
Base activated cola nut pod carbon (KPBC)	3.470	Nwodika *et al.*[15]
Acid activated cola nut pod carbon (KPBA)	5.760	Nwodika *et al.*[15]
Bottom ash	6.400	Gupta *et al.*[10]
Jamun seed powder biochar	8.000	Present study
Mesoporous molecular sieve of AI-SBA-16	70.080	Guan *et al.*[38]
Graphene based magnetic nanocomposite	89.400	Wang *et al.*[39]

CONCLUSION

The current study confirms that the JSPB is an effective, efficient and a low--cost adsorbent for the BF dye removal from synthetic waste water solution. The characterization shows that JSPB has good adsorption properties as it contains aromatic compounds and different elements like C, Mg, K, Si and Fe. The FT-IR

study reveals that biochar is rich in functional groups. The semi-crystalline surface of the biochar was revealed by the XRD analysis, which favours adsorption. The maximum removal efficiency and adsorption capacity of JSPB for BF dye removal was found to be 97 % and 8.0 g respectively at the optimum conditions of pH 8.01, concentration 100 mg L^{-1}, JSPB dosage 0.6 g, contact time 75 min and temperature 318 K. The adsorption capacity of JSPB is higher than other adsorbents (Table V) despite its fabrication through comparatively simple processes. The suitability of Temkin isotherm for both linear and non-linear forms indicate the uniform distribution of binding energy over the JSPB surface and also reveals that the adsorption heat for all molecules decreases with the increasing surface area of JSPB. Chemisorption behaviour of this process was confirmed by the linear pseudo-2nd order kinetic model. The negative values of ΔH^0 show the exothermic nature and the positive value of ΔS^0 indicates increase in randomness of the process. The overall study suggested that JSPB can be considered as eco-friendly and good adsorbent for the removal of cationic dyes.

ИЗВОД

УПОТРЕБА БИОУГЉА ОД СЕМЕНА *Syzyum cumini* ЗА УКЛАЊАЊЕ ФУКСИНСКЕ БОЈЕ ИЗ ВОДЕНОГ РАСТВОРА

DIVYA KOSALE, CHANDRAKANT THAKUR и VINOD KUMAR SINGH

Department of Chemical Engineering, National Institute of Technology Raipur, Raipur 492010, Chhattisgarh, India

Индустрија текстила, коже, боја и друге индустрије испуштају много боја у отпадне воде које могу имати велики утицај на животну средину и људски живот. Због тога је неопходно уклонити боју из отпадних вода пре њиховог испуштања и поновне употребе. У прошлости је предложено неколико поступака за уклањање и инактивацију боја, али је адсорпција стекла популарност због своје ефикасности и једноставне употребе. Употреба биоугљева као адсорбената добија на пажњи због њихове ниске цене, доступности и високе способности адсорпције. Ова студија је фокусирана на уклањање базног фуксина (BF) путем адсорпције ове боје, коришћењем биоугља у праху од семена *Syzyum cumini* као адсорбента. Биоугаљ је окарактерисан различитим анализама као што су: XRD, EDS, FTIR, TGA и SEM. Адсорпција је проучавана уз варирање параметара као што су pH, трајање контакта, температура, доза адсорбента и температура. Изотермна, кинетичка и термодинамичка испитивања су такође спроведена да би се разумео механизам адсорпције. Максимални капацитет адсорпције за BF боју је показао биоугаљ семена произведен на 500 °C. Ово истраживање открива да биоугаљ произведен од семена *Syzyum cumini* има значајан потенцијал за елиминацију BF боје из отпадних вода.

REFERENCES

1. B. Lellis, C. Z. Fávaro-Polonio, J. A. Pamphile, J. C. Polonio, *Biotechnol. Res. Innov.* **3** (2019) 275 (https://doi.org/10.1016/j.biori.2019.09.001)
2. G. Mezohegyi, F. P. van der Zee, J. Font, A. Fortuny, A. Fabregat, *J. Environ. Manage.* **102** (2012) 148 (https://doi.org/10.1016/j.jenvman.2012.02.021)

3. S. Punathil, D. Ghime, T. Mohapatra, C. Thakur, P. Ghosh, *J. Hazard. Toxic Radioact. Waste* **24** (2020) 2 (https://doi.org/10.1061/(asce)hz.2153-5515.0000534)
4. V. Chandane, V. K. Singh, *Desalin. Water Treat.* **57** (2016) 4122 (https://doi.org/10.1080/19443994.2014.991758)
5. V. Kumar, A. Khapre, C. Thakur, P. Ghosh, P. K. Chaudhari, *Int. J. Chem. React. Eng.* (2021) (https://doi.org/10.1515/ijcre-2021-0175)
6. S. Barakan, V. Aghazadeh, *Environ. Sci. Pollut. Res.* **28** (2021) 2572 (https://doi.org/10.1007/s11356-020-10985-9)
7. P. K. Navin, S. Kumar, M. Mathur, *Int. J. Eng. Res. Technol.* **6** (2018) 1 (https://www.ijert.org/research/textile-wastewater-treatment-a-critical-review-IJERTCONV6IS11015.pdf)
8. M. Paredes-Laverde, M. Salamanca, J. D. Diaz-Corrales, E. Flórez, J. Silva-Agredo, R. A. Torres-Palma, *J. Environ. Chem. Eng.* **9** (2021) (https://doi.org/10.1016/j.jece.2021.105685)
9. K. Sarayu, S. Sandhya, *Appl. Biochem. Biotechnol.* **167** (2012) 645 (https://doi.org/10.1007/s12010-012-9716-6)
10. V. K. Gupta, A. Mittal, V. Gajbe, J. Mittal, *J. Colloid Interface Sci.* **319** (2008) 30 (https://doi.org/10.1016/j.jcis.2007.09.091)
11. M. El-Azazy, A. S. El-Shafie, A. Ashraf, A. A. Issa, *Appl. Sci.* **9** (2019) (https://doi.org/10.3390/app9224855)
12. M. El Haddad, *J. Taibah Univ. Sci.* **10** (2016) 664 (https://doi.org/10.1016/j.jtusci.2015.08.007)
13. J. Qin, F. Qiu, X. Rong, J. Yan, H. Zhao, D. Yang, *Toxicol. Environ. Chem.* **96** (2014) 849 (https://doi.org/10.1080/02772248.2014.993642)
14. Priya, B. S. Kaith, U. Shanker, B. Gupta, *J. Environ. Manage.* **234** (2019) 345 (https://doi.org/10.1016/j.jenvman.2018.12.117)
15. N. Chekwube, O. D. Onukwuli, *Gazi Univ. J. Sci.* **30** (2017) 86
16. X. Zhang, J. Huang, Z. Kang, D. P. Yang, R. Luque, *Mol. Catal.* **484** (2020) 110786 (https://doi.org/10.1016/j.mcat.2020.110786)
17. S. Kalita, M. Pathak, G. Devi, H. P. Sarma, K. G. Bhattacharyya, A. Sarma, A. Devi, *RSC Adv.* **7** (2017) 27248 (https://doi.org/10.1039/c7ra03014b)
18. A. Sagar, A. Dubey, *Int.J. Chem. Studies* **7** (2019) 590 (https://www.chemijournal.com/archives/2019/vol7issue3/PartK/7-2-227-854.pdf)
19. M. El Haddad, *Integr. Med. Res.* **10** (2018) 664 (https://doi.org/10.1016/j.jtusci.2015.08.007)
20. J. N. Nsami, J. K. Mbadcam, *J. Chem.* **2013** (2013) 469170 (https://doi.org/10.1155/2013/469170)
21. K. I. Aly, M. M. Sayed, M. G. Mohamed, S. W. Kuo, O. Younis, *Micropor. Mesopor. Mater.* **298** (2020) 110063 (https://doi.org/10.1016/j.micromeso.2020.110063)
22. M. Stylianou, A. Christou, P. Dalias, P. Polycarpou, C. Michael, A. Agapiou, P. Papanastasiou, D. Fatta-Kassinos, *J. Energy Inst.* **93** (2020) 2063 (https://doi.org/10.1016/j.joei.2020.05.002)
23. D. Özçimen, A. Ersoy-Meriçboyu, *Renew. Energy* **35** (2010) 1319 (https://doi.org/10.1016/j.renene.2009.11.042)
24. D. Zhang, T. Wang, J. Zhi, Q. Zheng, Q. Chen, C. Zhang, Y. Li, *Materials (Basel)* **13** (2020) 1 (https://doi.org/10.3390/ma13245594)

25. E. O. Oyelude, F. Frimpong, D. Dawson, *J. Mater. Environ. Sci.* **6** (2015) 1126 (https://www.jmaterenvironsci.com/Document/vol6/vol6_N4/132-JMES-1383-2015-Oyelude.pdf)
26. V. K. Singh, A. B. Soni, R. K. Singh, *Orient. J. Chem.* **32** (2016) 2621 (https://doi.org/10.13005/ojc/320534)
27. W. Bessashia, Y. Berredjem, Z. Hattab, M. Bououdina, *Environ. Res.* **186** (2020) 109484 (https://doi.org/10.1016/j.envres.2020.109484)
28. F. Mashkoor, A. Nasar, Inamuddin, A. M. Asiri, *Sci. Rep.* **8** (2018) 1 (https://doi.org/10.1038/s41598-018-26655-3)
29. T. A. Khan, E. A. Khan, Shahjahan, *Appl. Clay Sci.* **107** (2015) 70 (https://doi.org/10.1016/j.clay.2015.01.005)
30. R. Bhattacharyya, S. K. Ray, *Polym. Eng. Sci.* **53** (2013) 2439 (https://doi.org/10.1002/pen.23501)
31. N. Abdus-Salam, A. V. Ikudayisi-Ugbe, F. A. Ugbe, *Chem. Data Collect.* **31** (2021) 100626 (https://doi.org/10.1016/j.cdc.2020.100626)
32. L. Wang, J. Zhang, A. Wang, *Colloids Surfaces, A* **322** (2008) 47 (https://doi.org/10.1016/j.colsurfa.2008.02.019)
33. S. Parimal, M. Prasad, U. Bhaskar, *Ind. Eng. Chem. Res.* **49** (2010) 2882 (https://doi.org/10.1021/ie9013343)
34. K. Patidar, M. Vashishtha, *J. Serbian Chem. Soc.* **86** (2021) 429 (https://doi.org/10.2298/JSC201103010P)
35. A. A. Babaei, S. N. Alavi, M. Akbarifar, K. Ahmadi, A. Ramazanpour Esfahani, B. Kakavandi, *Desalin. Water Treat.* **57** (2016) 27199 (https://doi.org/10.1080/19443994.2016.1163736)
36. D. Tian, X. Zhang, C. Lu, G. Yuan, W. Zhang, Z. Zhou, *Cellulose* **21** (2014) 473 (https://doi.org/10.1007/s10570-013-0112-3)
37. B. Singh, U. Shanker, B. Gupta, *J. Environ. Manage.* **234** (2019) 345 (https://doi.org/10.1016/j.jenvman.2018.12.117)
38. Y. Guan, S. Wang, C. Sun, G. Yi, X. Wu, L. Chen, X. Ma, *Chem. Pap.* **73** (2019) 2655 (https://doi.org/10.1007/s11696-019-00817-7)
39. C. Wang, C. Feng, Y. Gao, X. Ma, Q. Wu, Z. Wang, *Chem. Eng. J.* **173** (2011) 92 (https://doi.org/10.1016/j.cej.2011.07.041).

Waste hemp and flax fibers and cotton and cotton/polyester yarns for removal of methylene blue from wastewater: Comparative study of adsorption properties

MARIJA M. VUKČEVIĆ[1]*[#], MARINA M. MALETIĆ[2#], BILJANA M. PEJIĆ[1], NATAŠA V. KARIĆ[2#], KATARINA V. TRIVUNAC[1#] and ALEKSANDRA A. PERIĆ GRUJIĆ[1#]

[1]Faculty of Technology and Metallurgy, University of Belgrade, Karnegijeva 4, 11000 Belgrade, Serbia and [2]Innovation Center of the Faculty of Technology and Metallurgy, Karnegijeva 4, 11000 Belgrade, Serbia

Abstract: Waste hemp and flax fibers, and cotton and cotton/polyester yarns, available in large quantities from the textile industry, were used as cheap and effective sorbents for the removal of methylene blue from wastewater. Waste fibers and yarns were characterized by scanning electron microscopy, Fourier transform infrared spectroscopy, iodine sorption, water retention, and point of zero charge, as well as through the determination of crystallinity index and degree of surface crystallinity. The adsorption of methylene blue was optimized by examining the influence of contact time, initial concentration, temperature, and pH value. It was found that the more ordered structure of cotton and cotton/polyester yarns leads to lower adsorption capacities and better agreement with pseudo-second order kinetic and Langmuir isotherm model, while the more heterogeneous structure of flax and hemp fibers shows higher capacities for methylene blue adsorption, better described by the pseudo-first order kinetic and Freundlich isotherm model. Based on the obtained results, waste lignocellulosic fibers and yarns can be used for the discoloration of wastewater, thereby solving the problem of waste generated in the textile industry.

Keywords: textile waste; natural-based fibers; chemical composition; organic dye.

INTRODUCTION

The high consumption of energy and non-renewable natural resources, as well as the resulting climate changes require a serious approach to sustainable environmental protection criteria, in order to ensure a decent life in modern society and preserve resources for the coming generations. Material reuse is an

---

area of particular interest due to the large amount of waste produced around the world in various industries.[1,2]

The textile industry is one of the oldest and largest industries in the world, which tends to meet the ever-increasing demand for textile products that grow with the increase of the world's population.[3–5] Textile waste, which can be generated directly from the textile industry during the textile production processes, or post-consumer textile waste, which is created during consumer use and disposal, represents a group of reusable materials that can have different application possibilities.[3,6] The fact is that much more attention is paid to solving the problem of post-consumer textile waste (product reuse, material recycling, incineration and landfill)[7,8] than the one of the waste generated directly during textile production. Textile waste from production refers to raw textile materials, namely cellulose, protein, and synthetic fibers. Cellulose fibers are of vegetable origin, obtained from materials such as cotton, linen, hemp, ramie and straw; protein fibers are of animal origin, obtained mainly from wool, cashmere and silk, while synthetic fibers are obtained from petrochemical sources, *i.e.*, materials such as polyester, nylon, spandex, acrylic, and polypropylene.[3] These wastes are mainly disposed of by incineration and landfill, so, it is necessary to find ways to reuse them as materials with added value.[5] Another major problem in the textile industry is consuming a large amount of water used for scrolling, bleaching and dyeing processes. The textile industry is the second-largest polluter of water worldwide.[9] If contaminated water is not treated before discharge into natural reservoirs, this wastewater, due to its intense color, higher pH value, and high salt concentration, causes a decrease in photosynthetic activity, due to a deficiency of oxygen, which can be harmful to the aquatic ecosystem and human health.[9–11] According to environmental regulations, industries are required to remove dye from their wastewater before discharge into the environment. Numerous physical, chemical and biological methods may be used to remove dyes from wastewater in the textile industry. These methods mainly require specific equipment and high energy consumption, and an additional problem is the safe disposal of the removed products.[11–13] A process that provides low capital and energy costs, simplicity and speed, as well as high removal efficiency is adsorption.[10,13]

One of the effective ways to reuse textile waste is to convert them into adsorbents for wastewater treatment. Cellulose-based fibers and yarns can have exceptional adsorption properties and high absorption capacity, due to their specific structure and heterogenous chemical composition which implies the presence of different functional groups that acts as active sites for adsorption.[14] Summarizing all the above, it is concluded that the textile industry can be a perfect example of the reuse of textile waste material, to solve the problem of the

colored wastewater it creates. In this way, the needs for a cleaner environment and a circular economy are met at the same time.

This work examines the possibility of using waste hemp and flax fibers and cotton and cotton/polyester yarns, as cheap and effective sorbents for the removal of methylene blue from wastewater, with an emphasis on the influence that structural characteristics and chemical composition have on the adsorption properties.

EXPERIMENTAL

Fibers and yarns obtained as waste from different textile industries were used as adsorbents for the removal of methylene blue (MB). Short flax fibers (F_f) were obtained from Banja Luka, Republic of Srpska, Bosnia and Herzegovina,[15] while hemp fibers (H_f) were obtained from ITES Odžaci, Serbia. Waste cotton (C_y) and cotton/polyester (C_y/PES) yarns were obtained from SIMPO Dekor Vranje, Serbia.

Scanning electron microscopy (SEM JEOL JSM-6610LV) was used to determine the samples' morphological and structural characteristics.

The chemical composition of flax and hemp fibers and cotton yarns was determined by sequential removal of individual components from the structure of the fibers and yarns, which was in accordance with the Soutar and Bryden research.[16]

The surface functional groups' content was examined by Fourier transform infrared spectroscopy (Nicolet™ iS™ 10 FTIR spectrometer, ThermoFisher Scientific), in the range of 400–4000 cm^{-1}. The degree of surface crystallinity (Ci) was estimated based on the intensity of characteristic bands from the obtained FTIR spectra.[17] For flax and hemp fibers, and cotton yarns Ci was calculated as a ratio of the intensity of bands at 1368 and 2885 cm^{-1} (I_{1368}/I_{2885}), which were assigned to the in-the-plane C–H bending and C–H symmetrical stretching in cellulose and hemicelluloses.[18] Additionally, for the sample C_y/PES, the degree of surface crystallinity of the polyester component[19] was also calculated as the ratio between the intensity of the band at 1120 cm^{-1}, related to the O–CH$_2$ stretching, and the bend at 1100 cm^{-1}, related to the C–O stretching from amorphous polyester structure (I_{1120}/I_{1100}).

Iodine sorption values (ISV), were determined using the Schwertassek method:[15] yarn samples (0.3 g) were topped with iodine solution (2 cm^3 of KI$_3$), squashed, and squeezed for 3 min. Thereafter, the saturated sodium sulfate (100 cm^3, w(Na$_2$SO$_4$) = 200 g dm^{-3}) was added to the yarns and shaken for 1 h. The iodine concentration of the sample and blank was determined by titration with sodium thiosulfate (0.02 mol dm^{-3}). ISV was calculated as follows:

$$ISV = \frac{(b-t) \times 2.04 \times 2.54}{m_a} \ mg \ g^{-1} \tag{1}$$

where b and t are the volumes (cm^3) of Na$_2$S$_2$O$_3$ solution used for blank and sample titration, and m_a is the weight of absolute dry yarns (g). ISV was used for the determination of crystalline phase content (crystallinity index, X_K):[20]

$$X_K = 100 - \left(100\frac{ISV}{412}\right) \tag{2}$$

The standard centrifuge method (ASTM D 2402-01 2001) was used to assess the examined samples' water retention value (WRV).

The solid addition method[21,22] was used for the determination of pH at the point of zero charge (pH$_{PZC}$), for all the examined samples. To a series of PP tubes, 10 ml of 0.1 M KNO$_3$

was transferred, and the initial pH value of the solution (pH$_i$) was adjusted from 2 to 10 by adding either HCl or NaOH. 0.02 g of tested fibers and yarns were added to the tubes, which were securely capped immediately. The tubes were constantly shaken for 48 h and the final pH values (pH$_f$) were measured. The dependence of pH$_f$ *vs.* pH$_i$ was plotted, along with the tie line for which the final pH was considered equal to the initial pH. The intersecting point between those two lines was recognized as pH$_{PZC}$.

The adsorption was performed on 0.02 g of tested materials from 20 cm^3 MB solution (initial concentration of 20 mg dm^{-3}), at 25 °C in the batch system for 3 h with constant shaking (170 rpm). To examine the effect of pH on adsorption, the initial pH of the MB solution was adjusted to 2, 4, 6, 8 and 10. The influence that initial concentration has on materials adsorption capacities was examined under the same conditions, using the MB solution with the initial concentration ranging from 10 to 75 mg dm^{-3}. The influence of contact time was examined using 0.1 g of tested materials and 100 ml of MB solution (initial concentration of 20 mg dm^{-3}), while the effect of adsorbent mass (0.01, 0.02, and 0.05 g) was studied from 20 ml of MB solution (20 mg dm^{-3}). The concentration of MB solution was determined by UV––Vis spectrophotometry, while the amount of adsorbed MB (q_e in mg g^{-1}) was determined as:

$$q_e = \frac{V(C_0 - C_t)}{m} \tag{3}$$

where C_0 and C_t (mg L^{-1}) are the initial concentration, and the MB concentration in the solution after a defined time, respectively; V (L) is the solution volume and m (g) is the weight of adsorbents (C$_y$, C$_y$/PES, F$_f$ and H$_f$).

Kinetic studies were conducted using the following kinetic models: pseudo-first-order,[23] and pseudo-second-order kinetic model,[24] Elovich[25] and intra-particle diffusion model,[26] while Langmuir[27] and Freundlich[28] isotherm models were used to interpret the equilibrium adsorption data and determine the maximum adsorption capacities of examined samples. Equations for all models used are given in Table S-I of the Supplementary material to this paper.

To evaluate the influence that surrounding temperature has on the MB adsorption, the adsorption experiments were conducted in a temperature-controlled water bath, at 25, 35 and 45 °C. The thermodynamic parameters of the adsorption process were calculated using the following equations:[29]

$$\ln K = \frac{\Delta S}{R} - \frac{\Delta H}{RT} \tag{4}$$

$$\Delta G = \Delta H - T\Delta S \tag{5}$$

The values of ΔH and ΔS were obtained from the slopes and intercepts of ln K *vs.* the 1/T plot, and the values of ΔG were calculated from the corresponding values of ΔH and ΔS following Eq. (5).

RESULTS AND DISCUSSION

Hemp, flax and cotton fibers are natural fibers that are characterized by complex structures, and heterogeneous chemical compositions especially distinct for hemp and flax fibers. The main structural component of these fibers is cellulose, while secondary components are hemicelluloses, lignin, pectin, fats and waxes. The content of these chemical components varies depending on the type of fiber,

as well as on geographical location, cultivation methods, and primary processing. Hemp fibers generally contain 67.0–78.3 % of cellulose, 5.5–16.1 % of hemicelluloses, 2.9–3.3 % of lignin and 0.8–2.5 % of pectin,[16] while flax fibers may contain 64.1–76.0 % of cellulose, 11.0–20.6 % of hemicelluloses and 2–5 % of lignin and 1.8–2.3 % of pectin.[15] On the other hand, cotton fibers are mainly composed of cellulose (83–99 %), and may contain some lignin (up to 6 %) and hemicelluloses and pectin (up to 5 %).[30]

The quantity of these constituents and their location within the fiber structure has an influence on fibers' physicochemical and mechanical properties, especially sorption properties.

The chemical composition of the examined hemp and flax fibers and cotton yarns are given in Fig. 1. It was found that cotton yarns (sample C_y, and cotton component from sample C_y/PES) contain the highest amount of cellulose (94 %) while the hemp fibers contain the highest amount of non-cellulosic components (10.7 % of hemicelluloses, and 6.06 % of lignin).
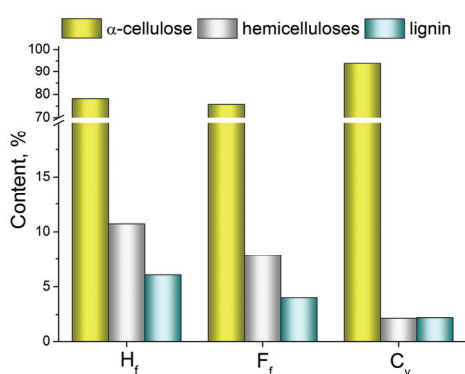

Fig. 1. Chemical composition of flax and hemp fibers and cotton yarns.

The morphology of tested fibers and yarns is examined by scanning electron microscopy (Fig. 2). The structure of flax and hemp fibers (Fig. 2a and b, respectively) is characterized by partially separated elementary fibers, which seem to be embedded in resinous substances (matrix of hemicelluloses, lignin and some pectin), and rough, uneven surface. This liberation of elementary fibers is more noticeable for flax than for hemp fibers, due to the higher content of lignin and hemicelluloses in the structure of hemp fibers. The cotton fibers within the C_y and C_y/PES structure are spirally twisted, with the structure looking like a twisted ribbon (Fig. 2c). Additionally, the polyester component from the sample C_y/PES is characterized by a straight filament, with a noticeable smooth surface.

The type, amount and availability of surface functional groups are influenced by the chemical composition and the location of the chemical components in the fiber structure. The qualitative examination of functional groups present on the surface of tested materials was performed by FTIR analysis.
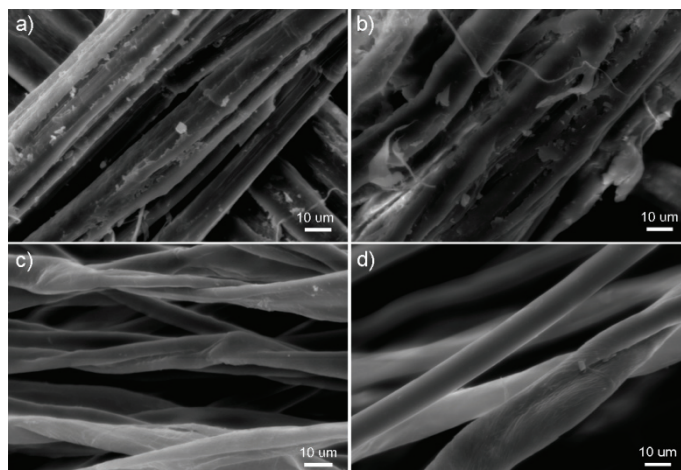
Fig. 2. SEM photographs of: a) H_f, b) F_f, c) C_y and d) C_y/PES.

FTIR spectra for all samples (Fig. 3) show a broad band around 3300 cm^{-1}, originating from the stretching of the O–H bond in hydroxyl groups. Peaks at 2850 and 2920 cm^{-1} originate from the symmetrical and asymmetrical vibrations of the C–H bond in methyl and methylene groups of cellulose and hemicelluloses[31] in the structure of all examined fibers and yarns. The peak near 1730 cm^{-1}, attributed to C=O stretching of carbonyl or ester groups of hemicelluloses,[31,32] is noticeable on the spectra of samples F_f and H_f. Bands in the region 1000–1370 cm^{-1}, are related to the C–O and C–C stretching in polysaccharides, cellulose, and hemicelluloses, while the peak around 890 cm^{-1} indicates the presence of glucopyranose ring in the structure of all examined samples. The broad band around 1630 cm^{-1}, observed for all samples, can be attributed to the aromatic skeletal vibration, or C=O stretching vibrations of hemicelluloses carbonyl groups.[31] Owing to the presence of polyester component, FTIR spectra of sample
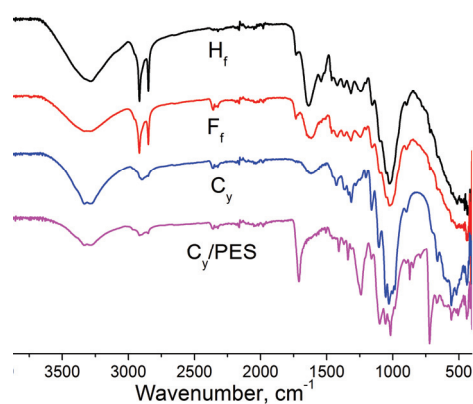

Fig. 3. FTIR spectra of flax and hemp fibers, and cotton and cotton/polyester yarns.

C_y/PES showed additional, intense peaks at 1710 and 1240 cm^{-1} that indicate the presence of the ester group, while the peak at 1505 cm^{-1} can be attributed to the skeletal vibrations of the aromatic systems in polyester chains.[33] Also, out-of--plane bending vibrations of the benzene ring in the polyester are displayed at 720 cm^{-1} (C–H and C=O) and 870 cm^{-1} (C–C).[33]

The degree of surface crystallinity (C_i), estimated based on the intensity of the characteristic bands obtained from FTIR spectra, is shown in Table I, along with the iodine sorption values (ISV), crystallinity index (X_K), water retention value (WRV), and point of zero charge (pH$_{PZC}$). The highest values for the degree of surface crystallinity and the crystallinity index were observed for C_y/PES, due to the presence of highly ordered polyester components and the highest content of α-cellulose in the cotton component. The highly ordered structure of C_y/PES results in lower iodine adsorption, while a smooth surface (Fig. 2), observed especially for the polyester component, leads to the lowest WRV. A similar trend in the physicochemical characteristics, shown in Table I, is observed for the sample C_y, whereby ISV and WRV show higher, and C_i and X_K lower values than C_y/PES, due to the less ordered structure, which is a consequence of the absence of polyester component. Samples F_f and H_f show much higher iodine adsorption and water retention than C_y and C_y/PES samples, as well as a lower degree of surface crystallinity and crystallinity index resulting from the more heterogeneous chemical composition and the location of the components in the fiber structure. Lower content of lignin in the secondary wall, and hemicelluloses in the interfibrillar region of F_f leads to the liberation of the elementary fibers (Fig. 2) and higher availability of α-cellulose on the fiber surface, making the F_f surface more crystalline than H_f. The more liberated fiber structure of F_f than H_f also results in better iodine sorption, while surface roughens and the presence of micropores and microcracks in the H_f surface leads to a higher WRV.

TABLE I. Material characterization: degree of surface crystallinity (C_i), iodine sorption values (ISV), crystallinity index (X_K), water retention value (WRV), and point of zero charge (pH$_{PZC}$)

Sample	C_i	ISV / mg I$_2$ g^{-1}	X_K / %	WRV / %	pH$_{PZC}$
H_f	0.960	132.2	67.91	51.20	5.12
F_f	0.977	160.3	61.09	41.07	4.12
C_y	0.981	84.0	79.61	32.34	5.90
C_y/PES	0.982[a]	55.1	86.63	15.55	5.48
	1.05[b]				

[a]Cotton component, [b]PES component

Adsorption characteristics of lignocellulosic fibers and yarns depend on the content of amorphous regions in cellulose and non-cellulosic components, cracks and cavities, as well as functional groups present on the absorbing surface.[16,34]

Accessible surface functional groups of fibers' chemical constituents (celluloses, hemicelluloses, lignin) are responsible for the surface charge and the acid–base behavior of tested samples. The pH_{PZC} values of tested samples were found to be in the range between 4.12 for F_f and 5.90 for C_y (Table I), indicating that in the water solution with pH higher than 5.90 surfaces of all tested samples will be deprotonated and negatively charged, so the adsorption of cationic MB will be favored.

The solution pH is an important factor that affects the adsorption of methylene blue through the ionization of surface functional groups along with the distribution and the morphology of dye molecules. The influence of the pH of MB solution on the adsorption capacities of examined samples is shown in Fig. 4.
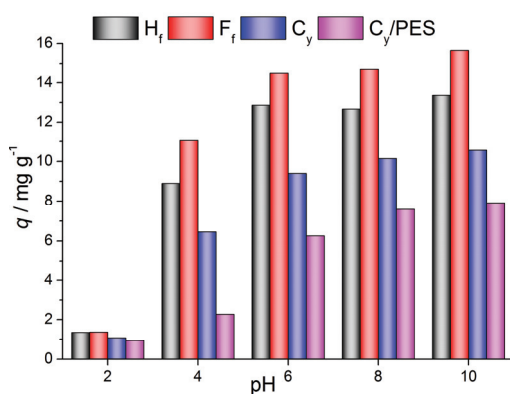

Fig. 4. Effect of the initial pH on the adsorption capacity.

Adsorption capacities increase rapidly with the increase of the solution pH from 2 to 6, while a further increase of pH slightly increases the adsorption capacities of tested samples, keeping the same trend of $F_f > H_f > C_y > C_y$/PES. Methylene blue is a cationic dye that is in the molecular form in the solution having a pH value lower than 4, while in the solution with a pH above 4, the MB^+ becomes dominant.[35] Additionally, in the solution having a pH above the pH_{PZC} value, the surface of tested samples is deprotonated and negatively charged, so an increase in the pH value of the solution positively affects the attraction and bonding of MB^+ species.

The influence that contact time has on the MB adsorption on tested samples is shown in Fig. 5a. Adsorption capacities follow the trend of $F_f > H_f > C_y > C_y$/PES, and increase with the contact time, reaching the equilibrium after 60 min of adsorption.

The process of MB removal from water solution using examined fibers and yarns is relatively fast since over 80 % of adsorption capacity was reached in the first 30 min. Experimental data were fitted with pseudo-first and pseudo-second order models (Fig. 5a), as well as with the intraparticle diffusion (Fig. 5b) and Elo-
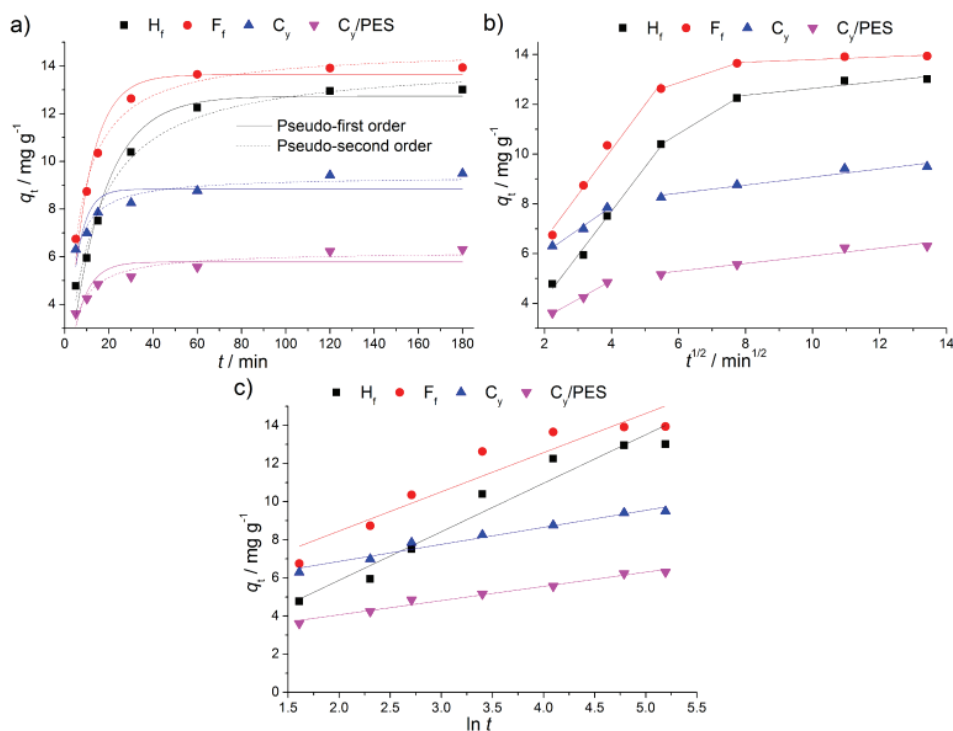
Fig. 5. Adsorption kinetic data fitted with pseudo-first and pseudo-second order (a),
intraparticle diffusion (b) and Elovich (c) model.

vich (Fig. 5c) models, and the obtained kinetic parameters are given in Table S-II of the Supplementary material. According to the correlation coefficients (R^2), adsorption of MB on all samples follow the pseudo-second order kinetic, while calculated adsorption capacity values ($q_{e,cal}$) indicate that the adsorption of MB onto H_f and F_f is better described by the pseudo-first order model. The values of pseudo-first and pseudo-second rate constants indicate that the adsorption process is faster on yarns than on fiber samples. This is also noticeable from the values of Elovich constant α that is related to the rate of adsorption in the beginning. Since the rate-controlling factor of the adsorption process may be the diffusion of adsorbate particles through the structure of the adsorbent, the intraparticle diffusion model was applied to the adsorption data. Multi-linear plots obtained by the intraparticle diffusion model indicate that MB adsorption onto H_f and F_f occurs through the three consecutive steps of fast external adsorption, intraparticle diffusion, and slow equilibrium adsorption, while the adsorption onto yarn samples proceeds through the external adsorption and equilibrium process. The highly ordered structure of yarn samples (C_i and X_K values), featured by smooth and nonporous cotton fibers and polyester filaments (Fig. 2), enables

only the fast adsorption onto the external surface of the yarn samples without the diffusion of the MB species into the yarn structure. Therefore, the adsorption capacities of the yarn samples are lower than for H_f and F_f, and limited by the number of active sites on the sample's external surface. The higher surface coverage of the yarn samples with MB species is confirmed by the values of Elovich constant β. On the other hand, higher adsorption capacities of F_f and H_f are the consequence of the more heterogeneous chemical composition and liberated fiber structure characterized by the surface roughens and the presence of micropores and microcracks.

Fig. 6 shows the influence that adsorbent mass has on the MB removal efficiency and the adsorption capacities of examined samples. For adsorbent mass 0.01 and 0.02 g removal efficiency is almost the same, while the highest removal efficiency was obtained for adsorbent mass of 0.05 g. Nevertheless, the adsorption capacities of all examined samples decrease with the increase of adsorbent mass.
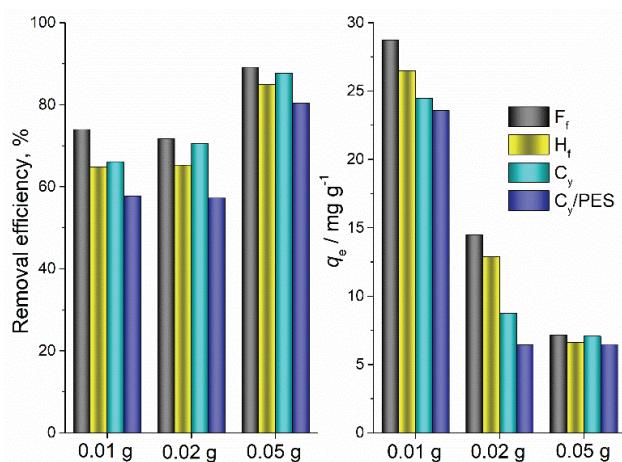

Fig. 6. The influence of adsorbent mass on MB adsorption.

The adsorption capacities of F_f and H_f increase with the initial concentration of MB solution (Fig. 7), while for samples C_y and C_y/PES, an increase in a concentration above 30 and 20 mg dm^{-3}, respectively, does not increase adsorption capacities, due to the surface saturation.

The obtained values for Langmuir and Freundlich parameters (Table II) are in agreement with the sample structure's influence on MB adsorption. The more amorphous and porous structure of H_f and F_f samples leads to higher maximal adsorption capacities (Q_0) and surface heterogeneity ($1/n$), whereby the Freundlich isotherm better describes the adsorption of MB on these samples. Samples

C_y and C_y/PES show lower adsorption capacities, more homogeneous surfaces, and better fits with Langmuir isotherm.
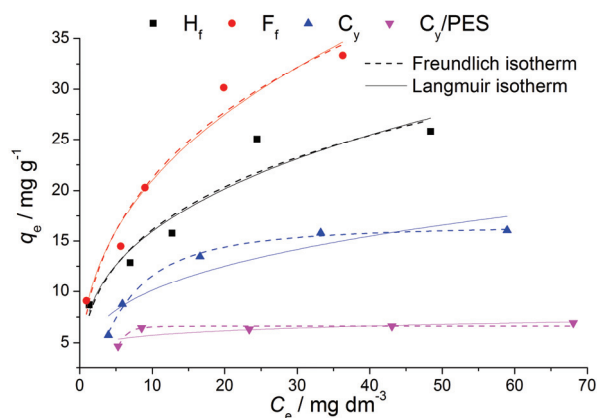

Fig. 7. The influence of initial concentration on MB adsorption: equilibrium adsorption data fitted with Langmuir and Freundlich isotherm.

TABLE II. Langmuir and Freundlich isotherm parameters for MB adsorption on examined fibers and yarns samples.

Sample	Langmuir isotherm			Freundlich isotherm		
	Q_0 / mg g^{-1}	b	R^2	K_f / mg$^{1-1/n}$L$^{1/n}$g^{-1}	$1/n$	R^2
H_f	104.063	0.0713	0.84306	7.350	0.337	0.89365
F_f	142.625	0.0601	0.92953	8.569	0.389	0.95157
C_v	16.630	0.0712	0.99077	4.987	0.307	0.84602
C_y/PES	6.618	0.000169	0.88299	4.502	0.105	0.50585

Thermodynamic studies revealed that MB adsorption onto tested fibers and yarns is an exothermic process (Table III) and that an increase in surrounding temperature leads to a decrease in the adsorption capacities (Fig. S-1 of the Supplementary material). The increase in temperature leads to higher MB solubility and a decrease in the attraction forces between the MB particles and the adsorbent surface.[36] The adsorption process is spontaneous for H_f and F_f at all tested temperatures, and for C_y at 25 and 35 °C, while the adsorption on C_y/PES is not spontaneous.

CONCLUSION

The conducted investigation was focused on reusing short and entangled flax and hemp fibers, and cotton and cotton/polyester yarns, obtained as waste from the textile industry, as a sustainable and renewable adsorbent for the purification of textile industry wastewaters. The adsorption properties of examined lignocellulosic fibers and yarns depend on chemical composition and the location of the structural constituents within the fiber structure. The higher content of α-cellulose and

TABLE III. Thermodynamic parameters for MB adsorption onto examined fibers and yarns

Sample	T / K	q_e / mg g^{-1}	Thermodynamic parameters		
			ΔG / kJ mol^{-1}	ΔH / kJ mol^{-1}	ΔS / kJ mol^{-1} K^{-1}
H$_f$	298.15	15.20	–2.95	–21.994	–0.064
	308.15	14.47	–2.31		
	318.15	12.88	–1.67		
F$_f$	298.15	13.95	–2.19	–24.443	–0.075
	308.15	13.28	–1.45		
	318.15	10.40	–0.70		
C$_v$	298.15	11.01	–0.72	–17.931	–0.058
	308.15	10.23	–0.14		
	318.15	8.90	0.44		
C$_v$/PES	298.15	8.09	0.84	–16.893	–0.059
	308.15	7.31	1.44		
	318.15	6.10	2.03		

the presence of polyester component led to the lower adsorption capacities of cotton and cotton/polyester yarns, while the adsorption process follows the pseudo-second order kinetic and can be described by Langmuir isotherm. On the other hand, more heterogeneous chemical composition and presence of non-cellulosic components in the structure of flax and hemp fibers, as well as fibrillated structure and presence of cavities and cracks on the fiber surface led to the higher capacities for removal of MB from water. The MB adsorption onto the heterogeneous surface of hemp and flax fibers is well described by the pseudo--first order kinetic model and Freundlich isotherm, whereby the intraparticle diffusion affects the rate of adsorption. Based on the obtained results, waste lingocellulosic fibers and yarns can be applied for the discoloration of wastewater, thereby solving the problem of wastes generated in the textile industry.

SUPPLEMENTARY MATERIAL

Additional data and information are available electronically at the pages of journal website: https://www.shd-pub.org.rs/index.php/JSCS/article/view/12170, or from the corresponding author on request.

ИЗВОД

ОТПАДНА ВЛАКНА КОНОПЉЕ И ЛАНА И ПРЕЂЕ ПАМУКА И ПАМУК/ПОЛИЕСТЕРА ЗА УКЛАЊАЊЕ МЕТИЛЕНСКО ПЛАВОГ ИЗ ОТПАДНЕ ВОДЕ: УПОРЕДНА АНАЛИЗА АДСОРПЦИОНИХ КАРАКТЕРИСТИКА

МАРИЈА М. ВУКЧЕВИЋ[1], МАРИНА М. МАЛЕТИЋ[2], БИЉАНА М. ПЕЈИЋ[1], НАТАША В. КАРИЋ[2], КАТАРИНА В. ТРИВУНАЦ[1] и АЛЕКСАНДРА А. ПЕРИЋ ГРУЈИЋ[2]

¹Технолошко–металуршки факултет, Универзитет у Београду, Карнегијева 4, 11000 Београд, и ²Иновациони центар Технолошко–металуршког факултета, Карнегијева 4, 11000 Београд

Отпадна влакна конопље и лана и пређе памука и памук/полиестра, добијена као отпад из текстилне индустрије, коришћена су као јефтини и ефикасни сорбенти за укла-њање метиленског плавог из отпадних вода. Узорци влакана и пређе су окарактерисани скенирајућом електронском микроскопијом, инфрацрвеном спектроскопијом са Фури-јеовом трансформацијом, сорпцијом јода, задржавањем воде, тачком нултог наелектри-сања, као и одређивањем индекса кристаличности и степена површинске кристалич-ности. У циљу оптимизације адсорпције метиленско плавог испитан је утицај времена контакта, почетне концентрације, температуре и pH вредности на ефикасност адсорп-ције. Показано је да пређа памука и памук/полиестера са већим уделом кристалних области у структури има нижи адсорпциони капацитет и боље се слаже са кинетичким моделом псеудо-другог реда и Лангмировом адсорпционом изотермом. С друге стране, влакна лана и конопље се одликују већим уделом аморфних области и нецелулозних компоненти у структури и показују већи капацитет адсорпције и боље слагање са кине-тичким моделом псеудо-првог реда као и са Фројндлиховом адсорпционом изотермом. На основу добијених резултата показано је да се отпадна лигноцелулозна влакна и пређа могу користити за обезбојавање отпадних вода, чиме се решава проблем отпада који настаје у текстилној индустрији и задовољавају све строжији захтеви у области заштите животне средине.

(Примљено 13. децембра 2022, ревидирано 15. марта, прихваћено 22. марта 2023)

REFERENCES

1. A. Briga-Sá, D. Nascimento, N. Teixeira, J. Pinto, F. Caldeira, H. Varum, A. Paiva, *Constr. Build. Mater.* **38** (2013) 155 (https://doi.org/10.1016/j.conbuildmat.2012.08.037)
2. Y. Wang, *Waste Biomass Valor.* **1** (2010) 135 (http://dx.doi.org/doi:10.1007/s12649-009-9005-y)
3. N. Pensupa, S.Y. Leu, Y. Hu, C. Du, H. Liu, H. Jing, H. Wang, C.S. Ki Lin, *Top. Curr. Chem.* **375** (2017) 189 (http://dx.doi.org/doi:10.1007/s41061-017-0165-0)
4. Yalcin-Enis, M. Kucukali-Ozturk, H. Sezgin, in *Nanoscience and Biotechnology for Environmental Applications*, K.M. Gothandam, S. Ranjan, N. Dasgupta, E. Lichtfouse, Eds., Springer Nature Switzerland AG, Cham, 2019, p. 29 (http://dx.doi.org/doi:10.1007/978-3-319-97922-9_2)
5. J. Rapsikevičienė, I. Gurauskienė, A. Jučienė, *Environ. Res. Eng. Manage.* **75** (2019) 43 (http://dx.doi.org/doi:10.5755/j01.erem.75.1.21703)
6. S. Rizal, K.H.P.S. Abdul, A.A. Oyekanmi, O.N. Gideon, C.K. Abdullah, E.B. Yahya, T. Alfatah, F.A. Sabaruddin, A.A. Rahman, *Polymers* **13** (2021) 1 (http://dx.doi.org/doi:10.3390/polym13071006)
7. D. Tian, Z. Xu, D. Zhang, W. Chen, J. Cai, H. Deng, Z. Sun, Y. Zhou, *J. Solid State Chem.* **269** (2018) 580 (http://dx.doi.org/doi:10.1016/j.jssc.2018.10.035)

8. M.D. Stanescu, *Environ. Sci. Pollut. Res.* **28** (2021) 14253
    (http://dx.doi.org/doi:10.1007/s11356-021-12416-9)
9. F. Parvin, S. Islam, Z. Urmy, S. Ahmed, A.K.M. Saiful Islam, *Biomed. J. Sci. Technol. Res.* **28** (2020) 21831 (http://dx.doi.org/doi:10.26717/BJSTR.2020.28.004692)
10. S. Mor, M.K. Chhavi, K.K. Sushil, K. Ravindra, *Environ. Dev. Sustain.* **20** (2018) 625
    (http://dx.doi.org/doi:10.1007/s10668-016-9902-8)
11. M.D. Tenev, A. Farías, C. Torre, G. Fontana, N. Caracciolo, S.P. Boeykens, *J. Sustain. Develop. Energy, Water Environ. Systems* **7** (2019) 667
    (http://dx.doi.org/doi:10.13044/j.sdewes.d7.0269)
12. S. Khamparia, D. Kaur Jaspal, *Front. Env. Sci. Eng.* **11** (2017) 1
    (http://dx.doi.org/doi:10.1007/s11783-017-0899-5)
13. S. Rangabhashiyam, N. Anu, N. Selvaraju, *J. Environ. Chem. Eng.* **1** (2013) 629
    (http://dx.doi.org/doi:10.1016/j.jece.2013.07.014)
14. M. Kostic, B. Pejic, M.Vukcevic, in *Chemistry of Lignocellulosics: Current Trends*, T. Stevanovic, Ed., Taylor & Francis Group/CRC Press, Boca Raton, FL, 2018, p. 3
    (https://www.crcpress.com/Chemistry-of-Lignocellulosics-Current-Trends/Stevanovic/p/book/9781498775694)
15. B.D. Lazić, B.M. Pejić, A.D. Kramar, M.M. Vukčević, K.R. Mihajlovski, J.D. Rusmirović, M.M. Kostić, *Cellulose* **25** (2018) 697 (https://doi.org/10.1007/s10570-017-1575-4)
16. Pejić, M. Vukčević, M. Kostić, in *Sustainable Agriculture Reviews 42*, G. Crini, E. Lichtfouse, Eds., Springer Nature Switzerland AG, Cham, 2020, p. 111
    (https://doi.org/10.1007/978-3-030-41384-2_4)
17. J.G.G. De Farias, R.C. Cavalcante, B.R. Canabarro, H.M. Viana, S. Scholz, R.A. Simão, *Carbohyd. Polym.* **165** (2017) 429 (http://dx.doi.org/10.1016/j.carbpol.2017.02.042)
18. Dai, M. Fan, *Vib. Spectrosc.* **55** (2011) 300
    (http://dx.doi.org/10.1016/j.vibspec.2010.12.009)
19. Donelli, G. Freddi, V.A. Nierstrasz, Paola Taddei, *Polym. Degrad. Stabil.* **95** (2010) 1542
    (http://dx.doi.org/10.1016/j.polymdegradstab.2010.06.011)
20. Fakin, V. Golob, K. Stana Kleinschek, A. Majcen, L. Marechal, *Text. Res. J.* **76** (2006) 448 (http://dx.doi.org/10.1177/0040517506062767)
21. M. Vukcevic, B. Pejic, M. Lausevic, I. Pajic-Lijakovic, M. Kostic, *Fiber. Polym.* **15** (2014) 687 (http://dx.doi.org/10.1007/s12221-014-0687-9)
22. N. Saha, M. Volpe, L. Fiori, R. Volpe, A. Messineo, M. Toufiq Reza, *Energies* **13** (2020) 4686 (http://dx.doi.org/10.3390/en13184686)
23. S. Lagergren, *Handlingar* **24** (1898) 1
24. Y. S. Ho, G. Mckay, *Process Biochem*. **34** (1999) 451 (http://dx.doi.org/10.1016/S0032-9592(98)00112-5)
25. W.J. Weber, J.C. Morris, *J. Sanit. Eng. Div. Am. Soc. Civil. Eng.* **89** (1963) 31
26. C. Aharoni, M. Ungarish, *J. Chem. Soc. Faraday Trans. 1* (1976) 265
    (https://doi.org/10.1039/F19767200400)
27. Langmuir, *J. Am. Chem. Soc.* **40** (1918) 1361
28. H.M.F. Freundlich, *Phys. Chem*. **57** (1906) 384
29. Harrou, E. Gharibi, H. Nasri, M. El Ouahabi, *SN Appl. Sci.* **2** (2020) 277
    (https://doi.org/10.1007/s42452-020-2067-y)
30. R.M. Kozasowski, M. Mackiewicz-Talarczyk, A.M. Allam, in *Handbook of Natural Fibres Volume 1*, R.M. Kozłowski, Ed., Woodhead Publishing Limited, Sawston, Cambridge, 2012, p. 56

31. H. Zhang, R. Ming, G. Yang, Y. Li, Q. Li, H. Shao, *Polym. Eng. Sci.* **55** (2015) 2553 (https://doi.org/10.1002/pen.24147)
32. M.A. Sawpan, K.L. Pickering, Alan Fernyhough, *Compos., A* **42** (2011) 888 (https://doi.org/10.1016/j.compositesa.2011.03.008)
33. A.A. Younis, *Egypt. J. Pet.* **25** (2016) 161 (http://dx.doi.org/10.1016/j.ejpe.2015.04.001)
34. S. Mihajlović, M. Vukčević, B. Pejić, A. Perić-Grujić, M. Ristić, K. Trivunac, *J. Nat. Fibers* (2021) 9860 (https://doi.org/10.1080/15440478.2021.1993414)
35. J.J. Salazar-Rabago, R. Leyva-Ramos, J. Rivera-Utrilla, R. Ocampo-Perez, F.J. Cerino-Cordova, *Sustain. Environ. Res.* **27** (2017) 32 (http://dx.doi.org/10.1016/j.serj.2016.11.009)
36. Salah Omer, G.A. El Naeem, A.I. Abd-Elhamid, O.O.M. Farahat, A.A. El-Bardan, He.M.A. Soliman, A.A. Nayl, *J. Mater. Res. Technol.* **19** (2022) 3241 (https://doi.org/10.1016/j.jmrt.2022.06.045).

Waste hemp and flax fibers and cotton and cotton/polyester yarns for removal of methylene blue from wastewater: Comparative study of adsorption properties

MARIJA M. VUKČEVIĆ[1]*, MARINA M. MALETIĆ[2], BILJANA M. PEJIĆ[1], NATAŠA V. KARIĆ[2], KATARINA V. TRIVUNAC[1] and ALEKSANDRA A. PERIĆ GRUJIĆ[1]

[1]Faculty of Technology and Metallurgy, University of Belgrade, Karnegijeva 4, 11000 Belgrade, Serbia and [2]Innovation Center of the Faculty of Technology and Metallurgy, Karnegijeva 4, 11000 Belgrade, Serbia

TABLE S-I. Theoretical models used for data examination

Model	Equation	Reference
Pseudo-first-order	$q_t = q_e \cdot \left(1 - e^{-k_1 t}\right)$	1
Pseudo-second-order	$q_t = q_e - \left(\dfrac{1}{q_e} + k_2 \cdot t\right)^{-1}$	2
Elovich	$q_t = \dfrac{1}{\beta} ln(\alpha\beta) + \dfrac{1}{\beta} \ln t$	3
Intra-particle diffusion	$q_t = k_{id} t^{1/2} + C$	4
Langmuir isotherm	$q_e = \dfrac{Q_o \cdot b \cdot C_e}{1 + b \cdot C_e}$	5
Freundlich isotherm	$q_e = K_F \cdot C_e^{1/n}$	6

– q_e and q_t (mg g^{-1}) are the amounts of MB adsorbed at equilibrium, and at the time t (min), respectively;

* Corresponding author. E-mail: marijab@tmf.bg.ac.rs

- k_1 (min^{-1}), k_2 (g $mg^{-1}min^{-1}$), and k_{id} (mg g^{-1} $min^{-1/2}$) are the rate constants,
- C (mg g^{-1}) is the intra-particle diffusion constant;
- α (g (mg min)$^{-1}$) and β (g mg^{-1}) are Elovich constants related to the initial adsorption rate and the extent of surface coverage and activation energy for chemisorption, respectively;
- C_e (mg dm^{-3}) is the MB equilibrium concentration,
- Q_o (mg g^{-1}) is the amount of solute adsorbed per unit mass of adsorbent required for monolayer coverage of the surface,
- b (dm^3 mg^{-1}) is a constant related to the heat of adsorption,
- K_F ($mg^{1-1/n}L^{1/n}g^{-1}$) Freundlich constant that indicates the adsorption capacity, and
- $1/n$ Freundlich parameter that indicates the heterogeneity of the adsorbent surface.

Table S-II. Kinetic parameters for MB adsorption onto H_f, F_f, C_y, C_y/PES

| Sample	H_f	F_f	C_y	C_y/PES
$q_{e,exp}$ / mg g^{-1}	13.01	13.94	9.49	6.31
Pseudo-first order model				
$q_{e,cal}$ / mg g^{-1}	12.73	13.63	8.83	5.78
k_1 / min^{-1}	0.06396	0.10777	0.19994	0.15134
R^2	0.96336	0.95320	0.67875	0.73348
Pseudo-second order model				
$q_{e,cal}$ / mg g^{-1}	14.21	14.73	9.38	6.22
k_2 / g $mg^{-1}min^{-1}$	0.00585	0.01102	0.03718	0.03795
R^2	0.98165	0.98712	0.93527	0.93455
Elovich model				
α / g (mg min)$^{-1}$	3.4699	17.078	262.30	23.473
β / g mg^{-1}	0.3930	0.48668	1.1194	1.3413
R^2	0.94105	0.8817	0.96306	0.97511
Intraparticle diffusion model				
$k_{i,1}$ / mg g^{-1} $min^{-1/2}$	1.76973	1.80789	0.93665	0.74877
C_1 / mg g^{-1}	0.63086	2.95116	4.15123	1.92006
R_1^2	0.98976	0.97795	0.96235	0.99202
$k_{i,2}$ / mg g^{-1} $min^{-1/2}$	0.82096	0.44953	0.16184	0.15323
C_2 / mg g^{-1}	5.89448	10.1698	7.45919	4.37612
R_2^2	1	1	0.90578	0.92013
$k_{i,3}$ / mg g^{-1} $min^{-1/2}$	0.13769	0.05198	-	-
C_3 / mg g^{-1}	11.2638	13.2772	-	-
R_3^2	0.73376	0.74817	-	-
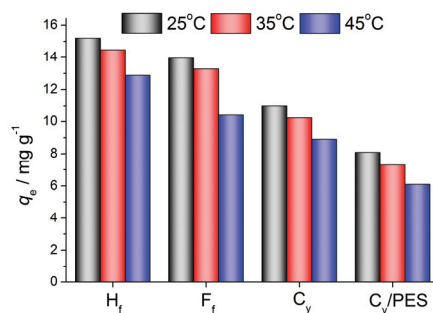
Fig. S-1. Effect of the initial temperature on the adsorption capacity.

REFERENCES

1. S. Lagergren, *Handlingar* **24** (1898) 1
2. Y. S. Ho, G. Mckay, *Process Biochem*. **34** (1999) 451 (http://dx.doi.org/10.1016/S0032-9592(98)00112-5)
3. W.J. Weber, J.C. Morris, *J. Sanit. Eng. Div. Am. Soc. Civil. Eng.* **89** (1963) 31
4. C. Aharoni, M. Ungarish, *J. Chem. Soc. Faraday Trans. 1* (1976) 265 (https://doi.org/10.1039/F19767200400)
5. Langmuir, *J. Am. Chem. Soc.* **40** (1918) 1361
6. H.M.F. Freundlich, *Phys. Chem.* **57** (1906) 384.